2012-12-14

Plume Dispersion: A New Flare Combustion and Plume Rise Model

Rahnama, Kamran

UNIVERSITY OF CALGARY

Plume Dispersion: A New Flare Combustion and Plume Rise Model

by

Kamran Rahnama

A THESIS

SUBMITTED TO THE FACULTY OF GRADUATE STUDIES

IN PARTIAL FULFILMENT OF THE REQUIREMENTS FOR THE

DEGREE OF MASTER OF SCIENCE

CHEMICAL AND PETROLEUM ENGINEERING DEPARTMENT

CALGARY, ALBERTA

December, 2012

Abstract

Air pollution from industrial sources is a continuing concern, especially near residential areas, where public health can be affected. Dispersion of plumes released from stacks depends on wind speed, plume emission rate, stack height, and other meteorological and stack variables. Plume rise is an important aspect of plume dispersion because it increases the apparent release height, which leads to lower ground-level concentrations. Plume rise models are therefore important components of air dispersion models. Plume rise linked with flare combustion has received only minimal attention in the scientific literature to date, despite its importance.

This thesis develops a numerical model of plume rise with flare combustion based on material, heat, mass, and momentum balances. The basis of the model was proposed by Scire et al. (2000) as Plume Rise Model Enhancements (PRIME) for plume rise and building downwash. Later on, De Visscher (2009) extended the PRIME model to account for flare combustion by keeping track of the amount of oxygen mixed into the plume. The current study is an extension of the work of De Visscher (2009) to account for the rate of reaction. The proposed model considers the reaction kinetics to produce more realistic and accurate results. Moreover, emissivity, which plays an important role in the heat conservation equations but which was only parameterized in the original model, is calculated explicitly to increase the accuracy of the model.

In the first step, a set of heat, material, and momentum conservation equations are proposed related to the wind speed and the stack parameters. The basic model is obtained by solving these equations simultaneously assuming instantaneous combustion. Then the kinetics of combustion to CO and CO_2 were considered as a model extension. The emissivity calculation was also enhanced to obtain more accurate results in the improved model. Finally, the air dispersion model CALPUFF was run according to the proposed flare model and a simpler and less realistic flare model by Beychok (2005) to compare results of the models.

This new flare method is simple enough to be embedded into the air dispersion modeling software (such as CALPUFF). Currently, regulatory models use variants of Beychok's (2005) approach, but these are not realistic. More sophisticated models exist (e.g. based on CFD), but

these are too complex to be used in combination with air dispersion models. Thus, this study offers a simple and reliable flare model to be used in air dispersion models.

Acknowledgements

First, I would like to express deep appreciation to my supervisor Dr. Alex De Visscher, for his guidance, support, and criticism throughout the course of my Master study and research. His wide knowledge, constructive advices and guidance from the initial to the final level enabled me to develop an understanding of the subject. His logical way of thinking is always an example for me.

My deep thanks to my family especially my brother Ramin and my sister in law Maryam for their unconditional love and support, and all my genuine helpful friends; Vahid, Ehsan, Mahsa, Behnoush, and Hashem for being great source of motivation and encouragement in many respects during the project and over the project in my day to day life.

I also would like to thank my official referees; Dr. Robert Gordon Moore, Dr. Jalal Abedi, and Dr. Craig Johansen for their helpful constructive comments and excellent advice.

Dedication

Dedicated to my beloved family back home; Hossein, Batoul, and Pooyan.

Table of Contents

List of Tables

List of Figures

List of Symbols

Symbol	Definition
ϕ	Centerline inclination of the plume [degrees]
m_{O_2}	Mass fraction of oxygen in the air []
$\frac{d\eta_{atm}}{dz}$	Ambient air lapse rate [K/m]
K_λ	Spectral extinction coefficient of material [m^{-1}]
$I_{\lambda 0}$	Intensity of radiation [W]
σ_λ	Scattering coefficient [m^2/g]
σ_a	Absorption cross section [m^2/g]
$\dot{c}$	Soot concentration [g/m^3]
c	Concentration [g/m^3]
c_p	Specific heat of air [J/kg K]
C_s	Stoichiometric mixing ratio [%]
D	Stack diameter [m]
E	Activation energy [cal/mol]
f	Burning mass fraction of flare []
F_b	Buoyancy flux parameter [m^4/s^3]
F_c	Coriolis force [N]
F_g	Gravity force [N]
F_m	Momentum flux parameter [m^4/s^2]
f_{mix}	Mass fraction of entrained air mixed into burning fraction of flare []
F_p	Pressure force [N]
F_s	Viscous force [N]
g	Gravitational constant [m/s^2]
H	Heat of combustion [kJ/kg]
h	Plank's constant [J.s]
h_{fv}	Vertical height of visible flame [ft]

k	Boltzmann constant [J/K]
L_f	Length of the flame [m]
MW	Molar weight of hydrocarbon [g/mol]
n	Stoichiometric factor []
NHV	Flare gas net heating value [Btu/ft^3]
OD	Optical density []
P	Pressure [Pa]
Q	Flare gas heat release [kJ/s]
r	Radius [m]
R	Ideal gas constant [Pa m^3/mol K]
r_i	Rate of reaction of component i [mol/m^3]
s	Stability parameter [s^{-2}]
S	Steric factor []
T	Temperature [K]
U_{atm}	Wind speed [m/s]
U_{sc}	Velocity of plume centerline [m/s]
X	Conversion of combustion []
y	Mass flow rate [kg/s]
y^m	Molar flow rate [mol/s]
β	Entrainment parameter in Y direction [m]
ε	Emissivity []
λ	Wavelength [nm]
ρ	Density [g/m^3]
σ	Stefan-Boltzmann constant [kJ/s m^2 K^4]
σ_y	Dispersion parameter in horizontal direction [m]
σ_z	Dispersion parameter in vertical direction [m]
α	Entrainment parameter in X direction [m]
α_B	Angle of flare to the vertical [degrees]
α_λ	Absorptivity at wavelength λ []

Subscript

a	Air
atm	Atmosphere
sc	Centerline

Chapter One: **Introduction**

Flaring is a common way for disposal of combustible vent gas in industrial plants. It is an essential safety requirement of industrial facilities like petroleum refineries, natural gas processing plants, and petrochemical plants. Flaring has been subject to governmental agencies regulations for proposed and operative hydrocarbon processing facilities for minimizing environmental hazards caused by these facilities.

A flare stack is designed to burn combustible gases released from hydrocarbon facilities. Combustible gases are ignited by a pilot flame and released into the ambient air. Flaring forms a plume which is a buoyant hot gas and rises and disperses in the atmosphere easily. As the temperature of the flame and consequently the plume increases, the plume rises higher and disperses more easily (Beychok, 2005).

Combustion of gases is widely used in various industries. The following two reasons support the combustion of the gases. First, many waste gases are considerably more harmful for human health as well as the environment than the gases produced in the combustion processes. This is of prime importance when we consider climate change. For instance, methane (CH_4) which is a common unwanted flammable gas in the oil and gas industry can be oxidized with O_2 in the surrounding air and produce CO_2 and H_2O as follows:

$$CH_4 + 2O_2 \rightarrow CO_2 + 2H_2O$$

It is widely accepted that methane is a stronger greenhouse gas than carbon dioxide (Forster et al., 2007). Second, in case of accidental release, acute health effects and explosion hazards are the motivation for flaring.

After burning the combustible plume, it is important to keep track of the contaminant transport. Some combustion products, such as SO_2, are still hazardous for human health and environment. Therefore, it is essential to predict the movement and concentration of any of the produced species downwind of the stack. This is of prime importance for industries close to urban areas. This information can then be compared to environmental standards to investigate if the pollutant concentrations exceed hazardous levels. If so, remedial actions must be taken.

Air dispersion modeling is a primary regulatory tool to predict source impacts. Modeling results are routinely used to set emission limits and emission conditions of air pollution sources. Other purposes of air dispersion modeling include the response to complaints concerning odors and/or opacity or the management of accidental releases.

Since dispersion of the plume produced by a flare is massively influenced by the flame characteristics such as temperature, height, and length of the flame, it is important to predict all these key influencing factors to perform an accurate air dispersion model simulation. Plume rise is well understood in non-reacting plumes, but few studies have considered plume rise associated with flare combustion. In this work, in the context of plume rise and air dispersion modeling, a new method is developed to model combustion in industrial flares. This new method should be simple enough to be embedded into air dispersion modeling software (such as CALPUFF) and more reliable than current flare models. Currently, regulatory models use variants of Beychok's (2005) approach, but these are overly simplistic and not realistic. More sophisticated models exist (e.g. based on CFD), but these are too complex to be used in combination with air dispersion models. Thus, the object of this study is to offer a simple and precise flare model to be used in air dispersion models.

For the sake of simplicity, flaring of pure methane (CH_4) gas is considered. In the first step, the model reflects instantaneous reaction of burning methane without considering the rates of reactions (burning CH_4 to CO and then oxidizing CO to CO_2). Then rates of reaction are included to obtain more realistic outcomes. Finally, results from the model are used in the air dispersion modeling software CALPUFF.

This dissertation consists of the following chapters: An overview of previous work is discussed in Chapter 2. Chapter 3 outlines a basic flare model based on the equations describing conservation of mass, momentum, and energy. In the fourth chapter, the rates of reaction of combustion are included in the model. This chapter also includes some improvements regarding the energy balance equation by offering an accurate method to calculate the emissivity. Then the results from this improved model are compared with field experimental data. The fifth chapter contains the results of including the flare model into the CALPUFF air dispersion model for

plume dispersion from flare combustion stacks. Finally, the last chapter of this thesis reviews the conclusions and outlines potential future work in this field.

Chapter Two: **Literature Review**

2.1 Air Dispersion Modeling

Air pollution was defined by Liu and Liptak (2000) as "the presence in the outdoor atmosphere of one or more contaminants (pollutants) in quantities and duration that can injure human, plants, or animal life or property (material) or which unreasonably interferes with the enjoyment of life or the conduct of business."

Sulfur dioxide (SO_2), carbon dioxide (CO_2), carbon monoxide (CO), nitrogen oxides (NO_x), particulate matter, smoke, haze, and volatile organic compounds (VOCs), such as methane (CH_4), and the aromatic compounds benzene and toluene ($C_6H_5CH_3$) are some examples of air pollutants. The manmade sources of these pollutants include transportation vehicles, industrial processes, power plants, municipal incinerators, etc. Many of these pollutants exhibit potentially toxic effects on the ecosystem and on human life. According to World Health Organization (WHO), respiratory infections, heart disease, and lung cancer are the main effects of air pollution (WHO, 2012). Ezzati et al. (2002) estimated the worldwide premature death burden due to outdoor air pollution at 800000 per year. The total death of air pollution in North America was estimated at 28000 annually in this study.

Regarding health effects of air pollutants released into the air by industrial facilities like petrochemical industries, natural gas processing plants, and petroleum refineries, governmental agencies have used some models to predict concentrations of contaminants and toxic materials discharged from the industrial plants, to regulate ambient air quality. These models are used to check if existing or proposed new plants are compatible with the acceptable concentration of pollutants based on National Ambient Air Quality Standard (NAAQS) in the United States and/or other nations. Predicting conditions in emergency situations is another use of these models. For instance, in the case of accidental releases of toxic materials or chemical substances in a petrochemical facility, these models can evaluate the affected area, ambient concentration, and also can be used for protective actions. So, based on the model results and meteorological conditions and considering the worst case scenario, locations and concentrations of pollutants

after accidental release are evaluated and protective actions will be taken. These models are called atmospheric dispersion models (Liu and Liptak, 2000).

The objective of air/atmospheric dispersion models is to estimate the concentrations of air pollutants or toxics, downwind of a single source or multiple pollution sources (Liu and Liptak, 2000). Atmospheric dispersion models use mathematical equations and algorithms to simulate the dispersion of the plume from various sources in the ambient air. These sources consist of industries, airplanes, cars, forest fires, etc.

Hence, an air dispersion model can be used for:

- Calculating optimum height of a stack
- Planning new facilities
- Managing existing emission rates
- Evaluating and comparing the impacts of existing emission rate with air quality guidelines, standards and criteria
- Measuring the risk and intensity of and preparing for emergency situations like, accidental hazardous release

Generally, models are divided into two classes: physical models and mathematical models. In physical models, a physical copy of the modeled object is made. A wind tunnel is an example of a physical model. A wind tunnel consists of a closed tubular tunnel with a powerful fan blowing air past the sample. This object can be an airplane or an industrial stack or any other solid sample to study the effects of air moving past solid objects. It helps to represent the reality in aerodynamic research. On the other hand, in mathematical models mathematical equations and relations and sometimes statistic calculations are used as the description of a real system. Computer simulation of the plume coming out of an industrial stack is an example of this type of model. Similarly, using mathematical concepts and language that relate the dispersion of pollutants into the air to the conditions of the atmosphere, air dispersion modeling is a mathematical model type (National Institute of Water and Atmospheric Research et al., 2004).

Using physical science (to calculate the transportation and diffusion of pollutant parcels in the air, by considering heat, momentum and mass balance) and chemistry (reacting pollutants together and with ambient air), the transportation, transformation, and dispersion of contaminants in the ambient air is calculated in air dispersion models. Air dispersion models are also known as: air quality models, atmospheric dispersion models, air pollution dispersion models, or atmospheric diffusion models.

Nowadays, most air dispersion models are computer programs, using the following information to calculate the concentration of contaminants:

- Topography data
- Meteorological data
- Emission source characteristics
    - Height of stack
    - Diameter of stack
    - Buildings around stack
- Emission specifications
    - Rate of emission
    - Temperature of plume
    - Contaminant specification

Figure 2-1 shows a schematic view of how atmospheric dispersion models use this information (National Institute of Water and Atmospheric Research et al., 2004).

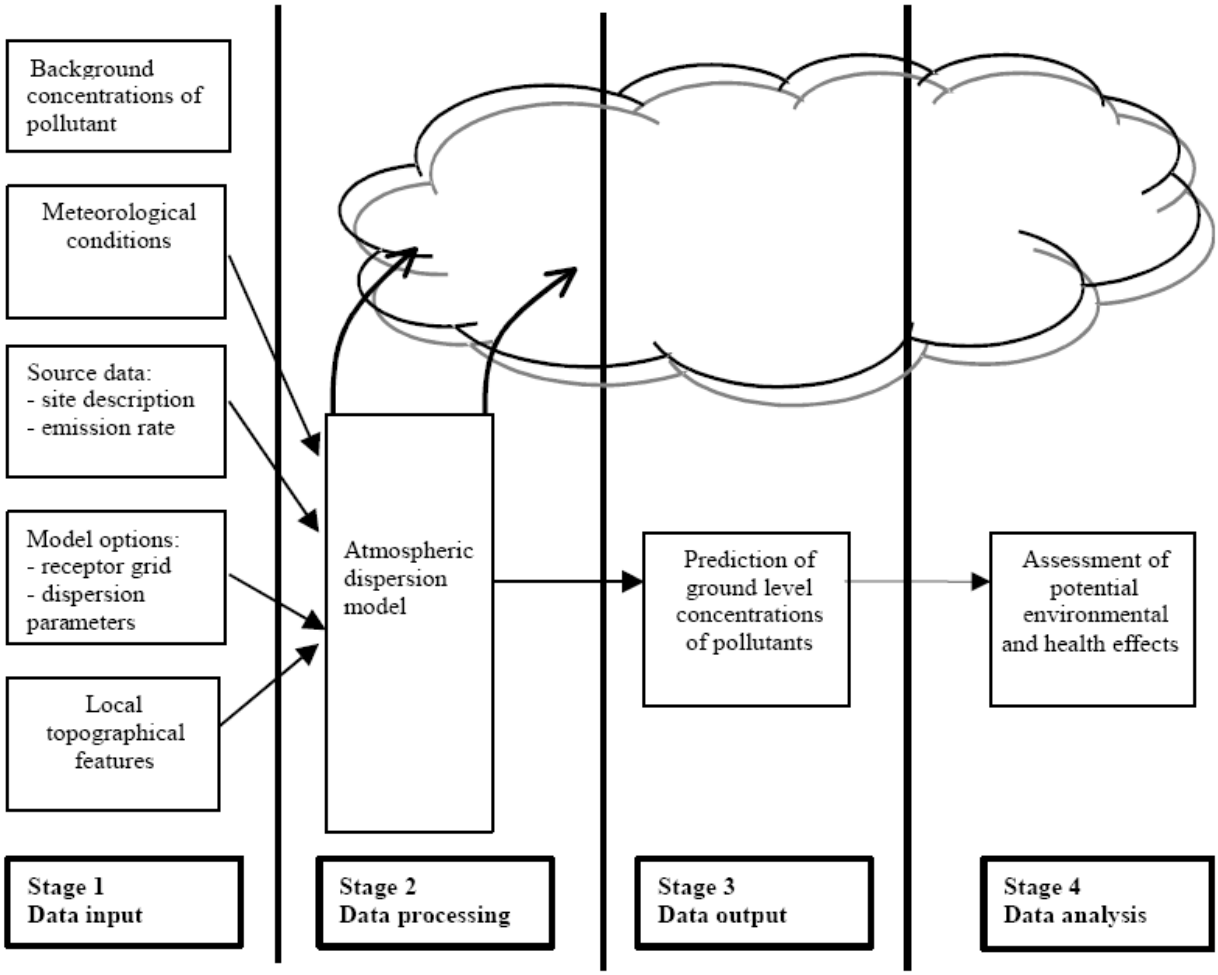

Figure 2-1: Schematic view of Air dispersion models (National Institute of Water and Atmospheric Research et al., 2004)

Based on the Guideline on Air Quality Models, developed by the EPA (2003), air dispersion models are divided into two levels of sophistication; screening and refined modeling. The first and easier level consists of comparatively simple equations, using the worst-case meteorological condition, to prepare a safe and conservative guess of the air quality affected by one or multiple sources. The main goal of this type of model is to determine if further investigation of the air quality impact is required. If the worst-case air quality does not exceed the National Air Quality Standards (NAAQS) or prevention of significant deterioration (PSD) concentration increments, then the source is not problematic, and further study is unnecessary. If the predicted worst-case

contaminant concentration exceeds the allowable concentration, the next level of sophistication, refined modeling, should be applied. Analytical techniques using more detailed meteorological and topographical data are used in the refined models, which provide more accuracy (EPA, 2003).

EPA classified the effective, practical, and well performing models for general conditions as "Appendix A" models. These models are shown in Table 2-1.

Table 2-1: U.S EPA preferred air quality dispersion models (Liu and Liptak, 2000)

Terrain	***Mode***	***Model***	***Reference***
Screening			
Simple	Both	SCREEN3	EPA, 1988;1992a
Simple	Both	ISC3	Bowers et al., 1979; EPA, 1987; 1992b; 1995
Simple	Both	TSCREEN	EPA 1990b
Simple	Urban	RAM	Turner and Novak, 1987; Catalano et al., 1987
Complex	Rural	COMPLEXI	Chico and Catalano, 1986; Source cede.
Complex	Urban	SHORTZ	Bjorklund and Bowers, 1982
Complex	Rural	RTDM3.2	Paine and Egan, 1987
Complex	Rural	VALLEY	Burt, 1977
Complex	Both	CTSCREEN	EPA 1987; Perry et al., 1990
Line	Both	BLP	Schulman and Scire, 1980
Refined			
Simple	Urban	RAM	Turner and Novak, 1987; Catalano et al., 1987
Simple	Both	ISC3	Bowers et al., 1979; EPA, 1987; 1992b; 1995
Simple	Urban	EDMS	Segal 1991; Segal and Hamilton 1988; Segal 1988
Simple	Both	CDM2.0	Irwin et al., 1985
Complex	Both	CTDMPLUS	Paine et al., 1987; Perry et al. 1989; EPA 1990a

Line	Both	BLP	Schulman and Scire, 1980
Line	Both	CALINE3	Benson, 1979
Ozone	Urban	UAM-V	EPA, 1990a
Coastal		OCD	DiCristofaro and Hanna, 1989

Technically, the industrial air (plume) dispersion models can be divided into two main categories; Gaussian plume dispersion models and advanced dispersion models. Currently, Gaussian steady state plume models are the most popular way to model plumes from industrial stacks. Although there are lots of limitations in applying these models, and sometimes results are not accurate enough, they can provide reasonable results when used in the proper conditions. On the other hand, advanced dispersion models use more sophisticated mathematical and computational methods and more fundamental properties of the atmosphere for describing dispersion. Hence, results based on these new generation dispersion models are more reliable and of course more computationally expensive (National Institute of Water and Atmospheric Research et al., 2004). The best results are obtained when a model is chosen that best suits the needs and resources of the modeler (De Visscher, 2013).

There are lots of factors we need to consider to choose an appropriate method of air dispersion modeling. To choose between Gaussian plume models and advanced air dispersion modeling we need a complete understanding of the atmospheric and emission source situation. In addition, we need to know how accurate we want our result to be and at what scale. For example, if the existence of an urban area more than 50 kilometers from the emission source forces us to be more conservative about modeling results, applying Gaussian plume models is not the best way. Since Gaussian models' results are not accurate enough for distances over 50 kilometers from the emission source, using the advanced air dispersion models is preferred in this case.

The following are some criteria that should be considered to decide what kind of modeling is to be used (National Institute of Water and Atmospheric Research et al., 2004):

- Whether the atmosphere in the modeled area is dry or humid
- Are large distance (>50 km) results important in the modeling or not
- Is the modeling domain a coastal area or not

- Is the pollutant neutral (conservative) or reactive with ambient air, or are reaction products important or not. It is the main issue for models treating SO_x and NO_x.

In the following part, Gaussian plume models and advanced air dispersion models will be discussed along with their application.

2.1.1 Gaussian Plume Models

Gaussian plume models use a Gaussian distribution of pollutants in two directions (lateral and vertical) to describe the specification of the plume and to calculate the plume concentration downwind of a source assuming steady state conditions (hourly). Different meteorological conditions lead to different plume shapes and characteristics. Gaussian models are effective for distances less than 50 kilometers from simple emission sources due to extrapolation of dispersion coefficients (National Institute of Water and Atmospheric Research et al., 2004; Arya, 1999). Dispersion coefficients are the standard deviation of the Gaussian distribution function that is responsible for distributing the plume in the vertical and horizontal (z and y) axis.

Gaussian models are easy to use, well understood, and widely accepted. They play an important role in the regulations and standards, however they are not always the most accurate and best models to use. Figure 2-2 represents a simple Gaussian plume shape used in modeling.

The equation for pollutant concentration in the Gaussian plume model, in the absence of boundaries, is as follows:

$$c = \frac{Q}{2\pi u \sigma_y \sigma_z} \exp\left(-\frac{1}{2}\frac{y^2}{\sigma_y^2}\right) \exp\left(-\frac{1}{2}\frac{(z-h)^2}{\sigma_z^2}\right)$$

Equation 2.1

Where: c = concentration at given point, g/m^3

Q = emission rate, g/s

u = wind speed, m/s

σ_y = dispersion parameters in the horizontal (lateral) direction (depends on distance from the source), m

σ_z = dispersion parameters in the vertical direction (depends on distance from the source), m

y = distance crosswind from the emission source, m

z = distance above the ground level, m
h = height of emission plume centerline above the ground level, m

The dispersion parameters are obtained from simple correlations, or from properties of atmospheric turbulence.

When the plume hits the surface (i.e., the ground or a water surface), the pollutant is usually not absorbed or only very slowly. This is incorporated in the model by assuming that the plume reflects on the surface. Then an imaginary source is defined in the underground so the plume behaves as if it reflects on the surface. In this situation Equation 2.1 is extended to:

$$c = \frac{Q}{2\pi\sigma_y\sigma_z}\exp(-\frac{1}{2}\frac{y^2}{\sigma_y^2})(\exp(-\frac{1}{2}\frac{(z-h)^2}{\sigma_z^2})\exp(-\frac{1}{2}\frac{(z+h)^2}{\sigma_z^2})) \qquad \text{Equation 2.2}$$

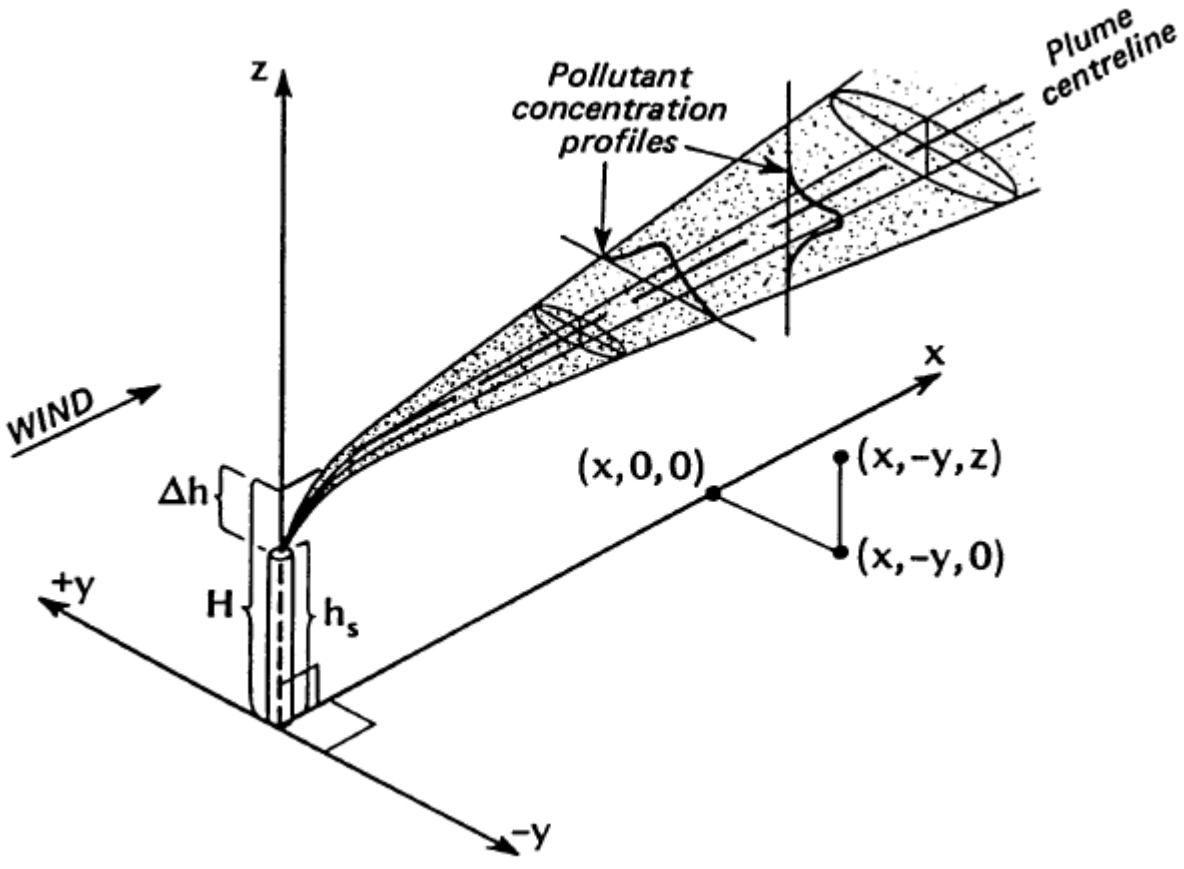

Figure 2-2: A typical Gaussian Plume (National Institute of Water and Atmospheric Research et al., 2004)

Generally, using Gaussian plume models are acceptable when (National Institute of Water and Atmospheric Research et al., 2004):

- Contaminants are unreactive chemically
- Topographical condition is simple with no slopes
- The meteorology does not vary much during small periods of time
- There are few periods of calm or light wind

These factors make the Gaussian models convenient tools in the modeling:

- They do not need an extensive numerical calculation - Gaussian models can be run on almost all computers without necessarily having a good processor.
- They are easy to use – they need only limited input data. They do not need complex meteorological data.
- They provide conservative results in the vicinity of the emission source.
- They are widely used even today – well known with a wide variety of users and well developed, so they are comparable between different studies.

AERMOD, CTDMPLUS, AUSPLUME, and ISCST3 are some examples of Gaussian air dispersion models.

2.1.2 Advanced Dispersion Models

Though Gaussian plume models are widely accepted in air quality assessments and regulation, sometimes more accurate and detailed results are desirable. Using more detailed data, advanced air dispersion models provide more dependable, accurate, and realistic modeling results. Advanced dispersion models perform more numerical calculations in order to run a simulation and thanks to access to high performance computers, these models have become more common. They can be categorized into three main groups based on the type of calculations; puff, particle, and grid point. In puff models, pollutant releases are represented by a series of puffs of material. Each puff represents a group of contaminant molecules whose volume increases due to turbulent mixing and they are transported by the model wind. The puffs are assumed to have a Gaussian concentration profile in three dimensions. Puff models are moderately expensive computationally. In particle models, released pollutants are represented by a stream of particles even if they are gas. In this type, pollutants are transported by the model wind and diffuse

randomly according to the model turbulence. Particle models are computationally more expensive than puff models. In grid point modeling, contaminants distribution is shown by concentration on a three-dimensional grid. This is the computationally most expensive type of model and is usually used for airshed modeling (National Institute of Water and Atmospheric Research et al., 2004).

Generally, the main difference between the Gaussian plume models and advanced dispersion models is that the advanced models need more complicated (three dimensional) meteorological information than the Gaussian plume models. The following are the situations where the advanced models provide better results than Gaussian plume models (National Institute of Water and Atmospheric Research et al., 2004).

- Chemical reaction between pollutants and ambient air is important.
- Appropriate and complete meteorological data is provided.
- Meteorological condition varies in the modeled field, so steady state Gaussian models cannot be applied.
- Source or receptors are located in steep or complex terrain.
- Pollutants accumulate in calm conditions or are re-circulated as the wind changes direction.
- Frequent periods of low wind speed are expected in the area.

Many modern atmospheric dispersion modeling programs contain pre and post-processor modules. These pre and post processor modules improve user friendliness of the interface and allow to input the meteorological, topographical and all other input data by pre-processor modules. Graphical output data, and/or plots of the affected area by pollutants can be obtained from post-processors modules.

The main example of advanced air dispersion models is the Gaussian puff model CALPUFF, which is used widely in industries. In Alberta it is the preferred model for regulatory applications.

2.2 CALPUFF

2.2.1 Background

Scire et al. (1990a, 1990b) developed a dispersion modeling system based on:

- A meteorological modeling package with diagnostic wind field generator, and capability of taking the results of a prognostic model (like MM5) as input data
- A Gaussian puff dispersion model with chemical removal, wet and dry deposition, complex terrain algorithm, building downwash, and plume fumigation
- Post processing programs for output fields of meteorological data, concentration and deposition fluxes

So, based on these components, considering the main needs in developing a new dispersion model, CALPUFF was designed originally to deal with these objectives:

- To treat time variable point and area sources
- To predict concentrations with averaging times from one hour to one year
- To deal with different modeling domains from tens of meters to hundreds of kilometers
- To be used for inert pollutants and those subject to linear removal and chemical conversion mechanisms
- To be used for rough or complex terrain situations

Then CALPUFF, after integrating into the CALGRID model (a photochemical model) and the Kinematic Simulation Particle (KSP) Model (a Lagrangian particle model, to complete the modeling system for both reactive and non-reactive pollutants) became more comprehensive. The Interagency Workshop on Air Quality Modeling (IWAQM) which consists of representatives from the U.S. Environmental Protection Agency (EPA), U.S. Forest Service, National Park Service, and U.S. Fish and Wildlife Service evaluated CALPUFF along with the other models and indicated that using CALMET/CALPUFF models with MM4 data (four dimensional meteorological data assimilation) could improve modeling performance over that of other models. Then, the use of CALMET/CALPUFF to estimate air quality impact was recommended by the IWAQM report (EPA, 1998) relative to the National Ambient Air Quality Standards (NAAQS) and Prevention of Significant Deterioration (PSD) increments. Then EPA

has categorized the CALPUFF modeling system as a Guideline ("Appendix A") model (see Table 2-1) which should be used for the regulatory application involving long range transport, and also, where non-steady-state effects may be important in a case-by-case basis for near-field usage.

As a part of work for IWAQM, U.S. EPA, the U.S.D.A Forest Service, the Environmental Protection Authority of Victoria (Australia), and the private industry in the U.S. and other countries, the CALMET and CALPUFF models have been changed, revised, and improved many times. The model has been made more appropriate for regional application, among other enhancements.

2.2.2 Overview of the CALPUFF Modeling System

As mentioned before, dispersion models are categorized into three groups depending on the way the air pollutants are represented by the model; Particles, Puffs, and Grid points. The CALPUFF modeling system is one of the "Puff" models. CALMET, CALPUFF, and CALPOST are three main components of the CALPUFF modeling system. Generally, CALMET is responsible for meteorological processing. This model develops hourly wind speed and temperature values on a three-dimensional gridded modeling domain. The CALPUFF model simulates dispersion and transformation process. It uses gridded fields generated by CALMET, which are incorporated throughout a simulation period to produce a distribution of puffs. Outputs of the dispersion simulating step (CALPUFF model) contain either hourly concentrations or hourly deposition fluxes calculated at receptors. Finally, CALPOST is used to process the output files generated by CALPUFF to calculate average values, percentiles and extreme values, extinction coefficients and related measures of visibility, and report these for each location. Figures 2-3 and 2-4 show an overview of elements used in the CALMET/CALPUFF modeling system.

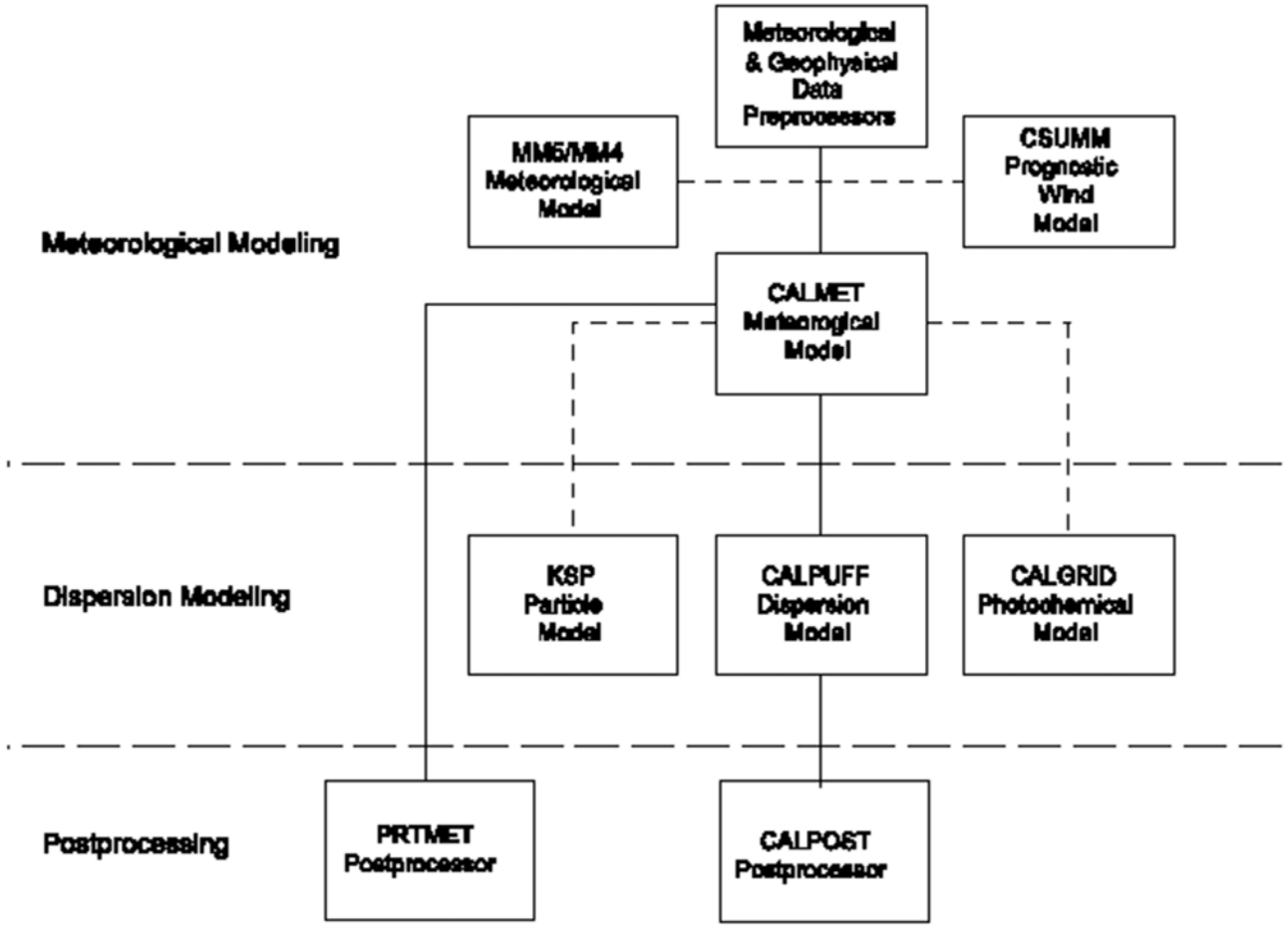

Figure 2-3: Overview of the program elements in the CALMET/CALPUFF modeling system (Scire et al., 2000)

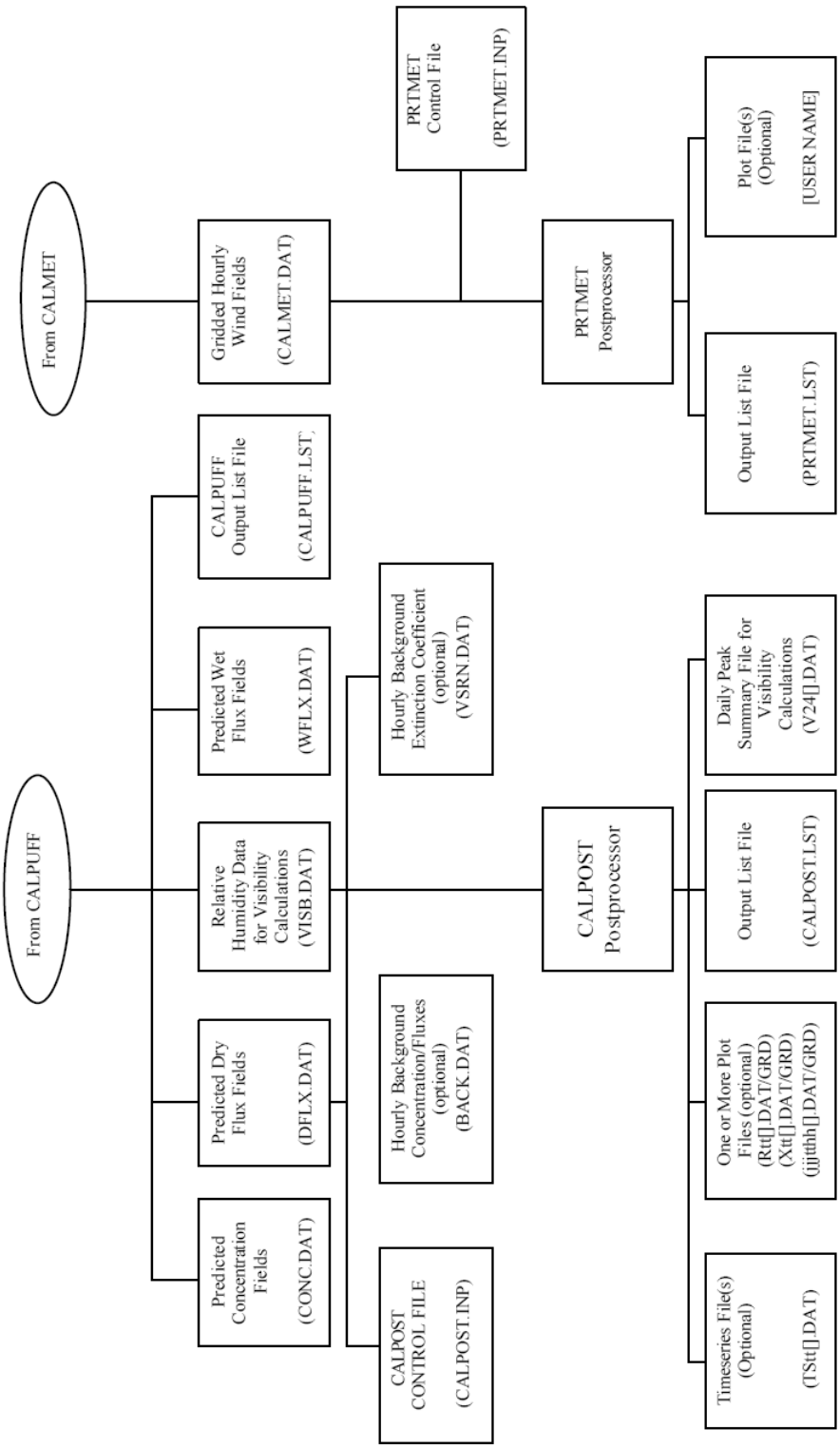

Figure 2-4: Postprocessing: CALPOST/PRTMET postprocessing flow diagram (Scire et al., 2000)

2.2.3 Puff Model Formulation

There is a fundamental similarity between Gaussian puff and Gaussian plume models. The mathematical description of a puff is based on the following equation:

$$\bar{c} = Q_p \varphi_x \varphi_y \varphi_z \qquad \text{Equation 2.3}$$

Where: Q_p = the emission contained in the puff, mg

In this equation φ_x and φ_y are defined in Lagrangian coordinates (i.e., in puff following coordinates) as:

$$\varphi_x = \frac{1}{\sqrt{2\pi}\sigma_x} \exp\left(-\frac{1}{2}\frac{X^2}{\sigma_x^2}\right) \qquad \text{Equation 2.4}$$

$$\varphi_y = \frac{1}{\sqrt{2\pi}\sigma_y} \exp\left(-\frac{1}{2}\frac{Y^2}{\sigma_y^2}\right) \qquad \text{Equation 2.5}$$

And φ_z is defined in Eulerian coordinates (i.e., terrain following coordinates) assuming puff reflection on the surface, as follows:

$$\varphi_z = \frac{1}{\sqrt{2\pi}\sigma_x} \left[\exp\left(-\frac{1}{2}\frac{(z-h)^2}{\sigma_z^2}\right) + \exp\left(-\frac{1}{2}\frac{(z+h)^2}{\sigma_z^2}\right)\right] \qquad \text{Equation 2.6}$$

To be able to describe a finite plume as a series of puffs accurately, a large number of very dilute puffs should be considered. This is the direct puff method for calculating the plume concentration (De Visscher, 2013). For the direct puff method to be effective, each source should emit at least one puff per second to resolve the plume near the source in some cases (Scire et al., 2000a). To solve this weakness, it is possible to define extra puffs near the receptors (Zannetti, 1981), or to merge puffs far from the source that are more closely spaced than necessary (Ludwig et al., 1977). The computational demands of these two improvements are still very large. Hence, two integrated methods have been proposed. The first method is called integrated puff method. It has been incorporated in MESOPUFF II (Scire et al., 1984a, b) and in CALPUFF. And the second one, the slug method, has been incorporated in CALPUFF (Scire et al., 2000). In these two methods some simplifying assumptions have been made to meet the

weakness of the direct puff method by using integrals to calculate the time-averaged concentration of a moving plum.

Assuming that the receptor is at the coordinates (x_r,y_r) and the puff center moves from (x_1,y_1) to ($x_1+\Delta x$,$y_1+\Delta y$), The final equation for the integrated puff method was offered as:

$$\bar{c}_{avr} = \frac{Q_p}{2\pi\sigma_y\sigma_x}\sqrt{\frac{\pi}{2a}}\exp(\frac{b^2}{2a}-\frac{c^2}{2})[erf(\frac{a+b}{\sqrt{2a}})-erf(\frac{b}{\sqrt{2a}})] \qquad \text{Equation 2.7}$$

Where: $a = \frac{(\Delta x)^2+(\Delta y)^2}{\sigma_y^2}$

$$b = \frac{\Delta x(x_1-x_r)+\Delta y(y_1-y_r)}{\sigma_y^2}$$

$$c = \frac{(x_1-x_r)^2+(y_1-y_r)^2}{\sigma_y^2}$$

Based on this method, the number of puffs needed for calculating the concentration accurately is reduced to one per hour (Scire et al., 2000a). This is the main equation which is implementing the plume concentration calculation in CALPUFF.

2.2.4 CALPUFF Features and Options

"CALPUFF is multi-layer, multi-species non-steady-state puff dispersion model which can simulate the effects of time-and space-varying meteorological conditions on pollutant transport, transformation, and removal" (Scire et al., 2000). Input of CALPUFF can be either three dimensional meteorological fields which are the output of the CALMET model, or just simply the meteorological data used to drive the AUSPLUME (Lorimer, 1986), CTDMPLUS (Perry et al., 1989), or ISCST3 (EPA, 1995) steady state Gaussian models.

CALPUFF also has many other options which include dealing with near-source effects like building downwash, longer range effects like vertical wind shear, chemical transformation, and over water transport. All the major features and options of the CALPUFF modeling system are summarized in Table 2-2.

Table 2-2: Major Features of the CALPUFF Model (Scire et al., 2000)

• **Source type**
  • Point source (constant or variable emissions)
  • Line source (source or variable emissions)
  • Volume sources (constant or variable emissions)
  • Area source (constant or variable emissions)

• **Non-steady-state emission and meteorological conditions**
  • Gridded 3-D field of meteorological variables (winds, temperature)
  • Spatially-variable fields of mixing height, friction velocity, convective velocity scale, Monin-Obukhov length, precipitation rate
  • Vertically and horizontally-varying turbulence and dispersion rates
  • Time-dependent source and emissions data

• **Efficient sampling function**
  • Integrated puff formulation
  • Elongated puff (slug) formation

• **Dispersion coefficient (σ_y, σ_z) option**
  • Direct measurements of σ_v and σ_w
  • Estimated values of σ_v and σ_w based on similarity theory
  • Pasquill-Gifford (PG) dispersion coefficient (rural areas)
  • McElroy-Poorler (MP) dispersion coefficients (urban areas)
  • CTDM dispersion coefficients (neutral/stable)

• **Vertical wind shear**
  • Puff splitting
  • Differential advection and dispersion

• **Plume rise**
  • Partial penetration
  • Buoyant and momentum rise
  • Stack tip coefficient
  • Vertical wind shear
  • Building downwash effects

• **Building downwash**   • Huber-Snyder method

- Schulman-Scire method

- **Sub-grid scale complex terrain**
  - Dividing streamline, H_d:
    - Above H_d, puff flows over the hill and experiences altered diffusion rates
    - Below H_d, puff deflects around the hill, split, and wraps around the hill

- **Interface to Emission Production Model (EPM)**
  - Time-varying heat flux and emission from controlled burns and wildfires

- **Dry deposition**
  - Gases and particulate matter
  - Three options:
    - Full treatment of space and time variations of deposition with a resistance model
    - User-specified diurnal cycles for each pollutant
    - No dry deposition

- **Overwater and coastal interaction effects**
  - Overwater boundary layer parameters
  - Abrupt change in meteorological conditions, plume dispersion at coastal boundary
  - Plume fumigation
  - Option to introduce sub-grid scale Thermal Internal Boundary Layers (TIBLs) into coastal grid cells

- **Chemical transformation options**
  - Pseudo-first-order chemical mechanism for SO_2, SO_4^{2-}, NO_x, HNO_3, and NO_3^- (MESOPUFF II method)
  - User-specified diurnal cycles of transformation rates
  - No chemical conversion

- **Wet removal**
  - Scavenging coefficient approach
  - Removal rate a function of precipitation intensity and precipitation type

- **Graphical user interface**
  - Point-and-click model setup and data input
  - Enhanced error checking of model inputs
  - On-line Help files

2.3 Plume Modeling and Plume Rise

In many cases of dispersion modeling, the transport of diffusing material after release cannot be considered as a passive phenomenon. Generally, the velocity and density of the released plume may be different from those of the ambient air, so the released puff or plume might rise or fall after being released from the stack. Therefore, for improving the modeling accuracy in these cases, we need to understand the effects of initial momentum or buoyancy on the trajectory of the plume or puff.

The different methodologies to model the plume rise can be divided into four main types; purely empirical formulas, empirical formulas based on dimension analysis, simple formulas based on material, heat, and momentum balance and finally equations based on Computational Fluid Dynamics (CFD) expressing heat, mass, and momentum balance (De Visscher, 2009; Arya, 1999).

1- **Purely empirical equations:** purely empirical plume rise formulas are based on statistical correlation and regression of observed plume rise with some relevant emission and atmospheric variables. These equations are simple and easy to use, but cannot be applied outside the range of conditions for which they have been tested (De Visscher, 2009). Briggs (1969) has provided a brief review of early empirical relations for the rise of buoyant plumes and momentum jets.
2- **Equations based on dimension analysis:** this method is also empirical, but based on dimension analysis and similarity. Briggs (1968) applied this method to derive a model for the plume rise for different source emissions and atmospheric conditions. These equations are relatively simple and accurate, but because many different cases need to be identified many different equations need to be used (De Visscher, 2009). Equations of this type are summarized in section 2.3.1.
3- **Simple momentum, energy, and mass balance equations:** This type of plume rise model is based on simple momentum, mass, and energy balances. All the equations are combined and form a set of differential equations, and all the model needs is to solve them numerically (De Visscher, 2009). This type is known as numerical plume rise model.

This dissertation is a study to extend the plume rise module PRIME (Plume Rise Model Enhancements) to include flare combustion. The PRIME plume rise module was based on Hoult and Weil's (1972) work (Schulman et al., 2000), and is used in the CALPUFF air dispersion model for simulating large buoyant area sources like forest fires (Scire et al., 2000). Simple conservation equations allow this type of model to be used easily in any air dispersion models (like CALPUFF), without requiring any extensive calculations.

4- **Computational Fluid Dynamics (CFD):** "Computational Fluid Dynamics (CFD) is in part, the art of replacing the governing partial differential equations of fluid flow with numbers and advancing these numbers in space and/or time to be obtain a final numerical description of complete flow field of interest" (Wendt, 1992). CFD is part of fluid mechanics, and uses numerical methods and algorithms to calculate and analyze problems related to fluid flows like a moving plume in the ambient air. This method involves the conservation of mass, momentum, and energy equations for buoyant plumes and momentum jets. This type of model can be the most accurate one between these four types of modeling, but it is the most intensive computationally. Since this method needs a large amount of calculations, sometimes simulating the trajectory of a plume in a large field, it requires super-fast computers with extensive memory space. Consequently, using CFD to model plume rise in air dispersion models is not the most practical approach. They are so computationally costly and time consuming, thus they are not appropriate for a real time application. Despite their complexity, their results are not 100% reliable (Argyropoulos, 2009).

The plume leaving the chimney from an industrial plant rises above the stack when it is either warmer than the surrounding air, which results in lower density rather than ambient air (buoyancy or thermal rise), or released at high velocity from the stack to give the exit gases enough kinetic energy to move upward (momentum rise). The effect of the thermal rise is more likely to have a dominant effect on the plume rise. Based on a rule of thumb, the buoyancy rise is dominant if the exit gas temperature is 10-15 K more than ambient air (Turner, 1994). Depending on the amount of turbulence in the surrounding air, the effect of buoyancy will be diluted after 3-4 minutes when a sufficient volume of ambient air is entrained into the plume,

decreasing its temperature to that of the ambient air. Also, in 30-40 seconds the effects of the momentum force will be degenerated (Turner, 1994).

Briggs (1965, 1968, 1969, 1972, and 1975) provided a set of plume rise equations based on dimension analysis. These equations are widely accepted and have been adopted by U.S. EPA and many others to be used in their stack gas dispersion models. A survey (1972) showed that about 43% of organizations (not including EPA) involved in the stack plume dispersion modeling in the U.S.A, Canada, and Japan were applying Briggs equations. Since the study, this usage has been probably grown even wider globally (Beychok, 2005).

2.3.1 Briggs Equations

Briggs (1969) divided plumes into four general types:

1- Cold jet plumes in calm conditions
2- Cold jet plumes in windy conditions
3- Hot, buoyant plumes in calm conditions
4- Hot, buoyant plumes in windy conditions

Briggs assumed that the movements of cold jet plumes are dominated mainly by their initial velocity momentum, however hot buoyant jet plumes are influenced more by their buoyancy momentum. Even though Briggs provided plume equations for all types of plumes, "the Briggs equations" which have become widely accepted are those for bent-over, hot buoyant plumes (Beychok, 2005).

Briggs (1965) considered six variables to formulate the plume rise phenomenon:

Momentum flux parameter: $F_m = \left(\frac{\overline{\rho}_s}{\overline{\rho}}\right) r_s^2 \overline{w}_s^2$ [m^4/s^2]

Buoyancy flux parameter: $F_b = \left(1 - \frac{\overline{\rho}_s}{\overline{\rho}}\right) g r_s^2 \overline{w}_s^2$ [m^4/s^3]

Stability parameter: $s = \frac{g}{T}\frac{d\theta}{dz}$ [s^{-2}]

Mean horizontal wind speed: $\bar{u}$ [m/s]

Time of travel: t [s]

Plume rise: Δz (transitional); Δh (final) [m]

Where: $\bar{\rho}_s$ = stack gas density, g/m^3

$\bar{\rho}$ = atmosphere air density, g/m^3

r_s = stack radius, m

$\bar{w}_s$ = vertical velocity of stack gas, m/s

g = gravitational acceleration, m/s^2

T = temperature of atmosphere, K

$\frac{d\theta}{dz}$ = potential temperature gradient

Transitional plume rise refers to the height Δz which a plume has risen by the time it reaches to certain location, while final plume rise indicates the height Δh which a plume has risen by the time it stops rising.

In a stable atmosphere, Briggs proposed the following equations to calculate the transitional plume rise:

Buoyancy-dominated: $$\Delta z = 1.6\left(\frac{F_b x^2}{\bar{u}^3}\right)^{1/3}$$ Equation 2.8

Momentum-dominated: $$\Delta z = 2\left(\frac{F_m x}{\bar{u}^2}\right)^{1/3}$$ Equation 2.9

And for final plume rise:

Buoyancy-dominated: $$\Delta h = 2.6\left(\frac{F_b}{\bar{u}s}\right)^{1/3}$$ Equation 2.10

Momentum-dominated: $$\Delta h = 1.5\left(\frac{F_m}{\bar{u}s^{1/2}}\right)^{1/3}$$ Equation 2.11

Since these equations tend to infinity when wind speed is very low, the final plume rise for very low wind speeds is changed to:

Buoyancy-dominated: $$\Delta h = 5.3\left(\frac{F_b}{s^3}\right)^{1/8}$$ Equation 2.12

Momentum-dominated: $$\Delta h = 2.4\left(\frac{F_m}{s}\right)^{1/4}$$ Equation 2.13

And when the atmosphere is near neutral (s=0) the above equations are replaced by:

Buoyancy-dominated: $$\Delta h = 400\frac{F_b}{\bar{u}^3}$$ Equation 2.14

Momentum-dominated: $$\Delta h = 3\frac{F_m}{\bar{u}^2}$$ Equation 2.15

Where plume rise is influenced by both momentum and buoyancy, Briggs (1975) suggested the following equation:

$$\Delta z = \left(\frac{3F_m x}{0.6^2\bar{u}^2} + \frac{3F_b x^2}{2\times 0.6^2\bar{u}^2}\right)^{1/3}$$ Equation 2.16

Arya (1999) summarized the above equation in Table 2-3.

Table 2-3: Plume rise prediction based on dimensional analysis (Arya, 1999)

Stability/Wind Condition	***Type of Rise/Plume***	***Buoyancy-dominated Plume***	***Momentum-dominated Plume***
Unstable and neutral/windy	Transitional/bent over	$\Delta z = 1.6\left(\frac{F_b x^2}{\bar{u}^3}\right)^{1/3}$	$\Delta z = 2\left(\frac{F_m x}{\bar{u}^2}\right)^{1/3}$
Stable/windy	Final/bent over	$\Delta h = 2.6\left(\frac{F_b}{\bar{u}s}\right)^{1/3}$	$\Delta h = 1.5\left(\frac{F_m}{\bar{u}s^{1/2}}\right)^{1/3}$
Stable/calm	Final vertical	$\Delta h = 5.3\left(\frac{F_b}{s^3}\right)^{1/8}$	$\Delta h = 2.4\left(\frac{F_m}{s}\right)^{1/4}$

Neutral/windy	Final/bent over	$\Delta h = 400 \frac{F_b}{\bar{u}^3}$	$\Delta h = 3 \frac{F_m}{\bar{u}^2}$

2.3.2 CFD Formulation

Computational fluid dynamics (CFD) is a branch of fluid mechanics that uses numerical methods and algorithms to solve and analyze problems that involve fluid flows. CFD applies numerical models for the governing transport equations for mass, energy, species, and momentum, the latter based on the Navier-Stokes equations. Because of the range of scales at which turbulent motions exist, direct simulation of atmospheric dynamics is impossible in practice with current computer technology. So, the smallest turbulence scales should be represented with some empirical models as they cannot be resolved by direct simulation. The two main methods to represent the smallest scales are *Reynolds averaged Navier Stokes (RANS)* and *large eddy simulation (LES)*.

The Navier-Stokes equations describe the momentum balance equation for fluids. The derivation of the Navier-Stokes equations is based on Newton's second law, considering the total force as the sum of a gravity force F_g, a Coriolis force F_c, a pressure force F_p, and a viscous force F_s which influence a fluid element with mass "m". Hence:

$$m \times acceleration = F_g + F_c + F_p + F_s \qquad \text{Equation 2.17}$$

Equations 2-18, 2-19, and 2-20 are the Navier-Stokes equations describing an incompressible Newtonian fluid.

$$\frac{\partial u}{\partial t} + u\frac{\partial u}{\partial x} + v\frac{\partial u}{\partial y} + w\frac{\partial u}{\partial z} = fv - \frac{1}{\rho}\frac{\partial p}{\partial x} + \nu\left(\frac{\partial^2 u}{\partial x^2} + \frac{\partial^2 u}{\partial y^2} + \frac{\partial^2 u}{\partial z^2}\right) \qquad \text{Equation 2.18}$$

$$\frac{\partial v}{\partial t} + u\frac{\partial v}{\partial x} + v\frac{\partial v}{\partial y} + w\frac{\partial v}{\partial z} = -fu - \frac{1}{\rho}\frac{\partial p}{\partial y} + \nu\left(\frac{\partial^2 v}{\partial x^2} + \frac{\partial^2 v}{\partial y^2} + \frac{\partial^2 v}{\partial z^2}\right) \qquad \text{Equation 2.19}$$

$$\frac{\partial w}{\partial t} + u\frac{\partial w}{\partial x} + v\frac{\partial w}{\partial y} + w\frac{\partial w}{\partial z} = -g - \frac{1}{\rho}\frac{\partial p}{\partial z} + \nu\left(\frac{\partial^2 w}{\partial x^2} + \frac{\partial^2 w}{\partial y^2} + \frac{\partial^2 w}{\partial z^2}\right) \qquad \text{Equation 2.20}$$

Where: u, v, and w = winds speeds in x, y, and z directions, m/s

v = kinetic viscosity, m^2/s

ρ = density, kg/m^3

p = pressure, Pa

f = Coriolis parameter (= $2\Omega \sin\square$, with Ω the angular velocity of the earth, and $\square$ the latitude)

2.4 The Effect of Plume Rise on the Downwind Concentration

As an illustration of the importance of plume rise on the ground-level concentration downwind of a source, an air dispersion calculation was made in the presence and in the absence of plume rise. The source was assumed to have a stack height of 50 m, and a pollutant emission flow rate of 50 g/s. The wind speed was assumed to be 3 m/s, ambient temperature 15 °C, plume temperature 65 °C. The stack radius is 37.5 cm (i.e., diameter 75 cm), and the emission flow velocity of the stack gas is assumed to be 5 m/s. Based on these data, a buoyancy flux parameter of 5.1 m^4/s^3 is obtained. Plume rise is calculated with the equations in Table 2-3 assuming near-neutral atmosphere.

The result of the calculations is shown in Figure 2-5. In the absence of plume rise, a ground-level concentration of up to 800 $\mu g/m^3$ can be expected, whereas plume rise lowers the maximum ground-level concentration to 270 $\mu g/m^3$. Clearly, accurate evaluation of plume rise is essential for the accurate estimation of the environmental impact of industrial emissions.

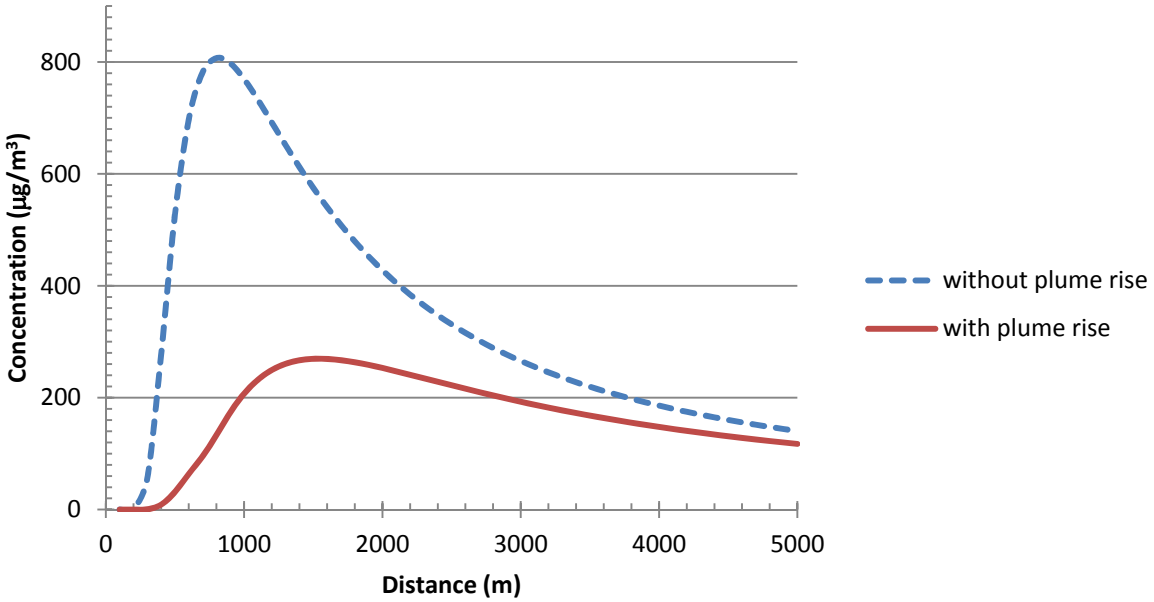

Figure 2-5: The effect of plume rise on the downwind concentration

2.5 Flare Modeling

Flaring in industrial plants has become a very common way of disposal of combustible vent gas. As mentioned in the Introduction section, it is widely used in the industry because of two main reasons; environmental and safety purposes. So, flaring has become an essential safety requirement of industrial facilities like petroleum refineries, natural gas processing plants, and petrochemical plants. It has also been part of governmental agencies regulations for proposed and working hydrocarbon processing facilities for minimizing environmental hazards produced by these facilities.

A flare stack is designed to burn combustible gases released by hydrocarbon facilities. For this purpose, combustible gases are ignited by a pilot flame and released into the ambient air. It is obvious that the plume formed by flaring is a buoyant hot plume, which will rise mainly by buoyancy rather than by momentum.

In some emergency cases, once a large volume of flammable gases has to be burnt, like in a fire situation, cooling water loss, overpressure in a process vessel, or compressor failure, the flaring gas flow rate in a single refinery flare might reach a value on order of 10^5 kg/h, with a heat

release rate of the order of 1000 MW for a few minutes. This shows the importance of safe disposal of large quantities of unwanted flammable gases in the oil industry. The influence of the ambient wind speed on the flare, its radiation field and the amount of radiation energy emitted from the flare, noise problems, the efficiency of the flare for burning any toxic gases, and the formation and dispersion of smoke and gaseous pollutants are subjects of studies by combustion scientists (Bruzustowski, 1976).

In this dissertation, a numerical study has been done to model the flare combustion and flare plume rise to be included in the air dispersion models like CALPUFF. CALPUFF includes a module that is currently used for plume rise and dispersion modeling for large area source, which is based on the work of Hoult and Weil (1972). This plume module does not include a flare modeling section. In other words, PRIME cannot predict the plume rise from flare combustion, or it does not allow for chemical reaction or heat production in the plume (De Visscher, 2009). Hence, an additional set of equations is needed for predicting the flare combustion in CALPUFF.

To model plume rise from flare combustion, the current practice is to use simple empirical equations to predict the flare size and orientation and the amount of air entrained into the flame. Based on these calculations, a "theoretical" source is defined located at the flame tip.

There are several equations describing the size of flames in the literature. Kalghatgi (1983) fitted empirical curves to a wind tunnel data set concerning the shape and size of turbulent hydrocarbon jet diffusion flames in a cross wind. He found that both flame height (h_f) and angles of flame to the vertical (α_B) were function of the ratio of wind speed to the stack exit speed (R). His derived empirical relations are:

$$h_f / D_\circ = (m_a / m)^{\frac{1}{2}} (6 + 2.35 / R + 20R) \qquad \text{Equation 2.21}$$

$$\alpha_B = 94 - (1.6 / R) - 35R \qquad \text{Equation 2.22}$$

Where: m_a, m = molecular weights of air and flare gas, g/mol

D_o = stack diameter, m

Beychok (2005) provides a set of equations predicting these features. In the Beychok flare model an American Petroleum Institute (1969) publication is used to describe the flame length as below:

$$L = 0.006 Q_c^{0.478} \qquad \text{Equation 2.23}$$

Where: L= flame length defined as length of the visible flame, ft

Q_c= flare gas heat release, Btu/hr

And for calculating the height of a flare stack flame, Beychok simply assumed that the angle of flame from the vertical is 45°. Hence, using the previous equation:

$$h_{fv} = L(\sin 45^\circ) = 0.707L$$
$$h_{fv} = 0.0042 Q_c^{0.478} \qquad \text{Equation 2.24}$$

Where: h_{fv}=vertical height of the flame

Steward (1978) published a study on flare size and developed a theoretical mathematical model for turbulent diffusion flames as follows:

$$\frac{L}{R} = 16.218 N^{0.2} \qquad \text{Equation 2.25}$$

Where: L = flame length, ft

R = stack exit radius, ft

N = a combustion parameter = $[Q_c^2 (r + w\rho_a / \rho)^2] / [R^5 (NHV)^2 \rho_a{}^2 g(1-w)^5]$

r = stoichiometric air: fuel ratio, lb air/lb of flared gas

w = a combustion parameter = $(rc_p T_a) / (rc_p T_a / NHV)$

NHV = flare gas net heating value, Btu/ft^3

g = gravitational constant of 417*10^{6}ft/hr^2

ρ_a = ambient air density, lbm/ft^3

ρ = fuel density, lbm/ft^3

T_a = air temperature, °R

c_p = specific heat of air of 0.24 Btu/lbm/°F

Q_c = flared gas heat release, Btu/hr

Some other equations for flare dimensions (downwind extent, area, and volume) were presented by Leahey et al. (1985) and Lehey and Schroeder (1987, 1990) as:

$$A_f = \frac{3927 D_\circ^2}{\beta_o C_s^2}\left[\frac{T}{T_\circ}\right]^{\frac{3}{2}}$$ Equation 2.26

$$V_f = \frac{7854 D_\circ^3}{\beta_\circ R^{\frac{1}{2}}}\left[\frac{T}{T_\circ}\right]^{\frac{3}{2}}\left[\frac{1}{C_s}\right]^{\frac{5}{2}}$$ Equation 2.27

$$h_f = \frac{5 D_\circ}{0.4 + 1.2}\left[\frac{T}{T_\circ C_s R}\right]^{\frac{1}{2}}$$ Equation 2.28

$$\beta_\circ = 0.4 + 1.2R$$ Equation 2.29

$$R = \frac{U}{V}$$ Equation 2.30

Which: A_f= area of flame, m^2
D_o = flare stack diameter, m
β_o = entrainment parameter
C_s = stoichiometric mixing ratio, (%)
T = flare stack temperature, K
T_o = ambient temperature, K (assumed to be 288K)
V_f = volume of the flame, m^3
R = ratio of wind speed to stack exit velocity
x_f = downwind extend of flame, m
h_f = elevation of flame above the stack top, m
U = wind speed, m/s
V = stack exit velocity

For determining the temperature of the flame some equations have been derived as well. For example, Beychok (2005) suggested calculating the adiabatic flame temperature, a procedure equating the heat released by combustion with the combusted gas heat content (enthalpy) at the combusted gas temperature:

$$n_f(NHV) = \sum(n_1 H_1 + n_2 H_2 + n_3 H_3 + n_4 H_4)$$ Equation 2.31

Where: NHV = fuel net heating value at 298K, cal/mol
n_f = mol of fuel
n_1 = mol of CO_2 in combusted gas = c

n_2 = mol of H_2O in combusted gas = 0.5h
n_3 = mol of N_2 in combusted gas = (1+x)(3.76)(c+.025h)
n_4 = mol of O_2 in combusted gas = x(c+0.25h)
c = carbon atoms per mole of fuel
h = hydrogen atoms per mole of fuel
x = (% excess air)/100
H_1,H_2,H_3,H_4 = enthalpies in cal/mol for the CO_2, H_2O, N_2, and O_2 in the combusted gas at the gas temperature T in K

In regards to these expressions for the specific combustion gas components:

$$H_{CO_2} = 7.70T + (2.65 \cdot 10^{-3})T^2 - (0.28 \cdot 10^{-6})T^3 - 2522.5 \quad \text{Equation 2.32}$$

$$H_{H_2O} = 8.22T + (0.075 \cdot 10^{-3})T^2 + (0.447 \cdot 10^{-6})T^3 - 2468 \quad \text{Equation 2.33}$$

$$H_{N_2} = 6.76T + (0.305 \cdot 10^{-3})T^2 + (0.043 \cdot 10^{-6})T^3 - 2042.7 \quad \text{Equation 2.34}$$

$$H_{O_2} = 8.27T + (0.13 \cdot 10^{-3})T^2 + (1.88 \cdot 10^{5})T^{-1} - 3107 \quad \text{Equation 2.35}$$

Where: H = cal/mol of heat content above 298K
T = combusted gas temperature, K

The combusted gas temperature can be calculated by trial-and-error selection of the temperature which satisfies both sets of equations above.

The factors which influence the size of the flame include: diameter of stack, height of stack, ambient air velocity, exit stack gas velocity, type of fuel, heating value of fuel, the heat loss by radiation, etc. As mentioned before, none of these equations incorporate all these influencing factors of the flame size of a flare.

Other than empirical equations, models based on computational fluid dynamics are another common approach for flare modeling. Fairweather et al. (1991) applied a finite-difference procedure to solve the flow equations to model the flare characteristics. In this study, length, trajectory, and temperature profile of the flame are investigated by solving the full three-dimensional forms of the partial differential conservation equations for mass, momentum, and scalar transport. Hernandez et al. (1995) and Lawal et al. (2010) also offered some flare models using a finite-volume procedure for solving the flow equations based on general assumptions similar to those employed by Fairweather et al. (1991). The flow field of all these studies are

based on Reynolds Averaged Navier Stokes (RANS) equations. Smith et al. (2009) presented another flare model using Large Eddy Simulation (LES) method to study the impact of H_2S on carbon and sulfur combustion.

When flare modeling is based on computational fluid dynamics, it is possible to incorporate all those influencing factors, but the problem in using them is that they are too sophisticated and need excess computational work, which make them almost impossible to be embedded into current air dispersion models to be used for real time application. So, more simple equations and solutions are needed to decrease the amount of computational work in air dispersion models.

In this study which is based on previous work of De Visscher (2009), a comprehensive set of equations has been derived to describe flares, incorporating all the factors that influence the flame size of the flare. Moreover, the solution procedure is easy enough to be included in air dispersion models like CALPUFF.

Since this model is a numerical solution of some ODEs (Ordinary Differential Equations) for describing the flame size, it can easily be embedded into the dispersion simulation software such as CALPUFF compared to other sophisticated models.

Chapter Three: **Basic Model – Considering instantaneous reaction**

3.1 Introduction

PRIME (Plume Rise Model Enhancements) is a popular plume rise model which has been developed for plume rise and building downwash (Schulman et al., 2000). This model is also used in CALPUFF to predict plume rise from large area sources. PRIME is an example of the third type of models mentioned in Section 2.3, which consists of a set of differential equations for the conservation of mass, momentum, and energy. Solving this set of ordinary differential equations numerically leads to predictions of the trajectory of a plume.

In the original model, 6 differential equations are responsible for predicting the plume rise using a numerical solution of the mass, energy, and momentum conservation laws. PRIME is unable to predict flare characteristics, so De Visscher (2009) extended PRIME to include flare combustion by keeping track of the amount of oxygen mixed into the plume. De Visscher (2009) added 3 more differential equations to PRIME to be able to account for the flare combustion. This model was fit to flame length correlations, but not to real data. Moreover, the entrainment factors in the mass balance were not optimal, and the specific heat of ambient air was taken constant throughout the flare and plume, despite a 2000°C temperature range.

The main purpose of this chapter is to improve the flare combustion model of De Visscher (2009) by optimizing the entrainment factors, and using temperature dependent values of the specific heat of ambient air. The entrainment factors are optimized by comparing the model results with real measured field data from literature instead of with correlations. These enhancements make the model more realistic.

Nine ordinary differential equations will be developed based on the conservation equations. They are then solved simultaneously along with some auxiliary equations. Though the model calculates the plume as a three dimensional object, it is essentially a one-dimensional model, because variables that define the plume as a three-dimensional object, like plume location along the x and z direction, and plume radius, are calculated as dependent variables of "s" which is the distance traveled by the plume. It is assumed that the plume cross-section is circular (De Visscher, 2009).

3.2 Model Development

The first step in this study is to obtain the differential equations describing the plume and flare behavior. The equations of the numerical plume rise model PRIME will be adopted, and extended to include flare combustion. Figure 3-1 below shows some variables in this numerical model and a schematic of the plume considered by the model.

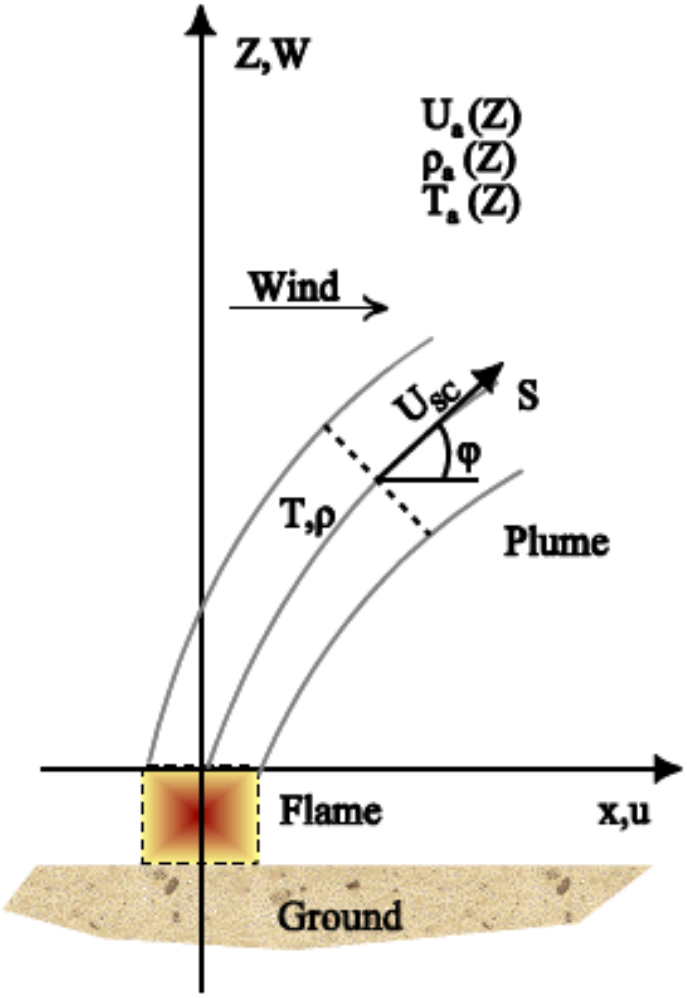

Figure 3-1: Schematic of the numerical plume rise model in CALPUFF (Scire et al., 2000)

PRIME includes the Equations 3.1 to 3.14 below.

The first equation is a mass balance for the rising plume. Based on this equation, the entrainment of ambient air into the plume during the plume trajectory "*s*" increases the mass of the plume while it is rising.

$$\frac{d}{ds}(\rho U_{sc} r^2) = (2r\alpha\rho_{atm}|U_{sc} - U_{atm}\cos\phi|) + (2r\beta\rho_{atm}|U_{atm}\sin\phi|) \quad \text{Equation 3.1}$$

Where: s = path length of plume centerline measured from the emission source, m

ρ = plume density, kg/m^3

U_{sc} = velocity of plume centerline, m/s

r = radius of plume, m

ρ_{atm} = density of atmosphere, kg/m^3

U_{atm} = wind speed, m/s

ϕ = centerline inclination, angle between plume path and the horizontal in the wind direction, degrees

α = plume entrainment parameter corresponding to velocity difference between plume centerline and wind in the parallel direction of the plume centerline = 0.11

β = plume entrainment parameter corresponding to velocity difference between plume centerline and wind in the normal direction of the plume centerline = 0.6

According to this equation there are two driving forces for entrainment of ambient air into the plume: shear along the plume ($U_{sc} - U_{atm}\cos\phi$) and shear across the plume ($U_{atm}\sin\phi$). In the left hand side of Equation 3.1, "$\rho U_{sc} r^2$" describes the mass of plume per unit of length, divided by π. From Equation 3.1, the parameter "$\rho U_{sc} r^2$" forms the first dependent variable of the model. All the equations in this model have been divided by π to simplify the equations.

To find differential equations relating the velocities of the plume and of ambient air, we need to distinguish between the vertical and horizontal components of plume velocity. If we consider "*u*" and "*w*" as the horizontal and vertical components of the plume velocity respectively, we have:

$$\frac{dx}{dt} = u \quad \text{Equation 3.2}$$

$$\frac{dz}{dt} = w \quad \text{Equation 3.3}$$

$$\frac{ds}{dt} = U_{sc} \quad \text{Equation 3.4}$$

Therefore, the second and third differential equations are derived from dividing Equations 3.2 and 3.3 by Equation 3.4:

$$\frac{dx}{ds} = \frac{u}{U_{sc}} = \cos\phi$$ Equation 3.5

$$\frac{dz}{ds} = \frac{w}{U_{sc}} = \sin\phi$$ Equation 3.6

In addition, *"U_{sc}"* can be calculated from "*u"* and "*w"* as below:

$$U_{sc} = \sqrt{u^2 + w^2}$$ Equation 3.7

The fourth differential equation is the momentum balance in the wind direction. The frame of reference chosen for momentum is the ambient wind. Hence, in this equation ambient air has no momentum, so the momentum of the plume is not changed by adding air into the plume. In other words, the momentum is calculated using the moving ambient air as an observer. Furthermore, it is assumed that all the air that experiences friction from the passing plume is entrained into the plume. Therefore, the only mechanism to change the momentum of the plume relative to the ambient air is the velocity gradient of the ambient air itself:

$$\frac{d}{ds}(\rho U_{sc} r^2 (u - U_{atm})) = -r^2 \rho w \frac{dU_{atm}}{dz}$$ Equation 3.8

Where: u = horizontal component of the plume speed, m/s
w = vertical component of the plume speed, m/s
z = height, m

The right hand side in this equation is related to wind shear, and the minus sign here means that the plume loses momentum by moving up into faster moving air layers.

The momentum balance equation for the vertical direction holds the same principle, but the assumption of zero vertical wind speed is taken, like in Equation 3.1. Hence, the difference between the gravitational and buoyant force is the generator of the vertical momentum change. The fifth differential equation is as follows:

$$\frac{d}{ds}(\rho U_{sc} r^2 w) = g r^2 (\rho_{atm} - \rho)$$ Equation 3.9

Where: g = gravitational acceleration, m/s^2

As with momentum, the enthalpy of the plume is taken relative to the enthalpy of ambient air. Hence, ambient air has zero enthalpy and does not affect the enthalpy of the plume when entrained into the plume. On the other hand, plume rise can have an effect on the enthalpy of the plume if the temperature changes due to plume rise differs from the temperature gradient (or lapse rate) of ambient air. Hence, the energy conservation equation can be written as:

$$\frac{d}{ds}(\rho U_{sc} r^2 (T - T_{atm})) = -\rho w r^2 \frac{d\eta_{atm}}{dz} + \frac{Q}{c_p} r^2$$

Equation 3.10

Where: T = temperature of flare, K

T_{atm} = temperature of ambient air, K

c_p = specific heat of air, kJ/kg K

Q = radiative heat loss per unit volume of the plume, (kJ/m^3)

$\frac{d\eta_{atm}}{dz}$ = lapse rate of ambient potential temperature which can be calculated as below:

$$\frac{d\eta_{atm}}{dz} = \frac{dT_{atm}}{dz} + \frac{g}{c_p}$$

Equation 3.11

Where $\frac{dT_{atm}}{dz}$ is the temperature gradient of ambient air (negative when the temperature declines with increasing height), and $\frac{g}{c_p}$ is the adiabatic lapse rate of a rising plume, i.e. the temperature change of the plume per meter of plume rise in adiabatic conditions. The adiabatic lapse rate is derived from thermodynamic principles in Appendix A.

The specific heat of air is obtained from the following formulation (Sandler, 1999) for the range of 273-2800 kelvin:

$$c_p = 28.088 + 0.197 \cdot 10^{-2} T + 0.48 \cdot 10^{-5} T^2 - 1.965 \cdot T^3$$

Equation 3.12

Where c_p is in *J/mol K*, and T is in *K*.

The last term describes the radiative heat loss from the plume to the ambient air. This term is important only initially when the plume temperature is high, and in the presence of combustion. Q in Equation 3.10 is the radiative heat loss per unit volume of the plume. It can be estimated as:

$$\frac{Q}{c_p} r^2 = -2\varepsilon\sigma r(T^4 - T_{atm}^4)/c_p \qquad \text{Equation 3.13}$$

Where: ε = emissivity of the plume

σ = Stefan-Boltzman constant = $5.76*10^{-11}$ kJ/s m^2 K^4

Schulman et al. (2000) proposed a value of 0.8 for ε for plume rise from large area sources. However, 0.8 is relatively high for small plumes.

Substituting Equations 3.11 and 3.13 into Equation 3.14, the last differential equation is obtained for the energy balance:

$$\frac{d}{ds}(\rho U_{sc} r^2 (T - T_{atm})) = -\rho w r^2 (\frac{dT_{atm}}{dz} + \frac{g}{c_p}) - \frac{2\varepsilon\sigma}{c_p} r(T^4 - T_{atm}^4) \qquad \text{Equation 3.14}$$

The term $(\frac{d}{ds}(\rho U_{sc} r^2 (T - T_{atm})))$ is the enthalpy change. In this equation it is equal to the sum of the heat the plume loses from radiation $(\frac{2\varepsilon\sigma}{c_p} r(T^4 - T_{atm}^4))$ and the change of enthalpy due to changes of the ambient air potential temperature $(\rho w r^2 (\frac{dT_{atm}}{dz} + \frac{g}{c_p}))$ with respect to the height. The lapse rate term which shows the altitude dependence of temperature is discussed in Appendix A.

Hence, we have six independent differential equations and six independent variables. All these differential equations are included in the PRIME plume rise model, and describe plume rise from large area sources like forest fires. To include flare combustion, we need to add some additional differential equations relating to the flare effects as well. De Visscher (2009) added four more ordinary differential equations to be solved along with the original equations to describe flare combustion.

First, De Visscher (2009) assumed complete mixing and instantaneous reaction in the flare. Then he calculated conversion of combustion *X,* by assuming that the amount of oxygen reacted with methane equals the amount of oxygen mixed into the plume:

$$X = \frac{\rho U_{sc} r^2 - (\rho U_{sc} r^2)_{s=0}}{(\rho U_{sc} r^2)_{s=0}} \cdot \frac{m_{O_2}}{n}$$ Equation 3.15

Where: m_{O_2} = mass fraction of oxygen in the air

n = stoichiometric factor, kg oxygen consumed per kg fuel combusted

In Equation 3.15, term $(\rho U_{sc} r^2)_{s=0}$ is the mass flow rate of initial fuel (pure methane) in the stack tip and $(\rho U_{sc} r^2 - (\rho U_{sc} r^2)_{s=0}) m_{O_2}$ relates the mass flow rate of oxygen entering into the plume.

To get a differential equation, the derivative with respect to "*ds*" is taken:

$$\frac{dX}{ds} = \frac{m_{O_2}}{n(\rho U_{sc} r^2)_{s=0}} \cdot \frac{d}{ds}(\rho U_{sc} r^2)$$ Equation 3.16

When the conversion of combustion reaches to 1 (X=1), it means that the entire combustible plume has been burned. In other words, it leads us to the end point of the flame. Therefore, the "*s"* amount related to *"X=1"*, shows the tip of the flare flame.

Solving all these equations yields dimensions of the flare, but these equations result in unrealistically short flames. The reason is the assumption of complete mixing during the plume. Complete mixing assumes that all the oxygen mixed into the plume has been reacted with the fuel and leads to flames that are unrealistically short. Therefore, it is assumed that mixing is incomplete and just part of the air mixed into the plume enters the burning section of the plume. Hence, the flame is subdivided to a burning mass fraction "*f"* and a non-burning mass fraction "*1-f*". Assuming that a constant portion of the air mixed into the plume, "f_{mix}", enters the burning section leads to extra mass and heat balance equations:

$$\frac{d}{ds}(f \rho U_{sc} r^2) = f_{mix} \frac{d}{ds}(\rho U_{sc} r^2)$$ Equation 3.17

$$\frac{d}{ds}(f \rho U_{sc} r^2 (T_f - T_{atm})) = (\rho U_{sc} r^2)_{s=0} \frac{H}{c_p} \frac{dX}{ds} - f(\frac{dT_{atm}}{dz} + \frac{g}{c_p}) \rho w r^2 - \frac{2\varepsilon\sigma}{c_p} f(T_f^4 - T_{atm}^4)$$

Equation 3.18

$$\frac{d}{ds}((1-f) \rho U_{sc} r^2 (T_{air} - T_{atm})) = -(1-f)(\frac{dT_{atm}}{dz} + \frac{g}{c_p}) \rho w r^2$$ Equation 3.19

Where H is the enthalpy of combustion in kJ/mol. Equation 3.18 is the heat balance for the burning section of flame and Equation 3.19 relates to the non-burning part of the flame.

De Visscher (2009) suggested a value of 0.0293 for "f_{mix}" to be concluded in the heat balance equations. This value was based on a model fit to empirical flame length equations.

Therefore, adding Equations 3.16 and 3.17 to the set of independent differential equations and substituting Equation 3.14 by 3.18 and 3.19 leads to nine independent differential equations describing characteristics of the flare.

3.2.1 Emissivity Calculation

Calculating an acceptable value for the emissivity plays an important role in flare modeling since it has a direct effect on the heat balance equations (Equation 3.18 and 3.19). Schulman et al. (2000) suggested a value of 0.8 for the emissivity of large area sources like forest fires. As large area sources are much bigger than flares, this emissivity is much higher than what is expected for flares, thus a different approach is required to obtain the flare emissivity.

Beychok (2005) suggested that 25% of the heat produced by combusted gas is lost by radiation at the end of the visible flame which is a conservative assumption that is not exceeded in practical conditions. Accordingly, to calculate the emissivity, we need to know the type of hydrocarbon burned in the stack and then determine the heating value of the gas. Thus, setting the percentage of heat loss by radiation to the amount of 25%, leads to an appropriate emissivity prediction.

A fraction of radiation heat loss occurs past the flame tip. Hence, it is evaluated at $s = 2\times$"flame length" because radiation is negligible past that point. The heat loss due to radiation is calculated with the following differential equation (De Visscher, 2009):

$$\frac{d(radiation-loss)}{ds} = \frac{2\sigma r}{c_p} \cdot \frac{\varepsilon(T_f^4 - T_{atm}^4)c_p}{(\rho U_{sc} r^2)_{s=0} H} \qquad \text{Equation 3.20}$$

Where: ε= emissivity of flare

H = heat of combustion, J/kg

All the independent differential equations along with independent variables are summarized in Table 3-1.

Table 3-1: Independent differential equations along with their independent variables

#	***Differential Equation***	***Variable***
1	$\frac{d}{ds}(\rho U_{sc} r^2) = (2r\alpha\rho_{atm}\lvert U_{sc} - U_{atm}\cos\phi\rvert) + (2r\beta\rho_{atm}\lvert U_{atm}\sin\phi\rvert)$	$\rho U_{sc} r^2$
2	$\frac{dx}{ds} = \frac{u}{U_{sc}} = \cos\phi$	x
3	$\frac{dz}{ds} = \frac{w}{U_{sc}} = \sin\phi$	z
4	$\frac{d}{ds}(\rho U_{sc} r^2 (u - U_{atm})) = -r^2 \rho w \frac{dU_{atm}}{dz}$	$\rho U_{sc} r^2 (u - U_{atm})$
5	$\frac{d}{ds}(\rho U_{sc} r^2 w) = g r^2 (\rho_{atm} - \rho)$	$\rho U_{sc} r^2 w$
6	$\frac{dX}{ds} = \frac{m_{O_2}}{n(\rho U_{sc} r^2)_{s=0}} * \frac{d}{ds}(\rho U_{sc} r^2)$	X
7	$\frac{d}{ds}(f\rho U_{sc} r^2) = f_{mix} \frac{d}{ds}(\rho U_{sc} r^2)$	$f\rho U_{sc} r^2$
8	$\frac{d}{ds}(f\rho U_{sc} r^2 (T_f - T_{atm})) = (\rho U_{sc} r^2)_{s=0} \frac{H}{c_p} \frac{dX}{ds}$ $- f(\frac{dT_{atm}}{dz} + \frac{g}{c_p})\rho w r^2 - \frac{2\varepsilon\sigma}{c_p} f(T_f^4 - T_{atm}^4)$	$f\rho U_{sc} r^2 (T_f - T_{atm})$
9	$\frac{d}{ds}((1-f)\rho U_{sc} r^2 (T_{air} - T_{atm})) = -(1-f)(\frac{dT_{atm}}{dz} + \frac{g}{c_p})\rho w r^2$	$(1-f)\rho U_{sc} r^2 (T_{air} - T_{atm})$
10	$\frac{d(radiation-loss)}{ds} = \frac{2\sigma r}{c_p} \cdot \frac{\varepsilon(T_f^4 - T_{atm}^4) c_p}{(\rho U_{sc} r^2)_{s=0} H}$	Radiation-loss

3.3 Results and Discussion

To calculate the dimensions of the flame, all the independent differential equations in Table 3-1 are solved in MATLAB. Based on initial conditions of the stack and meteorological situations,

the results change. Hence, to compare the results with observational data collected in the field, we need to set some parameters to correspond to the observational tests conditions. The parameters which are influenced by the stack and meteorological conditions include:

1- Heating value of fuel (kJ/kg fuel)
2- Heat of combustion (Watt)
3- Stoichiometric factor (in the study of pure methane its value equals 4)
4- Gas exit velocity (m/s)
5- Wind speed (m/s)
6- Atmosphere temperature (K)
7- Gas temperature (K)
8- Atmospheric entrainment parameters (m)

Along with all these parameters, it is assumed that the atmosphere is adiabatic ($\frac{dT_{atm}}{dz} = -\frac{g}{c_p}$) with a ground-level temperature of 15°C.

Leahey et al. (1987) collected some observed data of flame length and orientation of a flare, which is shown in Table 3-2 and 3-3. So, to compare these field data with modeling results we need to set all the stack influencing factors and ambient wind speed in the modeling codes as Table 3-2.

Table 3-2: Flare stack parameters for indicated test time (Leahey et al., 1987)

Test	***Time (MST)***	***Acid Gas (m^3h^{-1})***	***Fuel Gas (m^3h^{-1})***	***Molecular Weight ($g\ mol^{-1}$)***	***Flame Temperature (K)***	***Heat Content ($MJ\ m^{-3}$)***	***Exit Speed ($m\ s^{-1}$)***	***Wind Speed ($m\ s^{-1}$)***
March 7								
1	20:02-20:04	124	77	34.3	1353	17.6	7.6	1.3
2	20:16-20:18	126	60	35.6	1323	15.5	7.1	1.4
3	20:33-20:34	122	38	37.4	1213	12.5	6.1	1.4
March 8								
4	21:50-21:51	131	92	33.6	1273	18.6	8.5	2.8
5	21:56-21:57	124	49	36.5	1103	14.0	6.7	3.2

6	22:07-22:08	122	28	38.5	1073	10.7	5.8	3.0
7	22:25-22:26	122	0	42.8	673	4.1	4.6	3.2
8	22:33-22:34	122	16	38.1	823	8.1	5.3	2.8

Table 3-3: Observed values of hf/D and angle (Leahey et al., 1987)

Test	***hf/D***	α_B
1	10±3	54±6
2	10±2	51±8
3	8±1	53±5
4	9±3	64±10
5	4±0	73±2
6	4±2	72±10
7	2±1	68±12
8	2±2	70±11

Leahey et al. (1987) compared two flare variables: height of the flare divided by diameter of the stack (h_f / D) and angle of the flare to the vertical (α_B).

To run the model based on these input parameters, it is necessary to calculate the appropriate value for f_{mix}. Choosing proper value for f_{mix} is of prime importance for this part of study, since a small change in f_{mix} value leads to significant errors in calculating the flame characteristics.

For the first step f_{mix} is set for each data point to meet the results in Table 3-3. Hence, running the model for the initial conditions of observational data leads to the results offered in Table 3-4.

Table 3-4: Predicted values of hf/D and angle

		h_f/D		α_B (degree)	
Test	f_{mix}	***observed***	***predicted***	***observed***	***Predicted***
1	0.06	10±3	10.18	54±6	32
2	0.085	10±2	10.25	51±8	37

3	0.13	8±1	8	53±5	38
4	0.065	9±3	8.9	64±10	60
5	0.33	4±0	4	73±2	68
6	0.25	4±2	4	72±10	62
7	0.9	2±1	3	68±12	68
8	0.55	2±2	3	70±11	68

Table 3-4 shows the observed and predicted values for the height and angle of the flare. It shows that the theory tended to underestimate α_B and in some tests overestimated the height of the flare. This is related to the values of the entrainment factors. As discussed before in the model development section, α and β are the empirical parameters describing entrainment of the air into the plume corresponding to the difference of wind and plume speed in both directions. Scire et al. (2000) suggested a value of 0.11 and 0.6 for α and β, respectively, for area source plume rise. Subsequently, using an entrainment factor for large area sources in a model for industrial stack plumes, which are relatively small sources, has led to inaccuracies.

Since area sources, such as forest fires, are very large, the entrainment of some amount of ambient air into that huge volume has less influence on plume rise than the entrainment of ambient air into the relatively small and narrow industrial stack plume. In other words, on account of the fact that the proportion of "volume of ambient air entering into the plume" to the "initial volume of the plume" for the large area source is less than the industrial stack, ambient air entering the plume has more influence on the industrial stack plume rise than on large area source plume rise. Hence, the entrainment rate of atmospheric air into the industrial stack plume needs to be modified in this study.

Leahey et al. (1987) defined entrainment factor β as:

$$\beta = \beta_0 \left(\frac{\rho}{\rho_0}\right)^{1/2} \qquad \text{Equation 3.21}$$

Where: β_0=entrainment factor for a jet of density ρ_0, m

ρ_0=density of surrounding air, kg/m^3

ρ=density of a jet, kg/m^3

Which, according to Briggs (1975):

$$\beta_0 = 0.4 + 1.2\frac{U_{atm}}{U_{sc}} \qquad \text{Equation 3.22}$$

However, Briggs did not offer any formulation for the factor defining entrainment of atmospheric air parallel to the plume trajectory (α). Using Equation 3.22 instead of a constant value of β=0.6 did not improve the agreement between the model and the data.

It is assumed that the proportion of α/β of a large area source is the same as for a flare. In view of the fact that Leahey (1987) neglected the effect of α in the flare trajectory, we just manipulate the amount of α and β suggested by Scire et al. (2000) to fit the observed data. A correction factor of 1.6 provided the best agreement with the measurement data. Hence, the modified entrainment factors are:

α_{new}= *1.6* α

β_{new}= *1.6* β

Considering the new values for entrainment factors, predictions from the model are compared with the observed data collected in the field in Table 3-5.

Table 3-5: Observed and predicted values of hf/D and angle (including modified entrainment factors: α and β)

		h_f/D		***α_B (degree)***	
Test	f_{mix}	***observed***	***Predicted***	***Observed***	***Predicted***
1	0.07	10±3	10.9	54±6	45
2	0.085	10±2	10.1	51±8	49
3	0.13	8±1	8.39	53±5	51
4	0.065	9±3	7.54	64±10	68
5	0.33	4±0	3.36	73±2	75
6	0.25	4±2	4.26	72±10	70.1
7	0.9	2±1	2.1	68±12	70.1
8	0.55	2±2	2.7	70±11	65

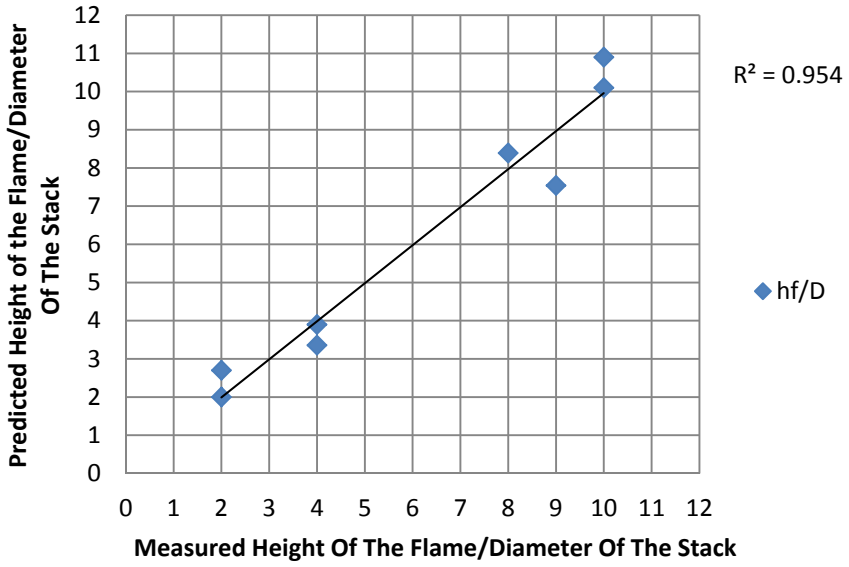

Figure 3-2: Observed and predicted values of hf/D (including modified entrainment factors)

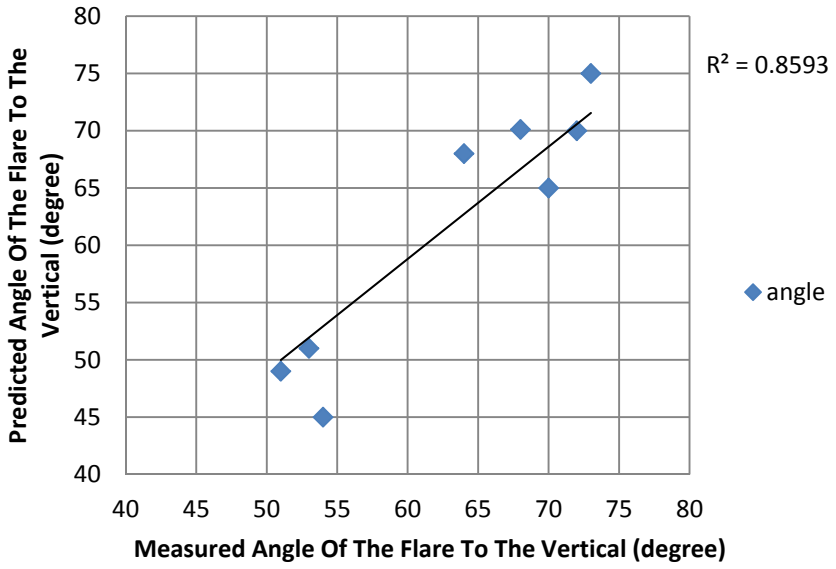

Figure 3-3: Observed and predicted angel of the flare to the vertical (including modified entrainment factors)

Values of observed h_f/D and α_B were compared to the predicted values in Figures 3-2 and 3-3. Predicted and observed values for each of the tests are also shown in Table 3-5. However, the results from test 4 seem to deviate from other results. Even in the model which is offered by the original study of Leahey et al. (1987) there is a considerable error for predicting the flare height

and angle regarding this test. It may be the result of of some inaccuracies in the measurements for this test. It is observed that the coefficient of determination (R^2) for Figure 3-2 would increase up to 0.983 (R^2=0.983) and for Figure 3-3 up to 0.881 (R^2=0.881) if the result of test 4 were omitted from the data set.

3.3.1 f_{mix} Calculation

In general, wind speed and stack exit speed are the main parameters influencing f_{mix}. To study their effects, Figure 3-4 is shown. Note that for the sake of simplicity, the proportion of the wind to stack exit speed is shown in this figure.

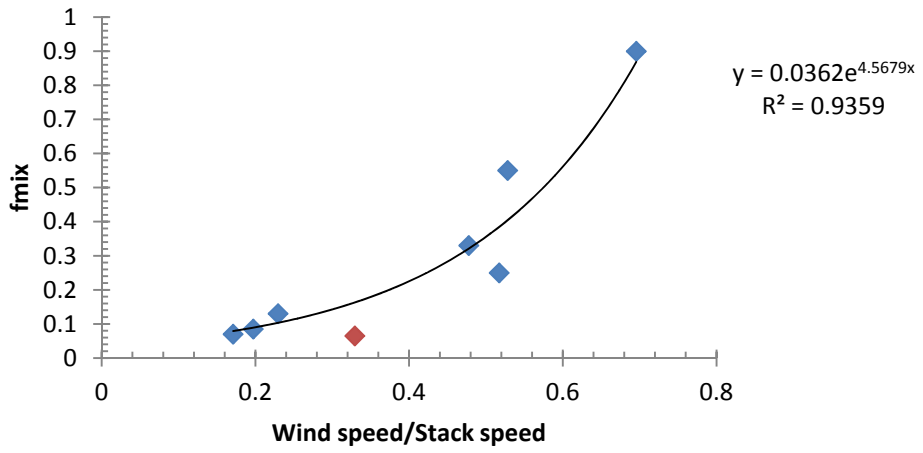

Figure 3-4: f_{mix} vs. proportion of the wind speed to the stack exit velocity

As shown in Figure 3-4, f_{mix} is directly correlated with the proportion of the atmosphere wind speed to the stack exit speed ($\frac{U_{atm}}{(U_{sc})_{s=0}}$). The bigger the proportion of the wind to the stack exit speed, the bigger f_{mix}. To model f_{mix}, different-structured equations were fitted to the experimental data shown in Figure 3-4 by regression to obtain the best equation for each structure. After comparing all the equations, the following exponential equation is found to yield the most accurate results:

$$f_{mix} = 0.0362 \exp(4.5679 \frac{U_{atm}}{(U_{sc})_{s=0}})$$

Height and angle of the flare are predicted using this proposed equation, and the results are given in Table 3-6 and Figures 3-5 and 3-6.

Table 3-6: Observed and predicted values of hf/D and angle (including modified entrainment factors: α and β, and formulated f_{mix})

		hf/D		***αB (degree)***	
Test	f_{mix}	***observed***	***Predicted***	***Observed***	***Predicted***
1	0.0791	10±3	10.1	54±6	44
2	0.0911	10±2	9.8	51±8	49
3	0.1054	8±1	9.7	53±5	53
4	0.1653	9±3	3.9	64±10	60
5	0.3208	4±0	3.4	73±2	75
6	0.3851	4±2	2.8	72±10	66
7	0.86	2±1	2.1	68±12	71
8	0.4048	2±2	3.4	70±11	68

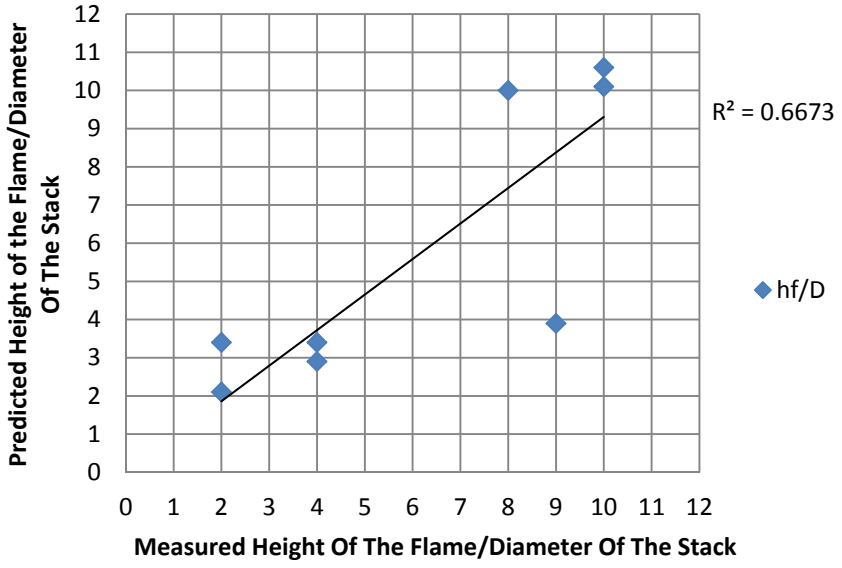

Figure 3-5: Observed and predicted values of hf/D (including modified entrainment factors and formulated f_{mix})

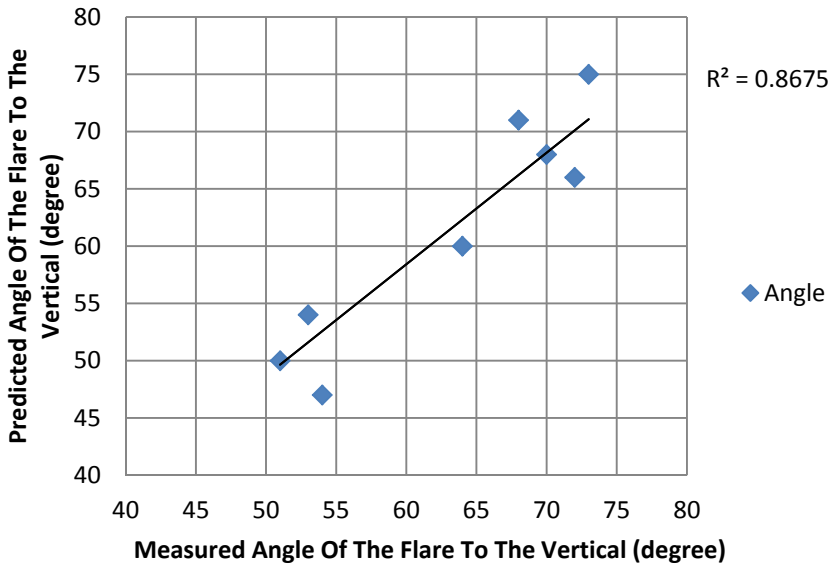

Figure 3-6: Observed and predicted values of angel of the flare to the vertical (including modified entrainment factors and formulated f_{mix})

As mentioned before, test 4 in this set of observed data seems to deviate from other observation results. Ignoring the results of test 4 leads to the following comparison between predicted and observed values in Figures 3-7 and 3-8.

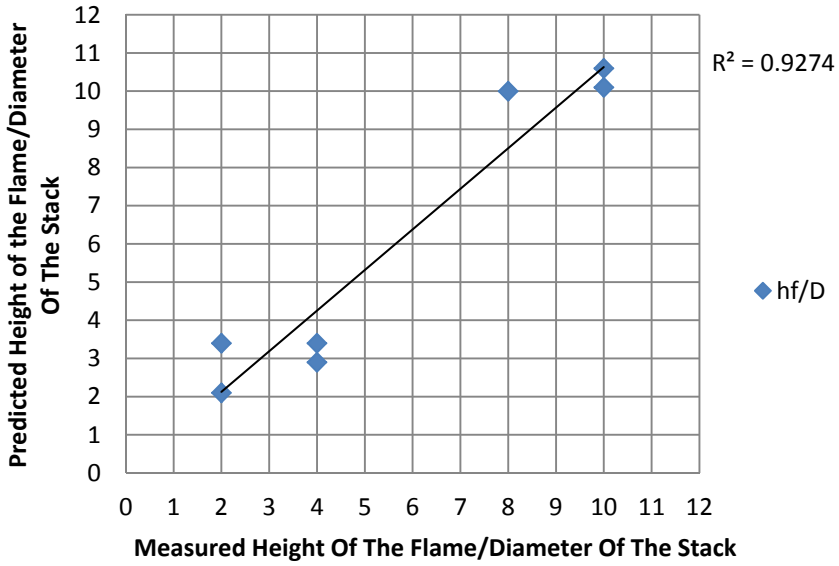

Figure 3-7: Observed and predicted values of hf/D (including modified entrainment factors and formulated f_{mix})

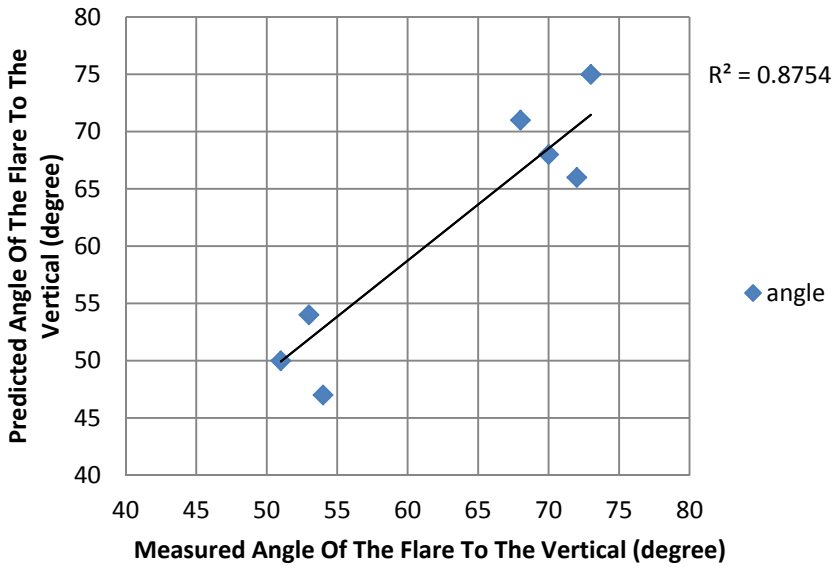

Figure 3-8: Observed and predicted values of angel of the flare to the vertical (including modified entrainment factors and formulated f_{mix})

According to Table 3-6 almost all the predicted values are within the confidence interval of the observed data except for test 4, where the model underestimates the height of the flare. Although the results from the field flare are based on a small number of observations, the agreement between the predicted and observed values verifies the accuracy of the model.

3.3.2 Basic Model Results

In the next chapter, some improvements are made to the model to include the rate of reaction, and then the new version of model is compared to this basic version. Thus, we need to run a sample calculation for an acceptable set of input data in both versions to be able to compare the results. For this set of calculations is it assumed that the combustion gas is methane (H=50000 kJ/kg, n=4), and the atmosphere is expected to be adiabatic ($\frac{dT_{atm}}{dz} = -\frac{g}{c_p}$) with a lapse rate of -0.00975 and ground level temperature of 15°C. All the other input data are shown in Table 3-7.

Table 3-7: Model conditions and parameters

Parameter	***Amount***	***Description***
U_{atm}	2	Wind speed (m/s)

T_{atm}	288	Temperature of atmosphere (K)
P_{atm}	101325	Pressure of atmosphere (Pa)
M_{gas}	0.016	Molar mass of flared gas (kg/mol)
T_{gas}	288	Initial temperature of flared gas (K)
D_{stack}	0.100695	Diameter of stack (m)
H_{stack}	20	Height of stack (m)
Q_c	10000	Heating value of fuel (kJ/s)
f_{mix}	0.0293	Burning mass fraction of plume

Running the codes for the above input data leads to the following results:

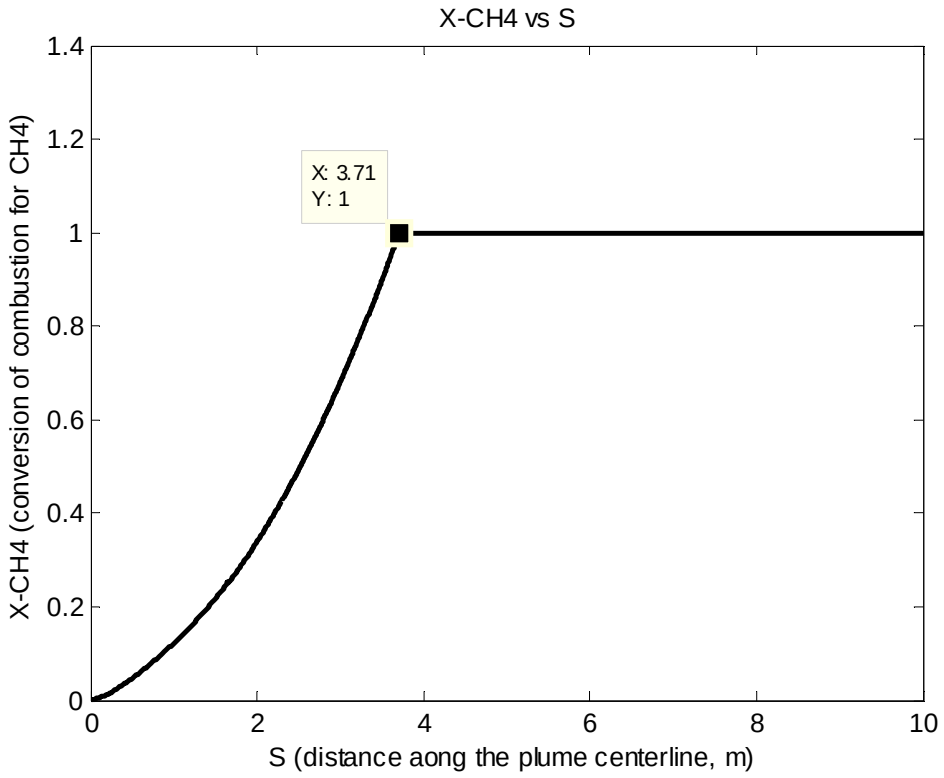

Figure 3-9: CH_4 conversion of combustion according to the initial condition of Table 3-7, basic model

The flare tip is the point where all the combustible gases, in this case pure methane, are burned. Based on Equations 3.15 and 3.16, the conversion of the combustion, *X*, is equal to 1 where there is no more combustible gas to be burned and after this point does not change. Hence, the

conversion of combustion can be used to determine the end point of the flame. As pointed out in Figure 3-9, the flame tip for the initial conditions given in Table 3-7 is at s=3.71 m. It means the flame length is equal to L_f=3.71 m. The height of the flare is calculated by solving Equation 3.6 for the flare tip length (s=3.71). The flare height calculation yields h_f=2.54 m.

To fulfill the assumption made in Table 3-7 of 25% radiation heat loss, different values of "ε" are substituted in Equation 3.20. The heat loss is calculated for each. The values "ε" which leads to 25% heat loss by radiation is calculated by trial and error, which yields ε=0.012. Based on this value for emissivity, the temperature profile in the flare and the subsequent plume trajectory is shown in Figure 3-10.

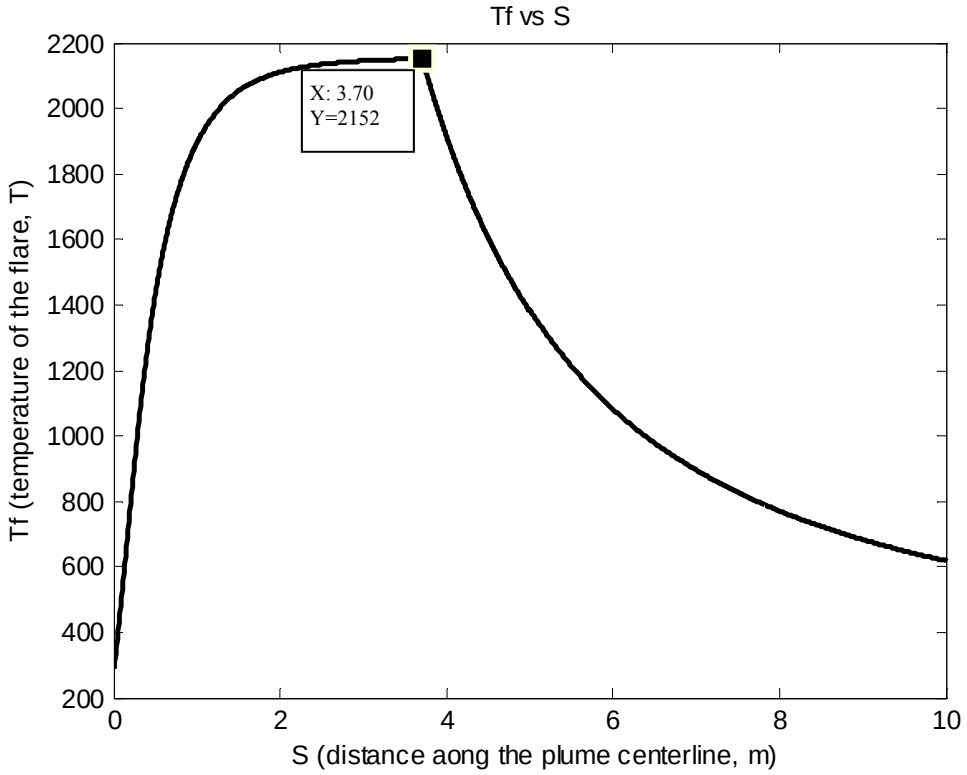

Figure 3-10: Temperature profile according to the initial condition of Table 3-7, basic model

The hottest point in the flare is just 1 centimeter before the flare tip at s=3.70 m. This temperature for the initial conditions of Table 3-7 is 2152 K. Right after this point, the temperature starts decreasing since all the combustible material has been burned. Entraining

fresh ambient air into the plume with low temperature (T_{atm}=298 K), along with lack of any burning gas accelerates this process.

In the next chapter, these results will be compared with the improved version of the model for the same initial meteorological and stack parameters to investigate the benefits of each model.

Chapter Four: **Improved Model**

4.1 Introduction

In the previous chapter, the flare model of De Visscher (2009) was improved by including a temperature dependent value of c_p, and by developing a relationship for f_{mix} that leads to an accurate fit between the model and the measured flame lengths. The purpose of the current chapter is to incorporate two further improvements to the model. The first improvement is considering the rate of reaction in the combustion of gases. The second one is to better calculate the energy which is emitted by radiation in the plume trajectory. The model developed in Chapter 3 assumed instantaneous reaction of combustion. Radiation energy calculation was also considered in a straightforward way by assuming that 25% of heat released from combustion is emitted by the radiation. According to these two assumptions (instantaneous reaction and 25% radiation energy loss) a basic, fast, and dependable model has been developed.

In the current chapter, the rate of reaction for oxidation of methane will be considered and then emissivity of the flare will be calculated more explicitly.

4.2 Model Development

4.2.1 Rate of Reaction Calculation

As discussed in the previous chapter, a methane flare is modeled. In the previous chapter we considered only one reaction as:

$$CH_4 + 2O_2 \longrightarrow CO_2 + 2H_2O \qquad \text{Reaction 4.1}$$

The reaction was assumed to be instantaneous. In reality, it is more accurate to describe the combustion of methane as two main reactions:

$$CH_4 + 1.5O_2 \xrightarrow{k_1} CO + 2H_2O \qquad \text{Reaction 4.2}$$

$$CO + 0.5O_2 \xrightarrow{k_2} CO_2 \qquad \text{Reaction 4.3}$$

Neither of these reactions is really instantaneous. The reaction rates r_1 and r_2 for Reactions 4.2 and 4.3, respectively, are (Cooper and Alley, 2011):

$$r_1 = r_{CH_4} = k_1[CH_4][O_2] \quad \text{Equation 4.1}$$

$$r_2 = r_{CO_2} = k_2[CO][O_2]^{0.5} \quad \text{Equation 4.2}$$

Where: [*i*] indicates concentration of species i, mol/cm^3

k_1 = rate constant of combustion of Reaction 4.2, cm^3/(mol.s)

k_2 = rate constant of combustion of Reaction 4.3, (1/s)(cm^3/mol)$^{0.5}$

r_{CH_4} = the rate of Reaction 4.2, mol/(cm^3.s)

r_{CO_2} = the rate of Reaction 4.3, mol/(cm^3.s)

As a first step in the development of the model, the combustion was assumed to occur in one step, as in Reaction 4.1, but with the reaction kinetics of Equation 4.1. In a second step, both reactions were considered.

The differential equations which describe combustion in the basic model are Equations 3.15 and 3.16 discussed in Chapter 3. We calculated these equations considering an instantaneous reaction of methane. These equations can no longer be used in the revised version of the model. To consider the rate of reaction of combustion, r_1 and r_2, we need to calculate the amount of conversion of combustion for methane (X_{CH_4}) and for carbon dioxide (X_{CO_2}) in Reactions 4.2 and 4.3. These reactions include conversion of fuel to carbon monoxide and then conversion of carbon monoxide to carbon dioxide.

To include the rates of reaction in the model, we have to express the conversion of combustion as a function of the rate of reaction, in contrast with Chapter 3 where the conversion of combustion was calculated assuming instantaneously reaction. To include the rate of reaction, it is necessary to calculate molar and mass flow rate of every single species in the reactions.

In a first step, for the calculation of the methane conversion, it was assumed that the methane is burned in just one reaction (Reaction 4.1) with reaction kinetics. Mole and mass flow rate formulations should be presented as functions of the independent variables of the differential equations presented in Table 3-1 to be included in the differential equations and solved.

All the mass flow calculations are based on the mass stoichiometric balance of combustion of methane, as follows:

$$CH_4 + 4O_2 \longrightarrow 2.75CO_2 + 2.25H_2O$$ Reaction 4.4

$$y_{CH_4} = (\rho U_{sc} r^2)_{s=0}(1 - X_{CH_4})$$ Equation 4.3a

$$y_{CO_2} = 2.75(\rho U_{sc} r^2)_{s=0} X_{CH_4}$$ Equation 4.3b

$$y_{H_2O} = 2.25(\rho U_{sc} r^2)_{s=0} X_{CH_4}$$ Equation 4.3c

$$y_{O_2} = [f\rho U_{sc} r^2 - (\rho U_{sc} r^2)_{s=0}]m_{O_2} - 4(\rho U_{sc} r^2)_{s=0} X_{CH_4}$$ Equation 4.3d

$$y_{N_2} = [f\rho U_{sc} r^2 - (\rho U_{sc} r^2)_{s=0}](1 - m_{O_2})$$ Equation 4.3e

Where: y_i = mass flow rate of species "i", divided by π, kg/s
m_{O_2} = mass fraction of oxygen in the air

And from the above equations the molar flow rate of each species can be calculated as:

$$y^m_{CH_4} = \frac{y_{CH_4}}{0.016}$$ Equation 4.4a

$$y^m_{CO_2} = \frac{y_{CO_2}}{0.044}$$ Equation 4.4b

$$y^m_{H_2O} = \frac{y_{H_2O}}{0.018}$$ Equation 4.4c

$$y^m_{O_2} = \frac{y_{O_2}}{0.032}$$ Equation 4.4d

$$y^m_{N_2} = \frac{y_{N_2}}{0.028}$$ Equation 4.4e

Where: y_i^m = molar flow rate of species "i", divided by π, mol/s

A methane material balance equation is derived for the flame. It describes the molar flow rate of methane as a function of the rate of reaction. Figure 4-1 shows a schematic of the material balance for methane in the path length of plume center line. As mentioned before, for the sake of simplicity area is divided by π.

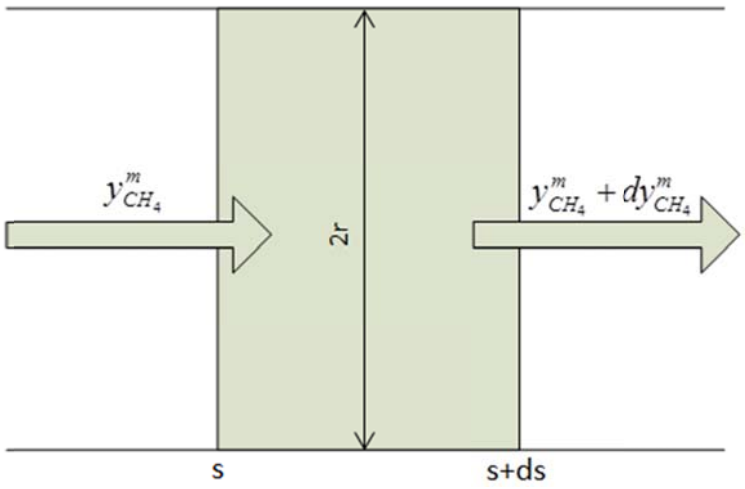

Figure 4-1: Flame material balance

$$area = r^2$$

$$volume = r^2 ds$$

$$dy^m_{CH_4} = r^2 ds(-r_{CH_4}) \qquad \text{Equation 4.5}$$

Where: r = radius of the plume, m

$y^m_{CH_4}$ = molar flow rate of methane, divided by π, mol/s

Rearranging Equation 4.5 yields:

$$\frac{dy^m_{CH_4}}{ds} = -r^2 r_{CH_4} \qquad \text{Equation 4.6}$$

Equations 4.3a and 4.4a can be combined into the above equation. Hence:

$$\frac{dy_{CH_4}}{ds} = -0.016 r^2 r_{CH_4} \qquad \text{Equation 4.7}$$

$$\frac{dy_{CH_4}}{ds} = \frac{d}{ds}[(\rho U_{sc} r^2)_{s=0}(1 - X_{CH_4})] = -(\rho U_{sc} r^2)_{s=0} \frac{dX_{CH_4}}{ds} \qquad \text{Equation 4.8}$$

Where: y_{CH_4} = mass flow rate of methane, divided by π, kg/s

Finally combining Equation 4.7 and 4.8 leads to:

$$\frac{dX_{CH_4}}{ds} = \frac{0.016 r^2 r_{CH_4}}{(\rho U_{sc} r^2)_{s=0}}$$ Equation 4.9

Equation 4.9 describes the conversion of the combustion of methane as a function of rate of reaction based on Reaction 4.1.

The full model incorporating the two combustion reactions requires both conversions X_{CH_4} and X_{CO_2}. The procedure for calculating X_{CO_2} is similar to the calculation of X_{CH_4}, but based on Reaction 4.3.

$$\frac{dX_{CO_2}}{ds} = \frac{0.016 r^2 r_{CO_2}}{(\rho U_{sc} r^2)_{s=0}}$$ Equation 4.10

This equation defines the conversion of combustion to CO_2. Hence, Equation 3.16 in the previous version of the model is replaced by Equations 4.9 and 4.10 in the new version of the model.

As with Reaction 4.4, the mass stoichiometric balance can be given by:

$$CH_4 + 3O_2 \longrightarrow 1.75CO + 2.25H_2O$$ Reaction 4.5

$$1.75CO + O_2 \longrightarrow 2.75CO_2$$ Reaction 4.6

According to the above mass stoichiometric reaction balances, the mole and mass flow rate of carbon monoxide can be obtained as:

$$y_{CO} = 1.75(\rho U_{sc} r^2)_{s=0}(X_{CH_4} - X_{CO_2})$$ Equation 4.11

$$y_{CO}^m = \frac{y_{CO}}{0.028}$$ Equation 4.12

Now we need to calculate the rate of reaction for CH_4 (r_{CH_4}) and CO_2 (r_{CO_2}) and then include them into the differential equations expressing the flare model.

Cooper et al. (1982) proposed a method for predicting an effective first-order rate constant "*k*" for hydrocarbon incineration. They combined collision theory with empirical data to suggest a

model which depends on the molecular weight and type of hydrocarbon. Based on their model the Arrhenius equation can describe the rate constant "*k*" as:

$$k = Ae^{-E/RT} \qquad \text{Equation 4.13}$$

Where: E = activation energy, cal/mol
A = pre-exponential factor, s^{-1}
R = ideal gas constant, 1.987 cal/mol-K
T = absolute temperature, K

The pre-exponential factor was given by:

$$A = \frac{Z' S y_{O_2} P}{R'} \qquad \text{Equation 4.14}$$

Where: Z' =collision rate factor
S = steric factor
y_{O_2} = mole fraction of oxygen
P = absolute pressure, atm
R' = gas constant, 0.08206 L-atm/mol-K

The collision rate factor is obtained from Figure 11-5 in Cooper and Alley (2011). A value of 1.011×10^{11} is obtained for methane.

The steric factor "*S*" (a factor to account for the effect of molecular geometry) can be calculated as (Cooper and Alley, 2011):

$$S = \frac{16}{MW} \qquad \text{Equation 4.15}$$

Where: MW = molar weight of hydrocarbon, g/mol

And the activation energy can be correlated with molar weight as:

$$E = -0.00966(MW) + 46.1 \qquad \text{Equation 4.16}$$

Once A and E have been estimated, k can be calculated from Equation 4.13 for a desired temperature in the plume, and then the rate constant of Equation 4.13 *considering first-order kinetics* for CH_4 can be given by:

$$k = \frac{Z' S y_{O_2} P}{R'} e^{-E/RT} \qquad \text{Equation 4.17}$$

Equation 4.17 defines the reaction rate constant considering first-order rate for CH_4. It means that the value of the reaction rate constant to be substituted in Equation 4.1, k_1, can be given by:

$$k_1 = \frac{Z' SP}{R'} e^{-E/RT} \qquad \text{Equation 4.18}$$

Provided that the mole fraction is used for $[O_2]$ in Equation 4.1, the rate of destruction of hydrocarbons to CO_2 depends on to the rate of destruction of CO. In some cases, the rate of destruction of CO is low enough to control the rate of overall reaction. The kinetics of CO oxidation has been studied by several researchers (Dryer and Glassman, 1973; Howard et al., 1973; Williams et al., 1969). Howard et al. (1973) published the following equation expressing the CO oxidation rate based on many experimental studies. This expression is valid over a wide range of temperatures (840-2360 K):

$$r_{CO} = 1.3e^{-30000/RT}[O_2]^{1/2}[H_2O]^{1/2}[CO] \qquad \text{Equation 4.19}$$

Where: $[H_2O]$, $[O_2]$, and $[CO]$ = concentration of H_2O, O_2, and CO, mol/cm^3

Compare to Equation 4.2:

$$k_2 = 1.3e^{-30000/RT}[H_2O]^{1/2} \qquad \text{Equation 4.20}$$

Therefore Equations 4.1 and 4.2 can be rewritten as:

$$r_{CH_4} = \frac{Z' Sy_{O_2} P}{R'} e^{-E/RT}[CH_4] \qquad \text{Equation 4.21}$$

$$r_{CO} = 1.3e^{-30000/RT}[O_2]^{1/2}[H_2O]^{1/2}[CO] \qquad \text{Equation 4.22}$$

The concentration terms can be expressed using independent variables in the Table 3-1 as:

$$[CH_4] = \frac{y^m_{CH_4}}{\sum y^m_i} \frac{P_{atm}}{RT_f} \qquad \text{Equation 4.23}$$

$$[CO] = \frac{y^m_{CO}}{\sum y^m_i} \frac{P_{atm}}{RT_f} \qquad \text{Equation 4.24}$$

Where $\sum y^m_i$ is the sum of the flow rates of all components.

The oxygen concentration is calculated with a pseudo-steady state approximation. It is assumed that the oxygen consumed in the reactions equals the oxygen provided by entrainment of air into the burning section of the flame.

$$[O_2] = [\frac{(-0.03 \cdot 20.5k_2[CO]) + \sqrt{(0.032 \cdot 0.5k_2[CO])^2 + 4 \cdot 0.032 \cdot 1.5k_1[CH_4]\frac{d(f\rho U_{sc}r^2)}{ds}\frac{m_{O_2}}{r^2}}}{2 \cdot 0.032 \cdot 1.5k_1[CH_4]}]^2$$

Equation 4.25

Combining the above four equations leads to:

$$\frac{dX_{CH_4}}{ds} = \frac{0.016r^2}{(\rho U_{sc}r^2)_{s=0}}\frac{Z'Sy_{O_2}P}{R'}e^{-E/RT}[CH_4]$$ Equation 4.26

$$\frac{dX_{CO}}{ds} = \frac{0.016r^2}{(\rho U_{sc}r^2)_{s=0}}1.3 * e^{-30000/RT}[O_2]^{1/2}[H_2O]^{1/2}[CO]$$ Equation 4.27

These are the final differential equations describing the rate of reaction. These equations substitute Equation 3.16 in Chapter 3, which was considered for an instantaneous reaction. They are responsible for the effects of the rate of reaction of CH_4 and CO in the model.

4.2.2 Emissivity Calculation

The emissivity of a material is its relative ability of emitting energy by radiation. It is equal to the ratio of energy radiated by the material to energy radiated by a black body at the same temperature. So a true black body has an emissivity value equal to 1. A blackbody is a hypothetical object that absorbs all radiation that falls on it. Emissivity depends on some factors including: temperature, emission angle, and wavelength.

Beychok (2005) assumed that 25% of the heat produced in flares is emitted by radiation. In the previous chapter, the emissivity was manipulated to meet this assumption. A value of ε=0.012 was found. Since radiation energy depends on various factors such as gas composition of the plume, concentration of soot in the plume, the temperature and the pressure, this is a rough

assumption and could be improved. Therefore, this section offers a method to calculate emissivity in a more explicit way.

In flare flames and their plumes, the main components are gas-phase species and small amounts of soot aggregates. They are diluted with the ambient air. At the flare and plume temperature the main components in the gas phase are transparent at visible wavelength. Light absorptivity and emissivity is then influenced just by soot and other aerosols present in the flame (Johnson et al., 2010). The contribution of the combustion process itself to the radiation emitted, which is called chemiluminescence, is relatively negligible (Perry and Green, 1984).

In methane flares, a large amount of water vapor is produced, but at the flare temperature no condensation of water vapor is expected (Johnson et al., 2010). Hence, water vapor, carbon dioxide, and soot are the constituents in the gas phase for the methane flare gas. Carbon monoxide does not absorb light to a significant extent. Some secondary particles in the form of sulfate and nitrate aerosols may transfer into the atmosphere due to the flaring of gas-phase sulfur dioxide and oxides of nitrogen (Hewitt, 2001). They will not be considered here.

Therefore, soot, water vapor, and carbon dioxide are the three main substances which are present in the plume of a methane flare. In the following three sections, emissivities of these substances are calculated separately and then total emissivity is obtained from the sum of each individual species' optical density.

4.2.3 Soot Emissivity Calculation

Soot emits a continuous spectrum in the infrared and visible regions. The existence of soot in the flame can often double or triple the radiation emitted by only the gaseous products (Siegel and Howel, 2002). Calculating the effects of soot in the flare radiation requires knowledge of the soot concentration and its distribution in the flame. The formulation derivation in this section is based on monochromatic light, and as a simplification assumption for the purpose of the model, it is assumed that this formulation applies to polychromatic light as well.

Kirchhoff's Law: Kirchhoff's law offers an important relation between absorptivity and emissivity for monochromatic light. Based on this law:

$$\alpha_\lambda = \varepsilon_\lambda \qquad \text{Equation 4.28}$$

Where: α_λ = fraction of incident radiation absorbed at wavelength λ
ε_λ = emissivity at wavelength λ

Beer–Lambert Law: consider monochromatic radiation of wavelength λ and initial intensity $I_{\lambda 0}$, which is incident on a layer of absorbing gas of thickness L. As radiation passes through the medium (Figure 4-2), its intensity reduces by absorption and scattering. The reduction in the intensity has been found proportional to the intensity of the beam, the thickness of the absorbing gas layer, and the concentration of absorbing molecules (Jones, 2000).

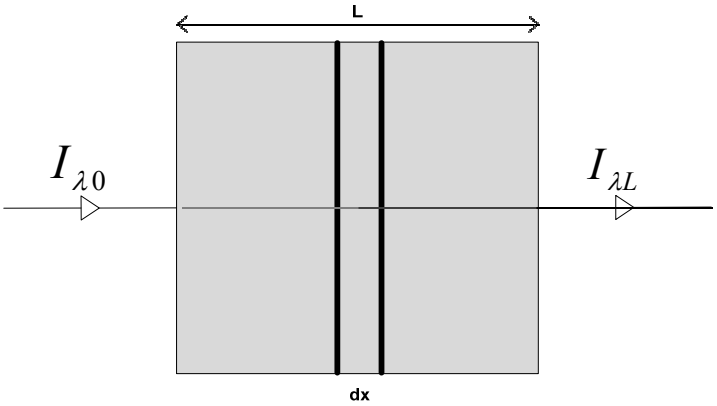

Figure 4-2: Schematic of beam passing through a layer of absorbing

Assume that that the beam intensity changes by dI_λ as it passes through an element of medium of thickness "*dx*", and a coefficient of proportionality K_λ is introduced that depends on the local properties of the medium, the light intensity decreases as:

$$dI_\lambda = -K_\lambda I_\lambda dx \qquad \text{Equation 4.29}$$

Where: K_λ = spectral extinction coefficient of material, m^{-1}

I_λ = radiation intensity, Watt

Since K_λ can be assumed to be independent of "*x*", the integration of Equation 4.29 over the length of the gas layer is given by:

$$\int_{I_{\lambda 0}}^{I_{\lambda L}} \frac{dI_\lambda}{I_\lambda} = -\int_0^L K_\lambda dx$$

Hence:

$$\frac{I_{\lambda L}}{I_{\lambda 0}} = \exp(-K_\lambda L) \qquad \text{Equation 4.30}$$

Equation 4.30 is known as Beer–Lambert law and predicts the intensity attenuation as light passes through a medium with absorbing and scattering effects.

The extinction coefficient is a function of temperature T, pressure P, concentration C_i of component i, and wavelength of incident radiation ($K_\lambda = K_\lambda(\lambda, T, P, C_i)$). It consists of two parts, the absorption coefficient a_λ and the scattering coefficient σ_λ:

$$K_\lambda(\lambda, T, P, C_i) = a_\lambda(\lambda, T, P, C_i) + \sigma_\lambda(\lambda, T, P, C_i) \qquad \text{Equation 4.31}$$

For small soot particles, such as soot produced in the methane flare, Mie theory (Siegel and Howel, 2002) suggests that the scattering cross section depends on $(\pi D / \lambda)^4$ while absorption cross section corresponds to $(\pi D / \lambda)$ with D the diameter of the particle. Hence, in this study, the scattering factor is negligible compare to the absorption cross section. Therefore, Equation 4.31 can be simplified to:

$$K_\lambda(\lambda, T, P, C_i) = a_\lambda(\lambda, T, P) \qquad \text{Equation 4.32}$$

The term $\frac{I_{\lambda L}}{I_{\lambda 0}}$ indicates the fraction of incident radiation of wavelength λ which is transmitted through the gas:

$$\frac{I_{\lambda L}}{I_{\lambda 0}} = \tau_\lambda = \exp(-a_\lambda L) \qquad \text{Equation 4.33}$$

Assuming negligible scattering, the monochromatic absorptivity is given by:

$$\alpha_\lambda = 1 - \tau_\lambda = 1 - \exp(-a_\lambda L) \qquad \text{Equation 4.34}$$

From Kirchhoff's law (Equation 4.28), monochromatic emissivity can be obtained as:

$$\varepsilon_\lambda = \alpha_\lambda = 1 - \exp(-a_\lambda L) \qquad \text{Equation 4.35}$$

In this study the absorbing gas layer (L) is assumed to be equal to the diameter of the plume which is $2r$.

Here a new term can be defined, the absorption cross section σ_a, which describes the absorptivity per unit of concentration as follows:

$$\sigma_a = \frac{a_\lambda}{\dot{c}} \qquad \text{Equation 4.36}$$

Where: σ_a = absorption cross section, m^2/g

$\dot{c}$ = concentration of medium (soot in this study), g/m^3

A wide range of soot specific absorption cross section is reported in the literature. For further investigations it is important to note that the wavelength dependence of σ_a is rather strong. This dependence is strong enough to make the values at the blue limit of visual spectrum more than twice the value at the red limit (Moosmuller et al., 1998). Hence, the range of observed absorption cross sections may be partly due to the range of wavelengths used in the experiments. However, a main part of this difference should be related to the different methods in assessing the soot mass concentration (Schnaiter et al., 2003).

Schnaiter et al. (2003) and Siegel and Howell (2002) suggested a relatively simple empirical relation for the absorption cross section as:

$$\sigma_a = \frac{c'}{\lambda} \qquad \text{Equation 4.37}$$

Where: λ = wavelength, nm

c' = constant, $nm.m^2/g$

For the calculation of c', the data of Colbeck et al. (1997) and Dobbins et al. (1994) was used (see Schnaiter et al., 2003). They found a σ value ranging from 6.0 to 8.1 m^2/g depending only slightly on the type of hydrocarbon fuel and the size of the soot aggregates for $\lambda = 632nm$. Solving for c', this leads to a c' value ranging from 3800-5100 $nm.m^2/g$.

For the calculation of λ, Wien's displacement law is used. Wien's displacement law formulates the wavelength λ_{max} at which the medium emits the maximum emissive radiant flux at the temperature of T. This law is derived by differentiation of Planck's law as:

$$\lambda_{max} = \frac{hc}{4.965kT} = \frac{2.898 \times 10^{-3}}{T} \qquad \text{Equation 4.38}$$

Where: h = Planck's constant, $6.62*10^{-34}$ J.s
c = speed of light, m/s
k = Boltzmann constant, $1.3806488*10^{-23}$ J/K
T = temperature, K

Using equation 4.38 and assuming c'=4000, σ_a can be obtained as a function of temperature.

The key premise in the calculation of the concentration of soot in the methane plume is using an emission factor. "Emission factors are representative values relating the quantity of an emission with an activity associated with the release of that emission" (Environment Canada, 2012). Emission factors offer an estimation of the average rate of emission (per unit of activity) of specific species. Johnson (2010) suggested the value of 0.2 kg soot/1000 m^3 fuel for the emission factor of methane flaring in the upstream oil and gas industry. Hence:

Initial volume flow rate of plume (m^3/s) = $\frac{\pi(\rho U_{sc} r^2)_{s=0}}{\rho_{s=0}}$

Mass flow rate of soot (kg soot/s) = $\frac{\pi(\rho U_{sc} r^2)_{s=0}}{\rho_{s=0}} \frac{EF}{1000} X$

Where: EF = emission factor of methane in the oil and gas upstream industry, 0.2 kg soot/1000 m^3 fuel
X_{CH_4} = conversion of combustion for methane

To calculate the concentration of soot, we need to divide the mass flow rate of soot by the volume of the plume:

$$\dot{c} = \frac{(\rho U_{sc} r^2)_{s=0}}{(\rho U_{sc} r^2)} \frac{\rho}{\rho_{s=0}} \frac{EF}{1000} X_{CH_4} \qquad \text{Equation 4.39}$$

Therefore absorptivity can be given by combining the above equation with equation 4.36 and 4.37 as:

$$\alpha_\lambda = 1 - \exp(-a_\lambda L) = 1 - \exp(-2c'r \frac{(\rho U_{sc} r^2)_{s=0}}{(\rho U_{sc} r^2)} \frac{\rho}{\rho_{s=0}} \frac{EF}{1000} X_{CH_4})$$ Equation 4.40

The term $a_\lambda L$ is called optical density or optical depth (*OD*). Hence, the optical density value for soot is given by:

$$OD_{soot} = 2c'r \frac{(\rho U_{sc} r^2)_{s=0}}{(\rho U_{sc} r^2)} \frac{\rho}{\rho_{s=0}} \frac{EF}{1000} X_{CH_4}$$ Equation 4.41

4.2.4 H_2O Emissivity Calculation

Other substances in the flame which influence the overall emissivity of the flame include water vapor and carbon dioxide. Leckner (1972) calculated the total emissivity of carbon dioxide and water vapor based on previous work by Hottel and Egbert (1942) using spectral data in a statistical model. His model is presented in the form of approximate empirical functions, which are required to be as simple as possible to be included in a computer program. His approximate empirical functions are within an error of less than 10% related to the emissivity calculated with spectral data. In the current and next section, H_2O and CO_2 emissivities are calculated using Leckner's (1972) method.

Total emissivity is dependent on pressure, temperature, and path length. Only at high temperature, the pressure dependence vanishes. For the calculation of the pressure dependence of emissivity, Leckner chose to reduce the total emissivity data at atmospheric pressure and various partial pressures of the emitting compound to emissivities at zero partial pressure of the emitting compound, ε_0. Then, using a pressure correction correlation, the actual emissivity ε_p, can be obtained from the emissivity at the partial pressure of the emitting substance.

The general form of the pressure correction relationship is a function of the total pressure, the partial pressure of the emitting substance, temperature, path-length, and gas components. For the sake of simplicity, an equivalent pressure P_E, is introduced. This equivalent pressure which is valid for water vapor and nitrogen is given by:

$$P_E = P_T (1 + 4.9 \frac{P_{H_2O}}{P_T} \sqrt{273/T})$$ Equation 4.42

Where: P_E = equivalent pressure, bar
P_T = total pressure (atmospheric pressure), bar
P_{H_2O} = partial pressure of H_2O, bar
T = temperature, K

For the next step, we need to define two parameters relating the dependence of the emissivity to the partial pressure, path length, and temperature as:

$$\lambda = \log(PL)$$
$$\tau = \frac{T}{1000} \qquad \text{Equation 4.43}$$

Where: PL = pressure-length, bar cm
T = temperature, K

An emissivity at constant pressure-length (PL) can be extrapolated to zero P by increasing L to infinity.

Similar to section 4.2.3 for the soot emissivity calculation, pressure-length is assumed to be equal to the diameter of the plume (L=2r) multiplied by the ambient pressure.

The maximum value of the actual emissivity divided by the reduced emissivity $[\frac{\varepsilon_p}{\varepsilon_0}]_{\max}$ is a function of equivalent pressure. Leckner (1972) presented an empirical equation relating this fraction:

$$[\frac{\varepsilon_p}{\varepsilon_0}]_{\max} = \frac{A \cdot P_E + B}{P_E + A + B - 1} \qquad \text{Equation 4.44}$$

Where: ε_p = actual emissivity at partial pressure of P of water vapor
ε_0 = reduced emissivity at zero partial pressure of water vapor
$A = 1.888 - 2.053\log\tau$, ($\tau = 0.75$ if T≤ 750K)
$B = 1.10\tau^{-1.4}$

Reduced Emissivity of Water Vapor: an emissivity chart for water vapor for a total pressure of 1 bar and zero partial pressure is presented by Leckner (1972). This is the hypothetical emissivity of a body of water vapor with infinite depth and zero partial pressure, so that the amount of water vapor on the path of the light is finite and non-zero. This diagram may be represented with two

polynomials of 2nd order (M=2, N=2) with a maximum error of less than ±5% for temperatures greater than 100°C:

$$\ln \varepsilon_0 = a_0 + \sum_{i=1}^{M} a_i \lambda_i$$
$$a_i = c_{0i} + \sum_{j=1}^{N} c_{ji} \tau^i$$

Equation 4.45

The coefficients c_{ji} are given in Appendix B.

4.2.5 CO_2 Emissivity Calculation

For carbon dioxide, the functions which define the pressure correction are similar to those of water vapor, but based on an equivalent pressure as:

$$P_E = P_T(1 + 0.28\frac{P_{CO_2}}{P_T})$$

Equation 4.46

Where: P_{CO_2} = partial pressure of CO_2, bar

The following empirical equation presents the relationship of the emissivities for carbon dioxide:

$$[\frac{\varepsilon_p}{\varepsilon_0}]_{\max} = \frac{A \cdot P_E + B}{P_E + A + B - 1}$$

The parameters A and B are given by:

$$A = 0.10\tau^{-1.45} + 1.0$$
$$B = 0.23$$

Equation 4.47

Finally the reduced emissivity calculation for CO_2 is the same as Equation 4.45 with different variables, given in Appendix B.

Overlapping: when carbon dioxide and water vapor are both present in a field, like in a methane flare, the total emissivity of these two substances is equal to the sum of emissivity of two gases minus a correction term due to overlap in some spectral regions:

$$\varepsilon_{H_2O+CO_2} = \varepsilon_{H_2O} + \varepsilon_{CO_2} - \Delta\varepsilon$$

Equation 4.48

And $\Delta\varepsilon$ can be obtained with the following equation:

$$\Delta\varepsilon = [\frac{\zeta}{10.7 + 101\zeta} - 0.0089\zeta^{10.4}]\lambda^{2.76} \quad \text{Equation 4.49}$$

Where: $\zeta = \frac{P_{H_2O}}{P_{H_2O} + P_{CO_2}}$

Calculating the emissivity of a mixture of water vapor and carbon dioxide leads to the overall optical density of those two species from Equation 4.35 as:

$$OD_{H_2O+CO_2} = \ln(1 - \varepsilon_{H_2O+CO_2})$$

4.2.6 Total Emissivity

From the Beer-Lambert-Bouguer law for monochromatic light, the total optical density of a mixture of gases and substances is equal to sum of optical density of each species. It is assumed for the purpose of the model that this law applies to polychromatic light as well. Since in a methane flare, water vapor, carbon dioxide, and soot are the main substances present, the total optical density for a methane flare can be obtained as:

$$OD_{total} = OD_{H_2O+CO_2} + OD_{soot} \quad \text{Equation 4.50}$$

Therefore, the total emissivity of a mixture of gases and soot for a methane flare is:

$$\varepsilon_{total} = 1 - \exp(-OD_{total}) \quad \text{Equation 4.51}$$

Now this new emissivity can be substituted into the heat balance equations in the set of independent differential equations.

4.3 Results and Discussions

In this chapter, the reaction of methane is broken down into two main sub reactions: the oxidation of methane to carbon monoxide, and the oxidation of carbon monoxide to carbon dioxide (Reactions 4.2 and 4.3). Separating the main reactions of burning the methane helps us to include the rate of reaction into the set of ordinary differential equations to model the flare. Based on the reaction rate constants in CH_4 and CO oxidation reactions, the controlling reaction

can be defined. The smaller reaction rate constant controls the reaction rate. Then a method is used to describe the radiation of the flare based on calculating the emissivities of the main substances in the flare flame separately. The main species responsible for radiating heat from the flare are CO_2, H_2O, and soot. The reason for extending the model with these additional calculations is to obtain more accurate flare model. Therefore, if the changes in the emissivity calculation and including the rate of reaction do not improve the accuracy of the flare markedly, it is computationally more efficient to use the basic model.

4.3.1 Improved Model Results

To compare the results of the improved version of the model (current chapter) with the basic version (previous chapter), the model is run with a set of sample input data from Section 3-3-2 summarized in Table 3-7:

Table 4-1: Sample input data

Parameter	***Amount***	***Description***
U_{atm}	2	Wind speed (m/s)
T_{atm}	288	Temperature of atmosphere (K)
P_{atm}	101325	Pressure of atmosphere (Pa)
M_{gas}	0.016	Molar mass of flared gas (kg/mol)
T_{gas}	288	Initial temperature of flared gas (K)
D_{stack}	0.100695	Diameter of stack (m)
H_{stack}	20	Height of stack (m)
Q_c	10000	Heating value of fuel (kJ/s)

Again, for this input data it is assumed that the combustion gas is methane (H=50000 kJ/kg, n=4), and the atmosphere is expected to be adiabatic ($\frac{dT_{atm}}{dz} = -\frac{g}{c_p}$) with a lapse rate of -0.00975 (K/m) and ground level temperature of 15°C. The meteorological condition is assumed to be calm and stable.

The version of the model considering methane combustion in a single step but with reaction kinetics yielded nearly exactly the same flame properties as the model with instantaneous kinetics, and will not be discussed here.

Solving the improved model based on the new equations from this chapter (4.26, 4.27, and 4.51) leads to the new height, length, and temperature profile for the flare.

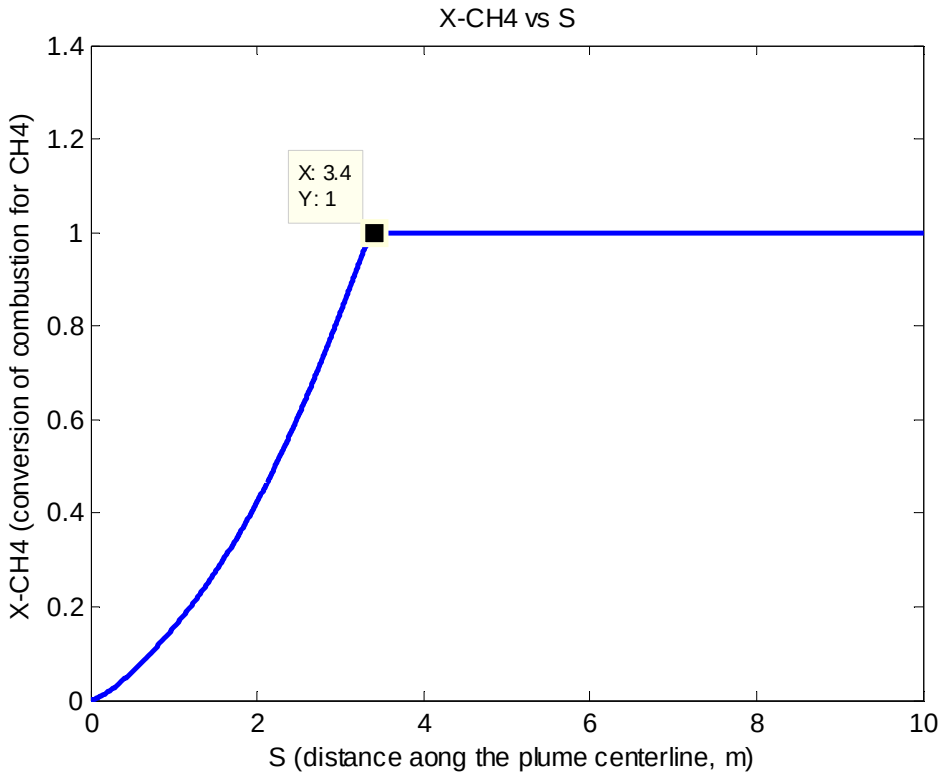

Figure 4-3: CH_4 conversion of combustion according to the initial condition of Table 3-7, improved model

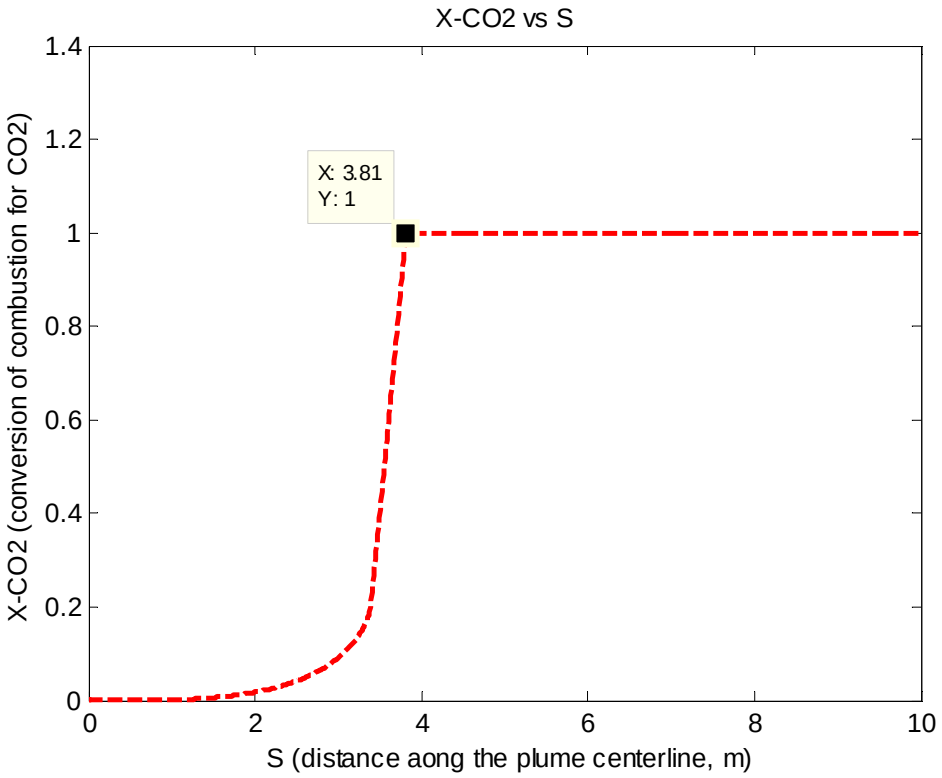

Figure 4-4: CO_2 conversion of combustion according to the initial condition of Table 3-7, improved model

Figure 4-3 shows CH_4 conversion of combustion profile. Based on this figure, all the methane is burned in the first 3.40 meters from the stack. After this point, there are still some amounts of CO to be burned and oxidized to CO_2. Hence, the CO_2 conversion of the combustion profile in Figure 4-4 indicates the flare tip at 3.81 meters.

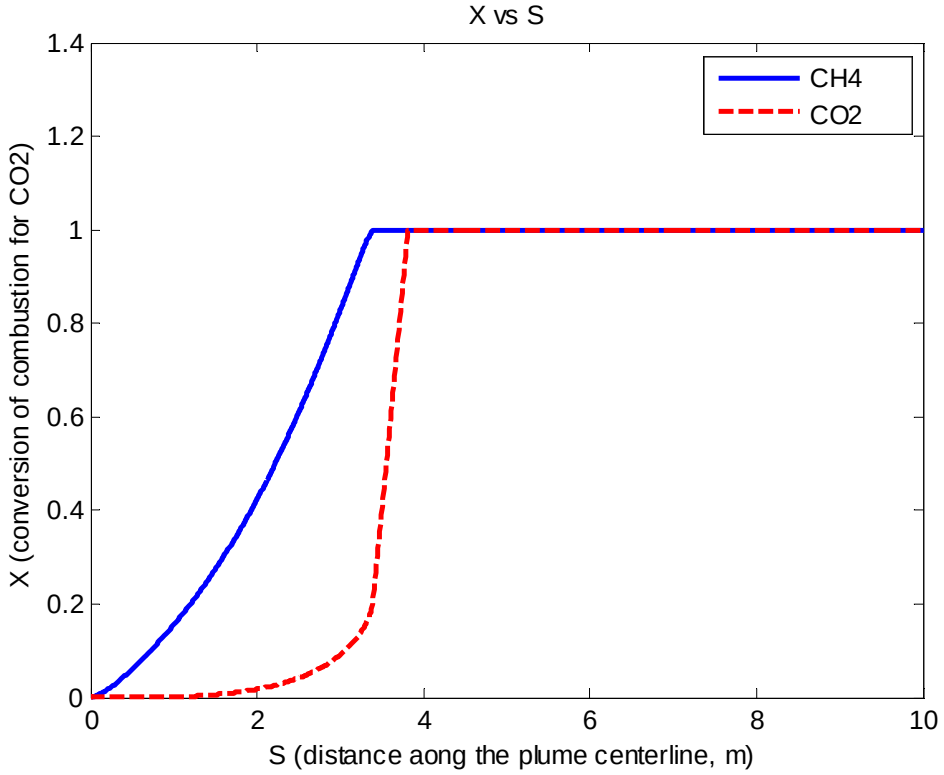

Figure 4-5: CO_2 and CH_4 conversion of combustion according to the initial condition of Table 3-7, improved model

Figure 4-5 compares the conversion of CH_4 with the conversion to CO_2 in the flame. The data indicate that combustion of methane is much faster than combustion of carbon monoxide. This is due to larger reaction rate constant for methane (k_1) compared with the reaction rate constant for carbon monoxide (k_2). In other words, in the very first step, oxygen tends to oxidize the methane (Reaction 4.2) rather than carbon monoxide (Reaction 4.3), and when almost all the methane is burned, near the flame tip, oxygen oxidizes the carbon monoxide to carbon dioxide. Hence, the controlling reaction here is burning of CO to CO_2 (Reaction 4.3).

A temperature profile is presented in Figure 4-6. In the temperature profile of the improved model, there is a peak at the end of the flame which is related to the conversion of carbon monoxide to carbon dioxide. The temperature profile reaches to 2220 K at s=3.80 m in its hottest point and then it decreases due to the cooling effect of entraining of cold ambient air (T_{atm}=298K) along with the lack of any burning gas.

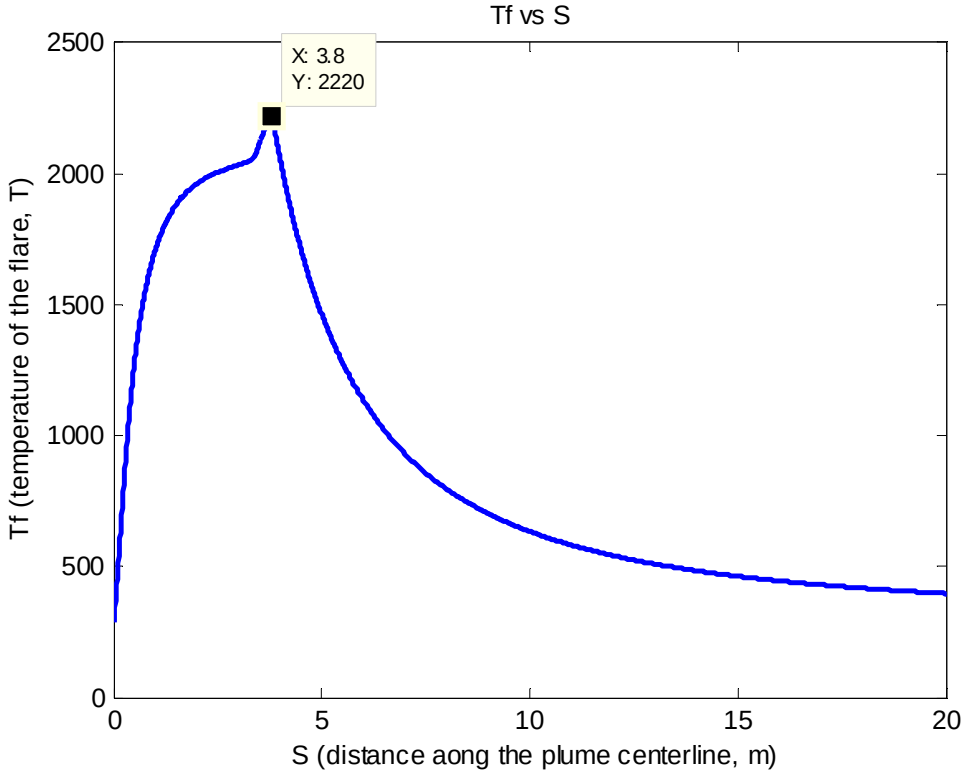

Figure 4-6: Temperature profile according to the initial condition of Table 3-7, improved model

In Chapter 3, it was found that the basic model predicts a flame length of 3.70 m, slightly shorter than the flame length found here. Longer flame lengths are expected for the modified model because the reaction kinetics slows down the overall process. However, the limited effect of kinetics may indicate that this is not an essential part of the model.

Figure 4-7 compares the CH_4 conversion profile of the flame from Chapter 3 (basic model) with the CO_2 and CH_4 conversions of the improved model.

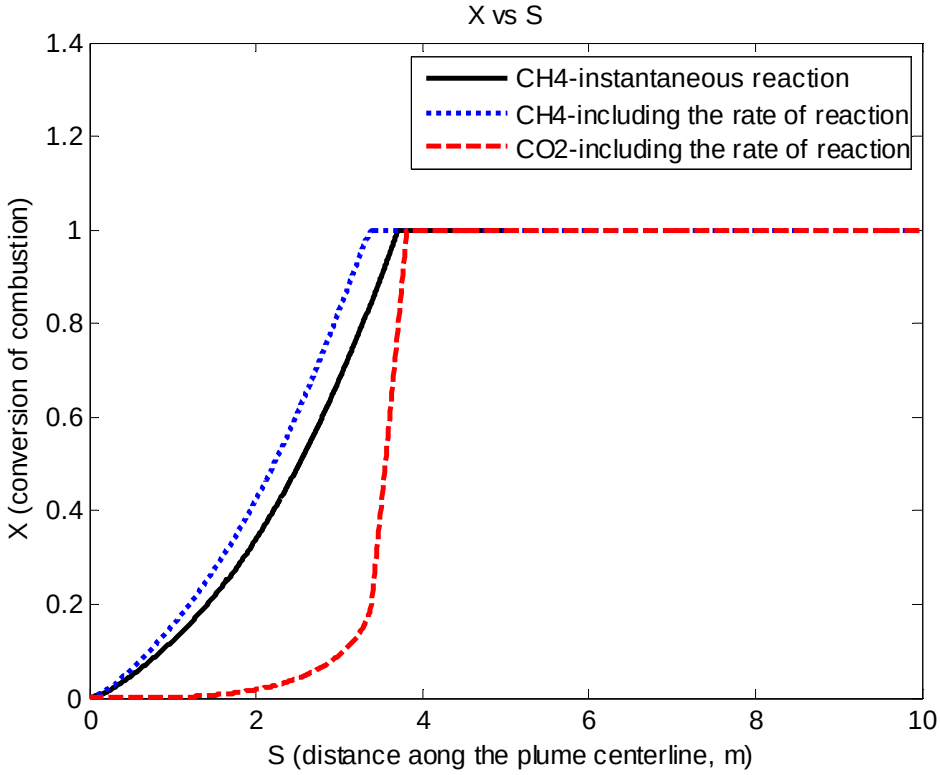

Figure 4-7: Conversion of combustion according to the initial condition of Table 3-7, improved model vs. basic model

In the improved model, emissivities of the main gaseous species (i.e., carbon dioxide and water vapor) and soot aggregates are calculated separately. The model results show that the gaseous components have negligible effects on the total emissivity of the flame, so heat radiation is mainly due to the presence of soot aggregates. However, at the beginning of the flame the emissivity of soot is as low as 10^{-6}. As more soot is produced the soot emissivity increases to ε_{soot}=0.0142. At the same time, the emissivities of CO_2 and H_2O decrease from the order of 10^{-5} to the order of 10^{-9} and 10^{-11}, respectively. Moreover, the total energy which is emitted as radiation is calculated as 9.7% of the total heat of combustion. This value is in agreement with GPSA (2012) which assumes 10% of radiation heat loss and considerably less than the 25% estimated by Beychok (2005).

The main difference between the temperature profiles of the basic and improved models is a sudden peak at the end of flare in the improved model. This peak is related to the last step of carbon monoxide oxidation, where all the methane is burned. Both profiles confirm that the

hottest point of the flare is the tip of the flame. The highest predicted temperature in the basic model is 2152K, while the value for the improved model is 2220K. The temperature difference between flare tips is 3%. Since the radiation is proportional to T^4, 3% difference in the flare temperature could potentially cause 12% difference in radiation which is a considerable amount. To justify this difference it is important to take a look at the temperature profile (Figure 4-8) precisely. The temperature profile for the basic model before the flare tip is slightly higher, while it predicts slightly lower temperatures after the flare tip than the improved model. Since the radiation calculation is based on the twice of the flare length, this difference in the flare temperature profile is negligible in average. Furthermore, the main factor affecting radiation is the calculation method for ε, as indicated before.

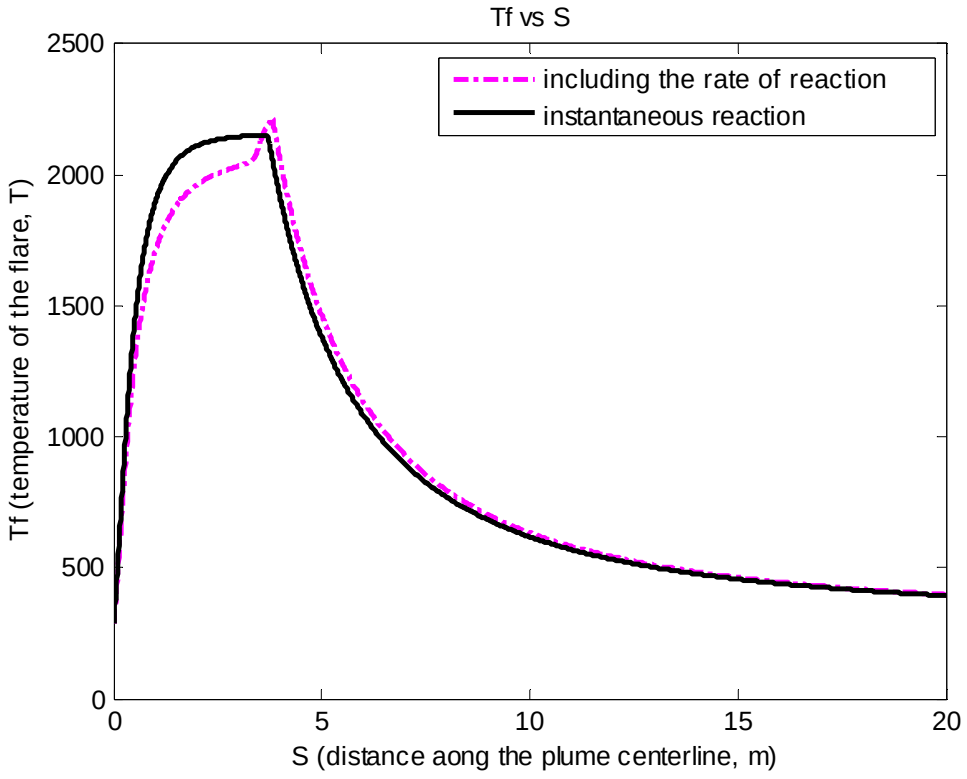

Figure 4-8: Temperature profile according to the initial condition of Table 3-7, improved model vs. basic model

Thus, a comprehensive comparison of the developed to the basic model leads to the following results:

- Conversion profiles show that CH_4 oxidation to CO dominates in most of the plume, whereas most CO_2 conversion occurs near the flame tip.
- Reaction kinetics is close to instantaneous.
- The models predict similar values for the length and temperature of the flame.

According to the above results, since performing the improved model does not improve the accuracy of flare characteristics prediction considerably, it is computationally beneficial to use the basic model. Thus, in the next chapter the effects of including the basic flare model in the CALPUFF air dispersion model will be discussed.

Chapter Five: **CALPUFF Simulation**

5.1 Introduction

The main goal of this research is to better predict the flare characteristics to be included in air dispersion models. CALPUFF is a widely accepted regulatory air dispersion model which is appropriate for both near field and far field applications. CALPUFF is one of the recommended models by EPA for regulatory applications, and it is the preferred regulatory model in Alberta. Hence, in this chapter the effects of applying the flare model result to the CALPUFF air dispersion model will be investigated.

CALPUFF version 7.9.0.06 does not include flare plume rise, but it includes stack plume rise. Hence, in this chapter flare characteristics are predicted with the model offered in Chapter 3, and then the dispersion simulation is performed based on the flare characteristics. To compare the dispersion results, another accepted flare model, offered by Beychok (2005), will also be considered to predict the flare height, temperature, and diameter. Then the dispersion simulation will be performed considering the predicted flame characteristics.

To include the effects of flare combustion in the dispersion model, we define a hypothetical stack based on the flare model results. The hypothetical stack's physical measurements are the same as the flare physical characteristics at the flame tip. The diameter, gas exit temperature, and gas exit velocity of the hypothetical stack are set as the diameter, temperature, and the vertical velocity of gas at the flare tip. The height of this new stack equals the height of original stack plus the height of the flame. In other words, the combusted gas plume rise and dispersion is defined to start at the end of the visible flame.

For a dispersion model calculation from a stack, all the parameters which need to be taken into account include:

1- Stack height
2- Stack diameter
3- Gas exit velocity
4- Gas exit temperature
5- Emission rate

Therefore, all the above parameters will be calculated in both flare models (Beychok and the flare model discussed in Chapter 3) and then used as input data for a dispersion model calculation in CALPUFF. Hence, we consider all the physical initial data based on the Table 3-5 for methane as the combustion gas (H=50000 kJ/kg, n=4). The data is shown in Table 5-1.

Table 5-1: Assumed input data for CALPUFF simulation

Parameter	***Amount***	***Description***
T_{atm}	288	Temperature of atmosphere (K)
P_{atm}	101325	Pressure of atmosphere (Pa)
M_{gas}	0.016	Molar mass of flared gas (kg/mol)
T_{gas}	288	Initial temperature of flared gas (K)
H_{stack}	20	Height of stack (m)
Q_c	10000	Heating value of fuel (kJ/s)

The model of Beychok (2005) discussed in section 5.3 or its variants are the basis of most flare dispersion modeling regulations.

5.2 CALPUFF Simulation Preparation

The CALPUFF modeling system includes three main modules: CALMET, CALPUFF, and CALPOST. CALMET is a meteorological model which produces a three-dimensional gridded modeling domain for hourly wind and temperature fields. CALPUFF is a transport and dispersion model that uses a puff model to represent a group of contaminant molecules whose volume increases due to turbulent mixing. In doing so, it takes advantage of the fields generated by CALMET. The output files of CALPUFF usually contain hourly concentrations for selected receptors locations. Then these files can be processed by CALPOST to produce layout that summarizes the results of the CALPUFF simulation.

Therefore, the first step for a dispersion model calculation is to prepare a CALMET field to be used in CALPUFF. The gridded domain was defined as outlined in Table 5-2.

Table 5-2: CALMET input data

Grid Origin (km)	X=600.16	Y=5690.607
Grid Spacing (km) = 0.9		

Number of Grid points	NX=204	NY=165
Number of Vertical Layers	NZ=10	
Vertical Layers position (m): 0, 20, 40, 80, 160, 320, 640, 1000, 1500, 2200, 3000		
UTM Zone: 11 Northern, Base Time Zone: (UTC-07:00) Mountain Time (US & Canada)		
Datum-Region: WGS-84		

The system used to sketch a part of a round Earth on a flat surface is called a map projection. Universal Transvers Mercator projection (UTM) and Lambert Conformal Conic projection (LCC) are the two main projections which are used in air dispersion modeling.

In the UTM grid the projection of the zone is on a cylinder wrapped around the Earth. Therefore the intersecting circle is a vertical (North-South) line at the center of the zone. The world is divided into 60 north-south zones, each covering a strip 6° wide in longitude and projects that strip on a separate plane. The zones are numbered consecutively beginning with zone 1 at 180-174° W and moving east to Zone 60, between 174° and 180° east longitudes. In each zone, coordinates are measured north and east in kilometers. The northing values are measured from zero at the Equator, in a northerly direction. The center of the zone (i.e., at the equator, at 3° latitude from both sides) the coordinates are x=500 km and y=0 (De Visscher, 2013; Turner and Schulze, 2007).

The shape of the Earth for computing positions that is assumed in the projection is referred to as the datum. Vertical datum is applied to determine the elevation, while horizontal datum is used to measuring the latitude and longitude of a point on the Earth's surface. The WGS-84 is a common standard datum.

To obtain the concentration profile, three sources (stacks) were defined in the domain along with their emission rates. The source information is shown in Table 5-3.

Table 5-3: Sources Information

Source Name	***X (km)***	***Y (km)***	***Base Elevation (m)***	***Emission Rate (g/s)***
P1	698.089	5736.437	1023.0	3.20

P2	694.023	5712.825	1128.0	2.99
P3	706.357	5698.485	1116.0	2.70

It is assumed that the emission is SO_2 which is released to the ambient atmosphere along with combusted methane.

For other stack parameters such as stack diameter, stack height, exit stack temperature, and exit stack velocity will be calculated using the Beychok method and the flare model which is offered in this study, based on the meteorological and geometrical data for a specific date. In this study we choose to simulate the dispersion modeling for June 15, 2002, for which meteorological calculations with CALMET were available (Fraser, 2011).

5.3 Flare Parameters Calculation Using Beychok Method

To calculate the plume rise from a flare stack, Beychok (2005) estimates the flare length to define the vertical and horizontal location of the flame tip. Based on an API publication (1969) he calculates the flare length as a function of the flare gas heat release as:

$$L = 0.006 Q_c^{0.478} \qquad \text{Equation 5.1}$$

Where: L = flame length, ft
Q_c = flare gas heat release, Btu/hr

Then he suggests the simple and conservative approach of assuming a constant angle of 45° of the flare to the vertical. Thus, the vertical height of the flare can be given as:

$$h_{fv} = L \sin 45^\circ = 0.707 L$$

Where: h_{fv} = vertical height of the visible flame, ft

Substituting into Equation 5-1 for the flame length L, leads to:

$$h_{fv} = 0.0042 Q_c^{0.478} \qquad \text{Equation 5.2}$$

Solving Equation 5.2 for the input data in the current case study in Table 3-5 leads to:

$$h_{fv} = 5.11 \text{m}$$

There are two important basic assumptions in the Beychok flare method that are helpful for calculating the temperature of the flare tip. The first assumption is that the flare stack flame entrains 175 percent excess air. The second assumption is that the flame loses 25 percent of its heat by thermal radiation. Therefore, to calculate the temperature of the flame at the flame tip based on the initial condition of Table 3-5, first the molar flow rate at the flame tip needs to be calculated. Assuming $Q_c = 10000\frac{kJ}{s}$ and $H = 50000\frac{kJ}{kg}$ for methane leads to $\frac{Q_c}{H} = 0.2\frac{kg\ CH_4}{s}$ or $12.5\frac{mol\ CH_4}{s}$, that is, for this initial condition 12.5 mol of methane is released to the ambient air per second. Thus, according to Reaction 4.11, 12.5 mol of methane needs 25 mol of oxygen to be burnt in a 100% efficiency situation. Assuming 175% excess air enters into the flame, 68.75 moles of oxygen are mixed into the flame (25+1.75*25=68.75 mol oxygen). Supposing air consists of 21% oxygen and 79% nitrogen, it means for 12.5 mol methane released in the air, 327.38 mol of air enters into the flame section.

In this method it is assumed that 25% of the heat produced in the flare combustion is released by thermal radiation, so for $Q_c = 10000\frac{kJ}{s}$ just $7500\frac{kJ}{s}$ heats up the 327.38 moles of air. In other words, each mole of air is heated up for 22.91kJ ($\frac{7500\frac{kJ}{s}}{327.38\frac{mol-air}{s}} = 22.91\frac{kJ}{mol-air}$ or $5475.62\frac{cal}{mol}$). Here combusted gas temperature can be obtained by equating the combustion heat release from the flare with the air heat content (enthalpy) at the flare temperature. The thermal properties of air are used here instead of thermal properties of the gas mixture, because the combustion gas consists of over 90% air. The effect of gas composition on the buoyancy of a plume resulting from its temperature rise is negligible. On a molar basis the specific enthalpy of oxygen and nitrogen is given by (Beychok, 2005):

$$H_{N_2} = 6.76T + (0.305\cdot 10^{-3})T^2 + (0.043\cdot 10^{-6})T^3 - 2042.7 \qquad \text{Equation 5.3a}$$

$$H_{O_2} = 8.27T + (0.13\cdot 10^{-3})T^2 + (1.88\cdot 10^{5})T^{-1} - 3107 \qquad \text{Equation 5.3b}$$

Where: H_{N_2}, H_{O_2} = heat content of nitrogen and oxygen above 298K, cal/g-mol
T = flare temperature, K

In Equations 5.3a and 5.3b the enthalpy is zero at 298 K.

Hence, the total heat content of air at the flare tip can be given by the sum of nitrogen and oxygen enthalpy as:

$$H_T = 0.79H_{N_2} + 0.21H_{O_2} = 5476.62\frac{cal}{mol} \qquad \text{Equation 5.4}$$

Where: H_T = heat content of air above 298K, cal/g-mol

Since flare combustion heats up the air, the total heat content of air should be equal to the heat produced by the flare. Substituting Equation 5.3a and 5.3b into Equation 5.4 yields:

$$5475.62 = 1.0771T + (0.26825\cdot 10^{-3})T^2 + (0.0397\cdot 10^{-6})T^3 + (0.3948\cdot 10^{5})T^{-1} - 2266.2$$

Solving the above equation gives a flare tip temperature equal to 1042.53K (T_{tip}=1042.53K).
To calculate the gas exit velocity and radius of the flare tip we assume the plume as an ideal gas, and that momentum is conservative in the vertical direction, that is, the ambient wind has no vertical vector component. Then we need to solve the momentum conservation and ideal gas law equations.
The momentum conservation equation can be given by:

$$(\frac{d_{exit}}{2})^2 U_{exit}^2 \rho_{exit} = (\frac{d_{tip}}{2})^2 U_{tip}^2 \rho_{tip} \qquad \text{Equation 5.5}$$

Where: d_{exit}, d_{tip} = diameter of the stack and flare tip, m
U_{exit}, U_{tip} = gas exit velocity and vertical velocity of the flare tip, m/s
ρ_{exit}, ρ_{tip} = the gas exit and flare tip density, kg/m^3

And from the ideal gas law:

$$\frac{V}{nT} = \frac{R}{P} = \text{constant}$$

Consequently:

$$\frac{V_{exit}}{n_{exit}T_{exit}} = \frac{V_{tip}}{n_{tip}T_{tip}} \qquad \text{Equation 5.6}$$

Where: V_{exit}, V_{tip} = volume of gas exiting the stack and at the flare tip, m^3

n_{exit}, n_{tip} = number of mole of gas exiting the stack and at the flare tip, mol

T_{exit}, T_{tip} = temperature of the exit gas and the flare tip, K

Then, the volume (in this case volumetric flow rate), density, and gas exit velocity can be calculated by:

$$V_{exit} = (\frac{d_{exit}}{2})^2 U_{exit}$$ Equation 5.7a

$$V_{tip} = (\frac{d_{tip}}{2})^2 U_{tip}$$ Equation 5.7b

$$\rho_{exit} = \frac{PM_{CH_4}}{RT_{exit}}$$ Equation 5.8a

$$\rho_{tip} = \frac{PM_{air}}{RT_{tip}}$$ Equation 5.8b

$$U_{exit} = \frac{Q_C}{H\rho_{exit}\pi(\frac{d_{exit}}{2})^2}$$ Equation 5.9

Where: M_{CH4}, M_{tip} = molecular weight of methane and air, kg/mol

P = atmospheric pressure, Pa

Hence, substituting Equations 5.6, 5.7a, 5.7b, 5.8a, 5.8b, and 5.9 into Equation 5.5 and solving for d_{tip} gives us the diameter of the flare tip. Then Equation 5.5 is solved for U_{tip}.

Therefore, assuming the initial conditions of Table 5-1, the Beychok method predicts the characteristics of the flare tip as:

$T_{tip} = 1042.53K$

$U_{tip} = 0.67 \, m/s$

$d_{tip} = 7.44m$

$h_{fv} = 5.11m$

According to the Beychok method, ambient wind does not influence the flare characteristics, such as flare angle and flare height. It is important to mention again that to obtain the height of the hypothetical stack we have to add the height of the flame to the original stack height. In this case the apparent height of the new stack is equal to 25.11m. Thus, the above flare characteristics can be used in the dispersion model as shown in Table 5-4.

Table 5-4: Source input data according to the Beychok method

Source Name	***X (km)***	***Y (km)***	***Base Elevation (m)***	***Emission Rate (g/s)***	***Stack Height (m)***	***Stack Diameter (m)***	***Exit Velocity (m/s)***	***Exit Temperature (K)***
P1	698.089	5736.437	1023.0	3.20	25.11	7.44	0.67	1042.53
P2	694.023	5712.825	1128.0	2.99	25.11	7.44	0.67	1042.53
P3	706.357	5698.485	1116.0	2.70	25.11	7.44	0.67	1042.53

5.4 Flare Parameters Calculation Using the New Flare Model

Contrary to the Beychok model, all the flare characteristics highly depend on the ambient wind speed in the new flare model. Beychok suggests the simple assumption that the flame is tilted 45° from the vertical, which may cause big errors in the prediction of the flare height at low and high wind speed. Obviously, a flare tends to have a nearly vertical flame at low wind speed and nearly horizontal flame at high wind speed. Since the wind speed varies continuously, considering the effects of wind speed on the prediction of the flare parameters prediction would increase the accuracy of the model considerably.

To take the wind speed into account, it is necessary to find out the wind speed exactly at the top of each original stack. Using the postprocessor PARTMET for CALMET output data, all the wind vectors are accessible for all the vertical defined layers. Since the original stack height is 20 meters, the new hypothetical stack is placed somewhere in the second vertical layer (20-40 m). So the wind speed values are gathered from the second layer of air. To obtain a comprehensive comparison, different wind speed values for different times on June 15, 2002 are chosen. Table 5-5 shows the wind speed values for different times in the second layer of air for the sources defined in Table 5-3.

Table 5-5: Wind speed for different times at top of sources

time	*Wind speed at P1 (m/s)*	*Wind speed at P2 (m/s)*	*Wind speed at P3 (m/s)*
06:00	0.7581	0.4815	0.1315
08:00	0.66	0.27	0.27
19:00	8.46	11.46	8.99

Using the basic model to predict the flare parameters using these wind speed values yields the source input data for different times in Table 5-6. The exit temperature is a weighted average of the burning and non-burning parts of the flame.

Table 5-6: Source input data according to the flare model of this study

Source Name	*X (km)*	*Y (km)*	*Base Elevation (m)*	*Stack Height (m)*	*Stack Diameter (m)*	*Exit Velocity (m/s)*	*Exit Temperature (K)*
HR 06:00							
P1	698.089	5736.437	1023.0	25.20	1.14	2.58	336.4
P2	694.023	5712.825	1128.0	26.81	1.01	2.90	363.5
P3	706.357	5698.485	1116.0	30.46	0.84	3.47	359.9
HR 08:00							
P1	698.089	5736.437	1023.0	25.68	1.01	2.68	365.4
P2	694.023	5712.825	1128.0	28.72	0.91	3.22	361.3
P3	706.357	5698.485	1116.0	28.72	0.91	3.22	361.3
HR 19:00							
P1	698.089	5736.437	1023.0	20.62	2.25	1.56	522.7
P2	694.023	5712.825	1128.0	20.38	2.51	1.55	642.2
P3	706.357	5698.485	1116.0	20.58	2.28	1.56	534.1

5.5 Results and Discussion

Running the CALPUFF dispersion model for input data of Table 5-4 and Table 5-6 provides files which contain hourly concentrations and fluxes evaluated at the selected sources. Then CALPOST is used to process these files and summarize the results by identifying average and peak concentrations. Figures 5-1 to 5-6 are the concentration profiles for various times based on the Beychok flare model and the flare model developed in this study.

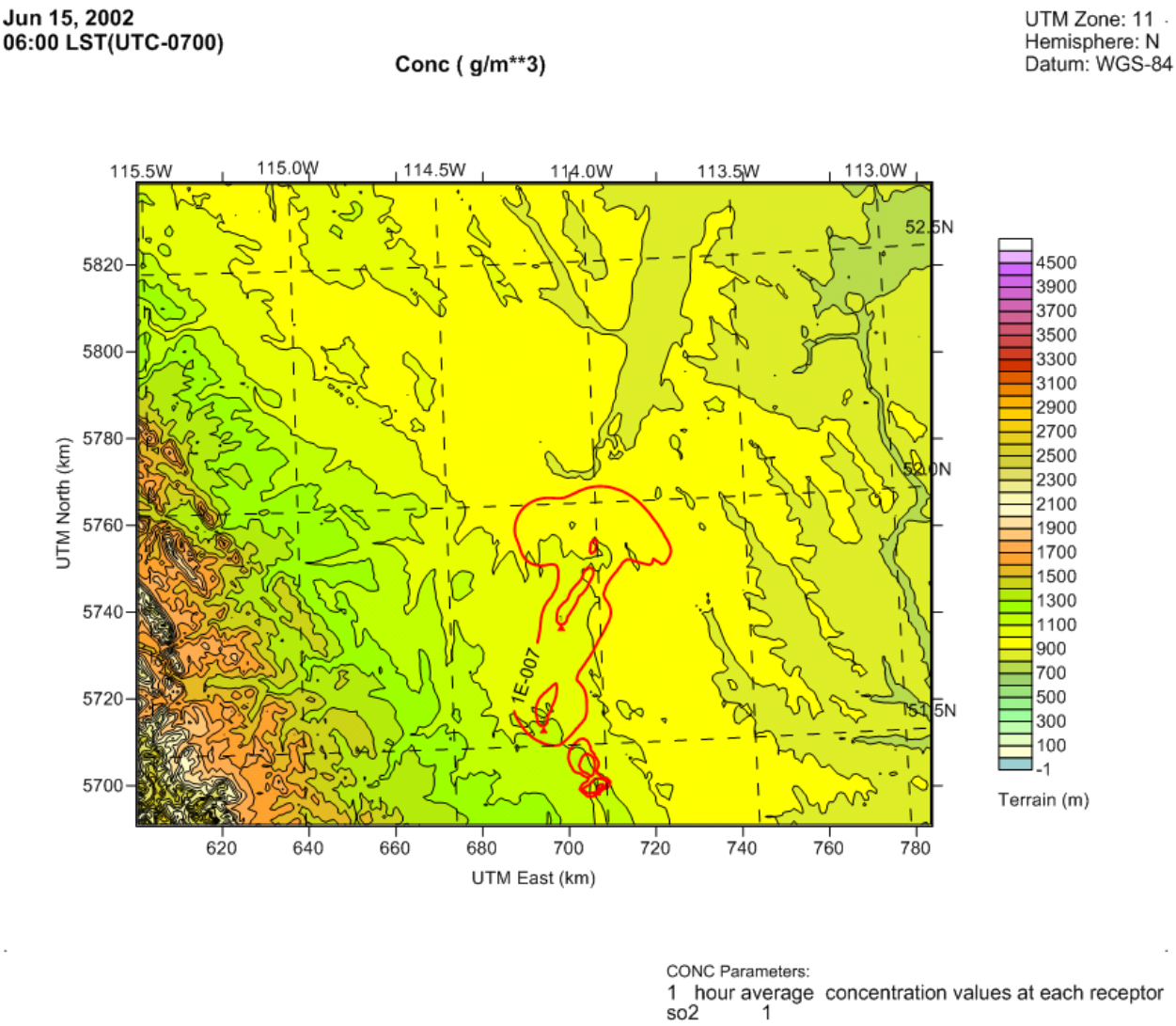

Figure 5-1: Concentration profile based on the Beychok flare model, hr 06:00

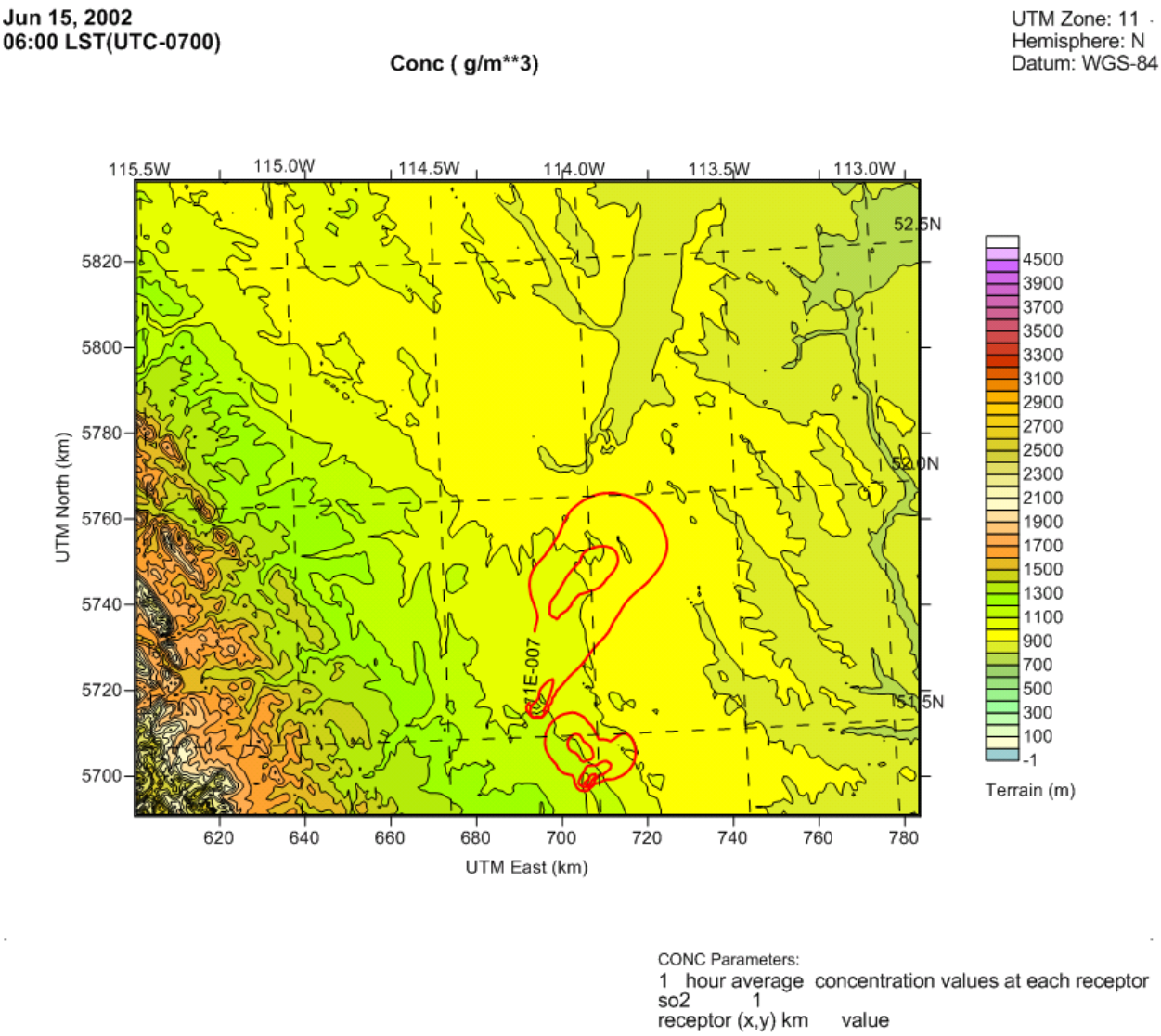

Figure 5-2: Concentration profile based on this study flare model, hr 06:00

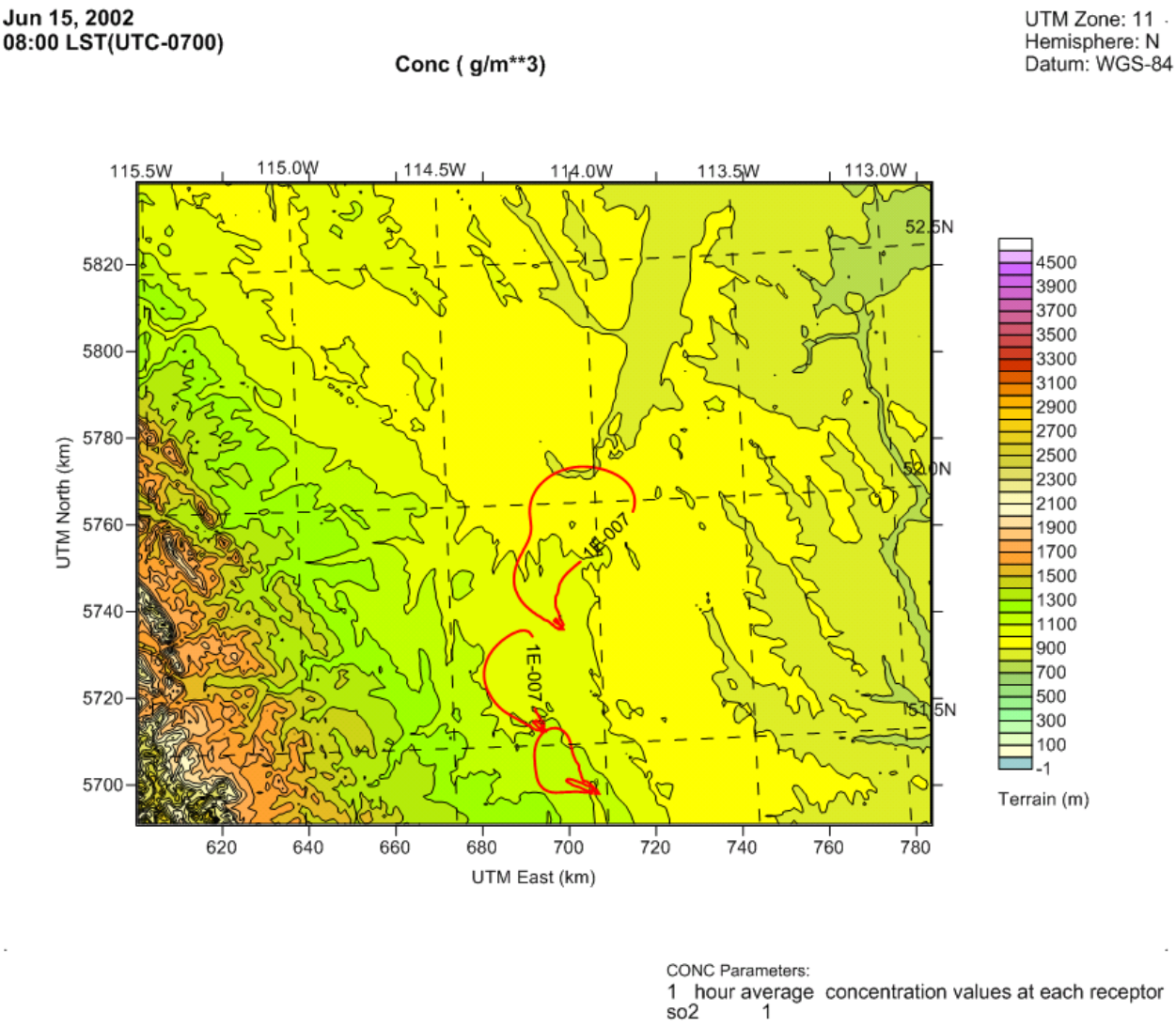

Figure 5-3: Concentration profile based on the Beychok flare model, hr 08:00

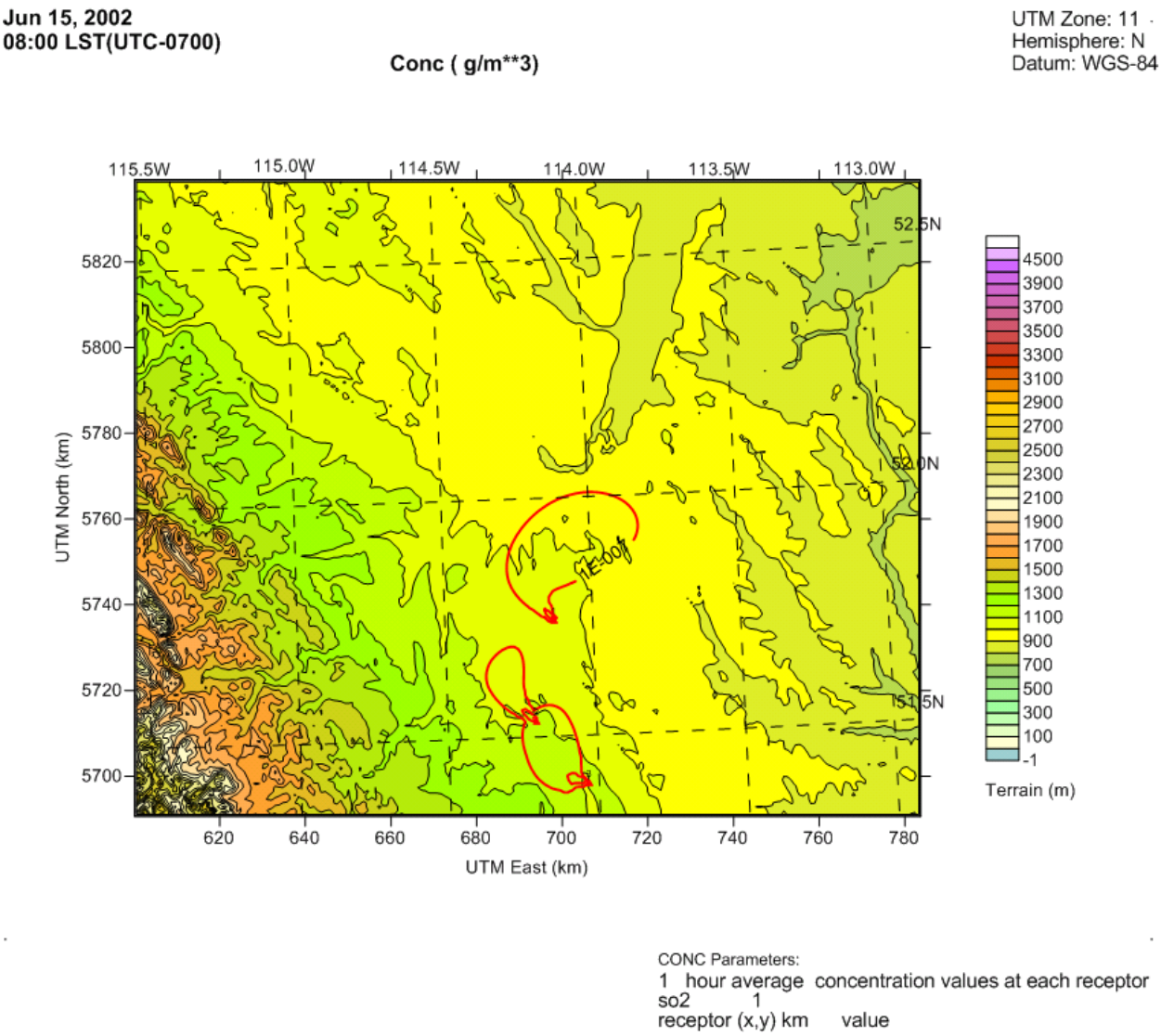

Figure 5-4: Concentration profile based on this study flare model, hr 08:00

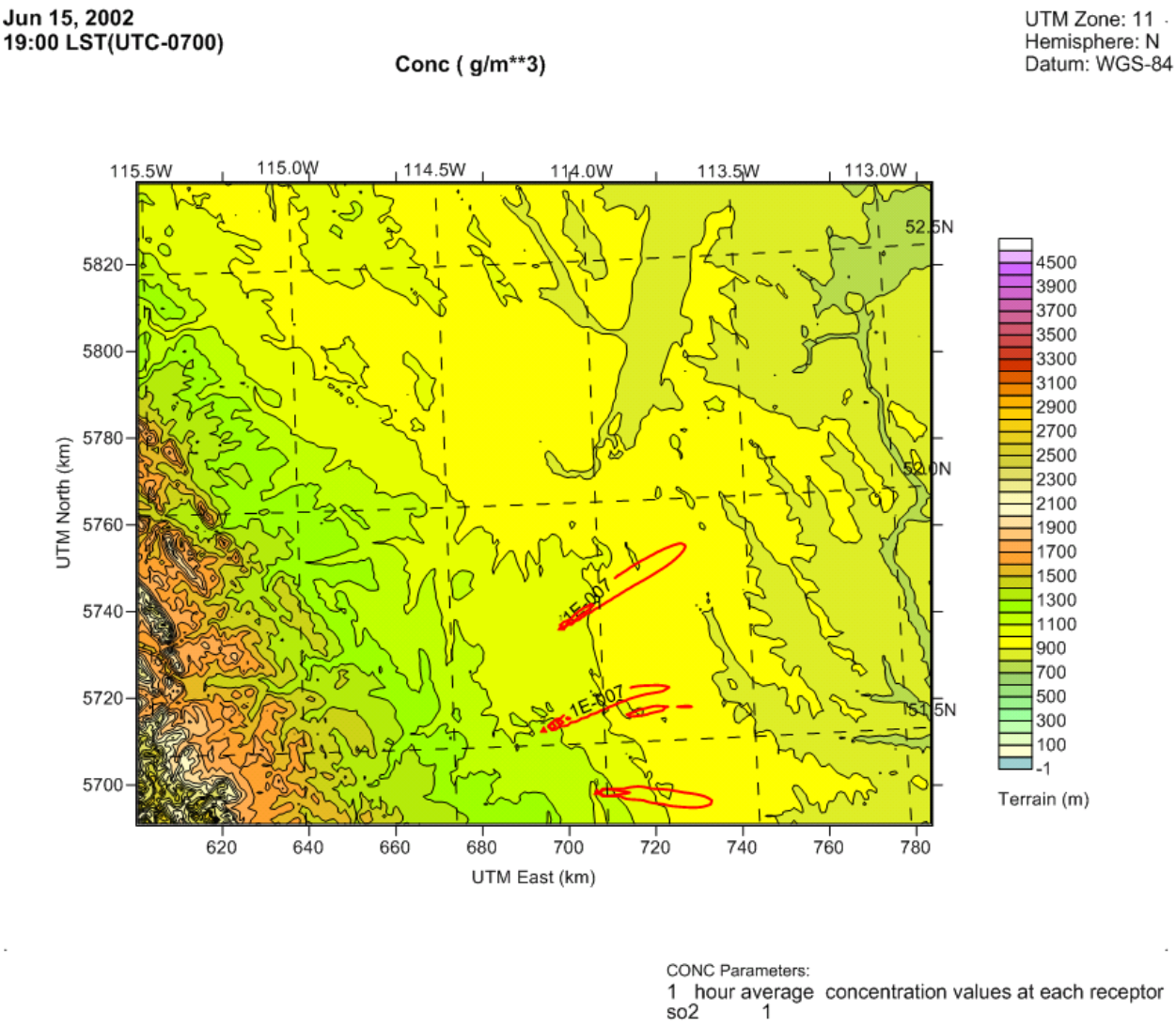

Figure 5-5: Concentration profile based on the Beychok flare model, hr 19:00

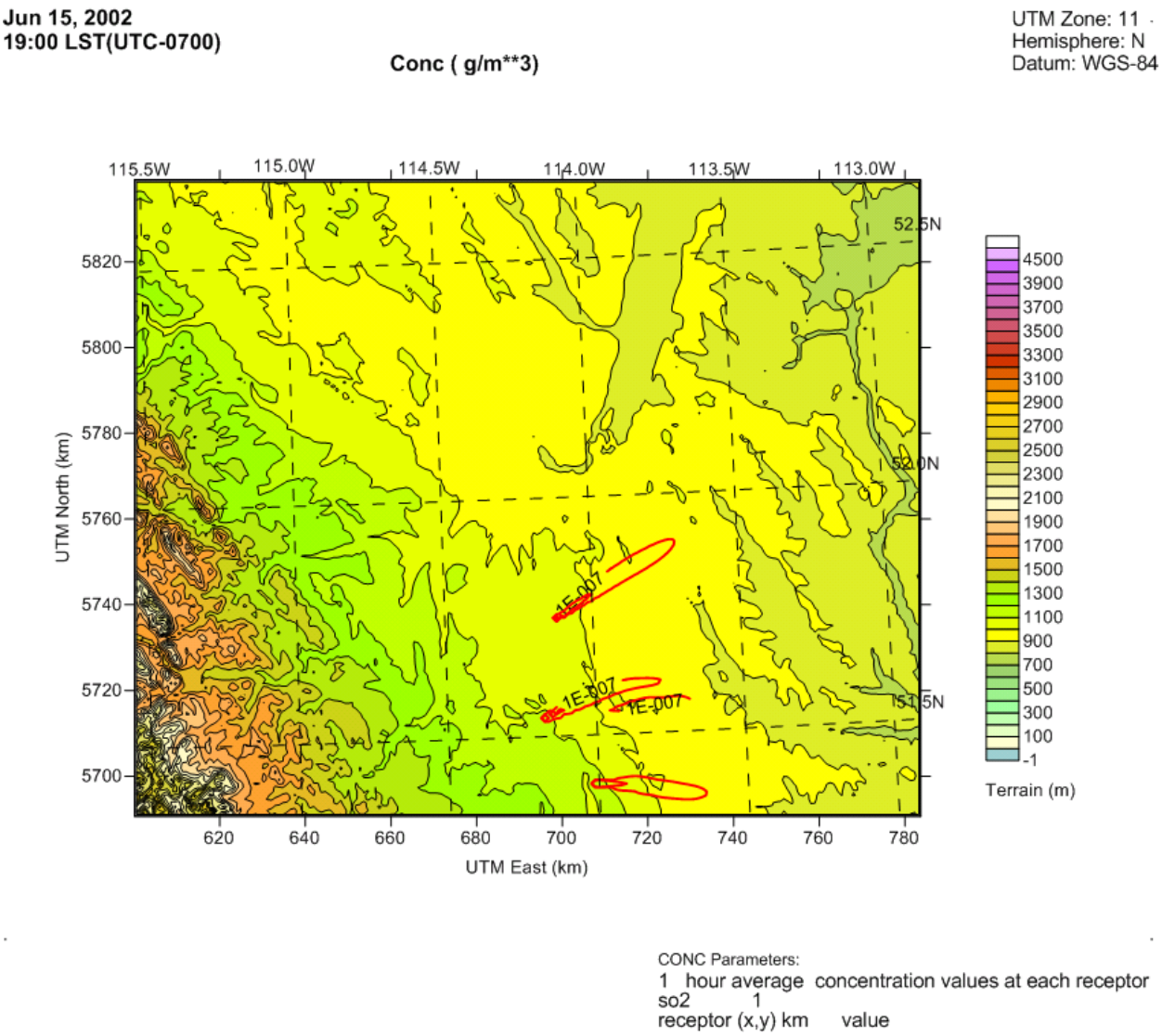

Figure 5-6: Concentration profile based on this study flare model, hr 19:00

Applying Surfer mapping software (Golden Software Inc., Golden, Colorado) for CALPOST output files help us to compare these concentration profiles precisely.

Figures 5-7 to 5-11 compare the ground level concentrations of SO_2 for each simulation in some constant latitude and longitude for different sources.

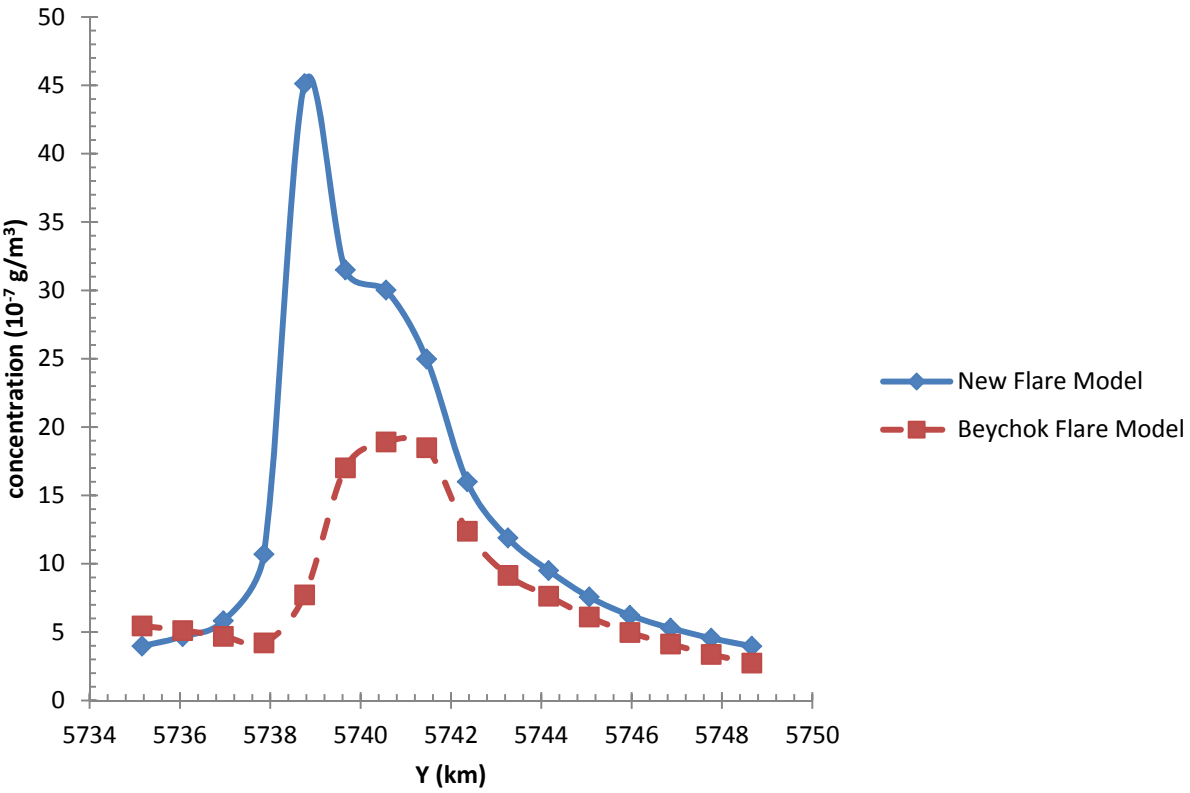

Figure 5-7: Concentration of SO_2 at hr 06:00 for X=699.56 km, near P1

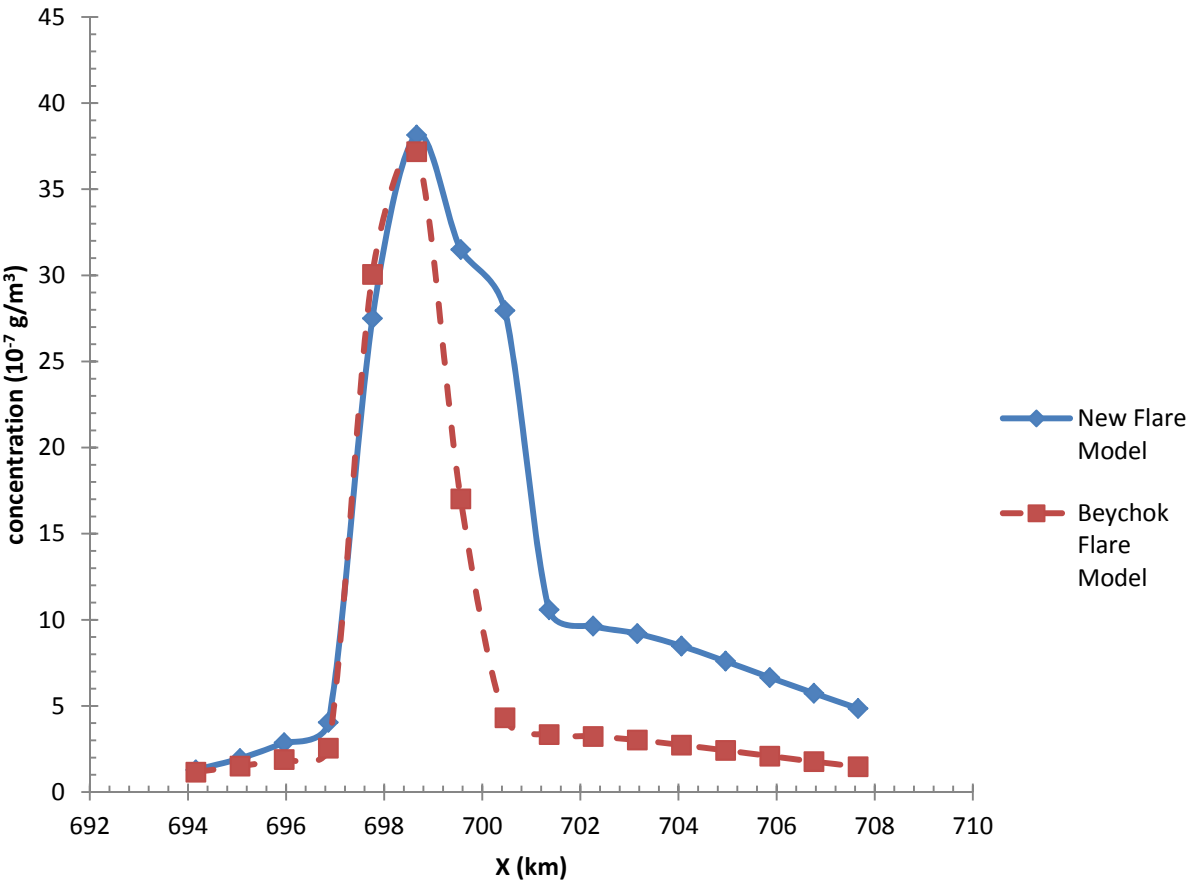

Figure 5-8: Concentration of SO_2 at hr 06:00 for Y=5739.66 km, near P1

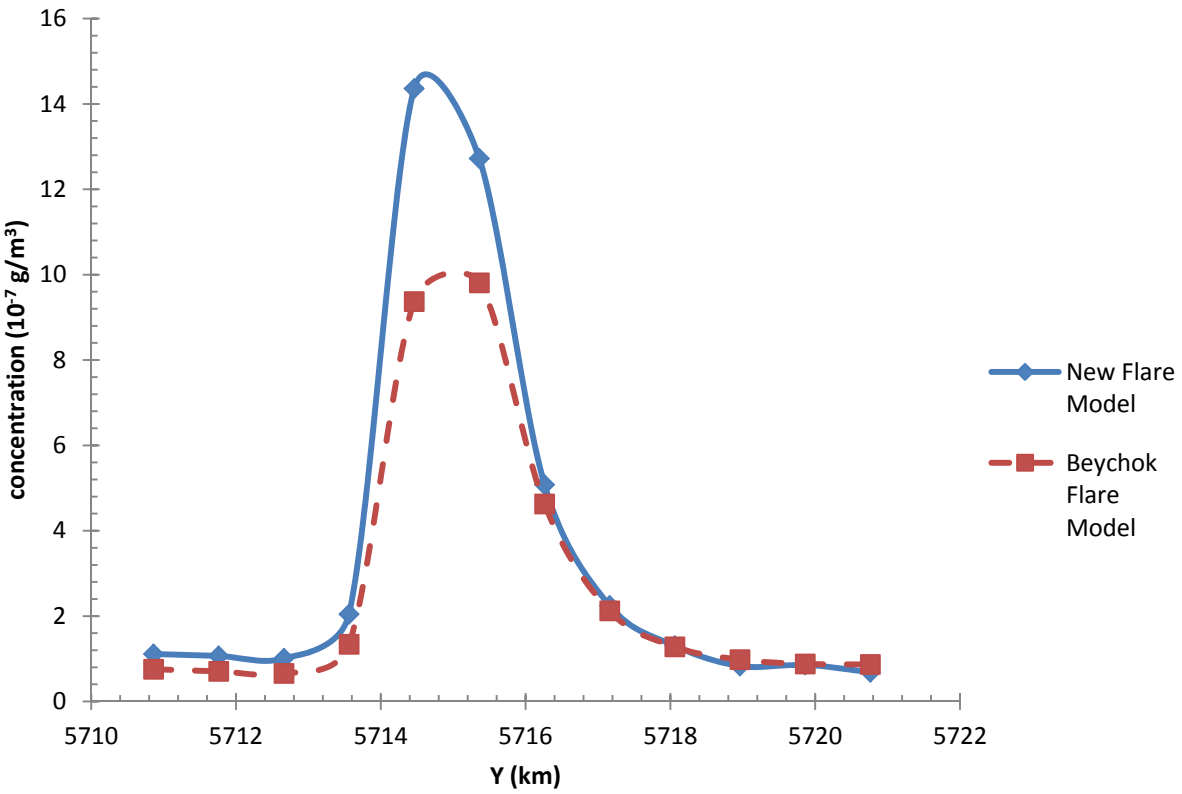

Figure 5-9: Concentration of SO_2 at hr 08:00 for X=691.46 km, near P2

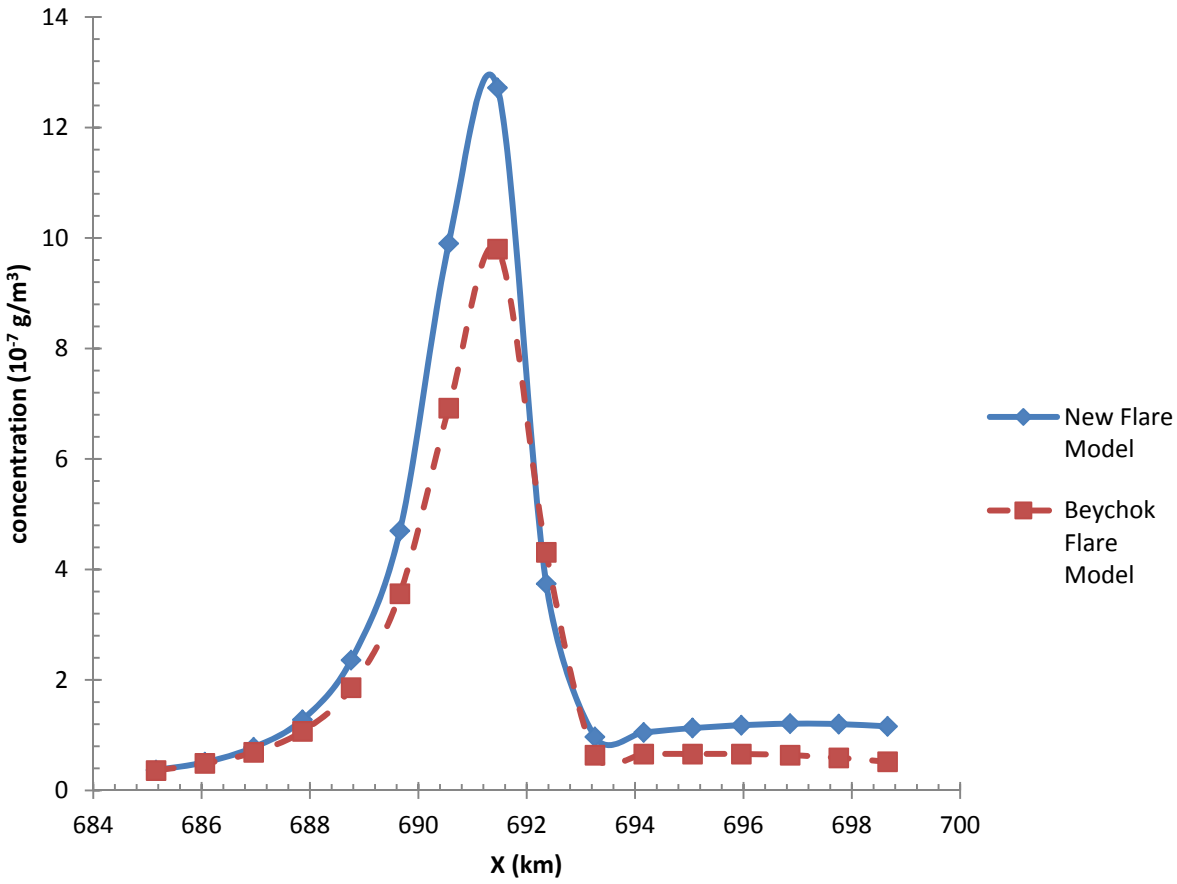

Figure 5-10: Concentration of SO_2 at hr 08:00 for Y=5715.36 km, near P2

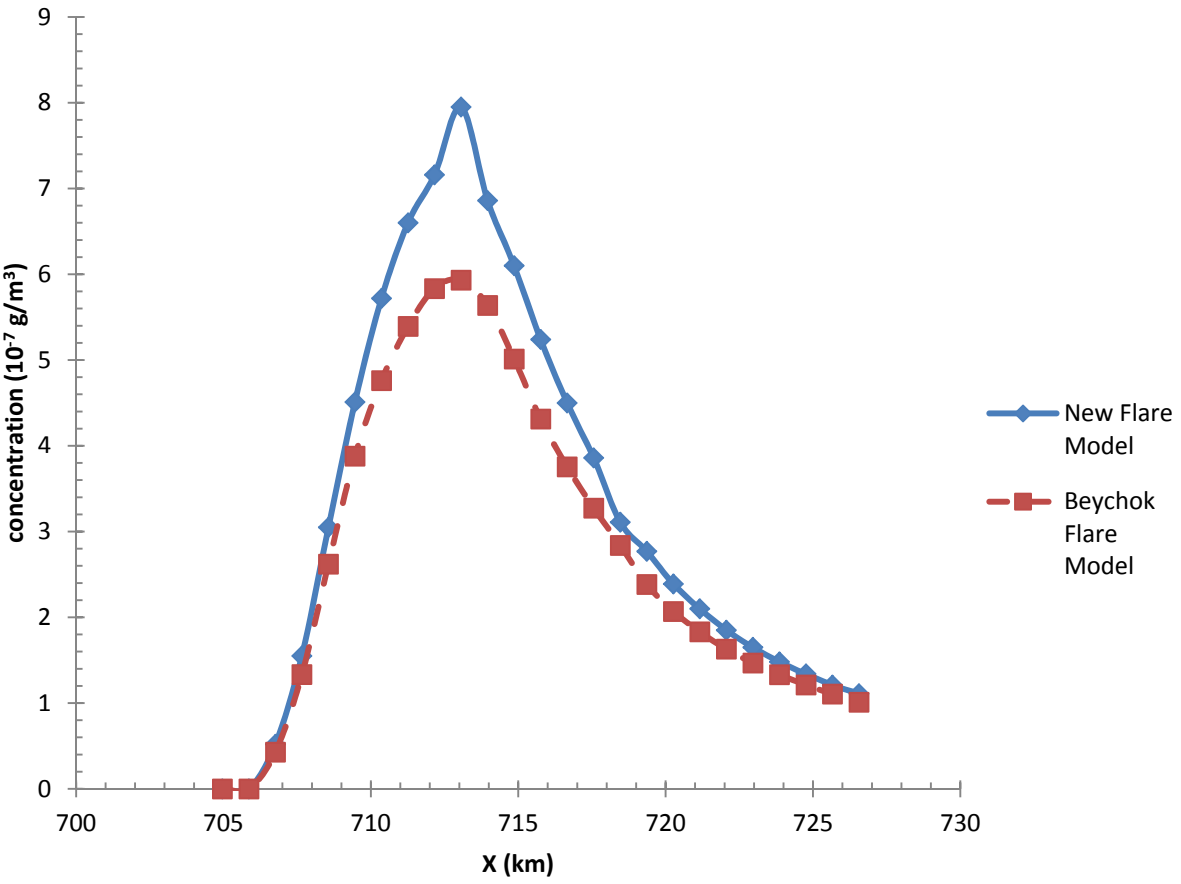

Figure 5-11: Concentration of SO_2 at hr 19:00 for Y=5697.36 km, near P3

As is shown in the above figures, the simulation based on the new flare model generally predicts a higher concentration of the pollutant than the simulation based on the Beychok flare model for the near field. In some cases, especially for moderate wind speed, both approaches have almost the same results. This is due to height of the flare which is predicted to be similar in both flare models. However, the results vary by a factor of two in the case of low or high wind speed.

On the other hand, for the far field the results are completely different. For areas far from sources, it is the Beychok flare model which predicts higher concentration. Figures 5-12 and 5-13 show the concentration of the pollutant far from any sources in some random coordinates.

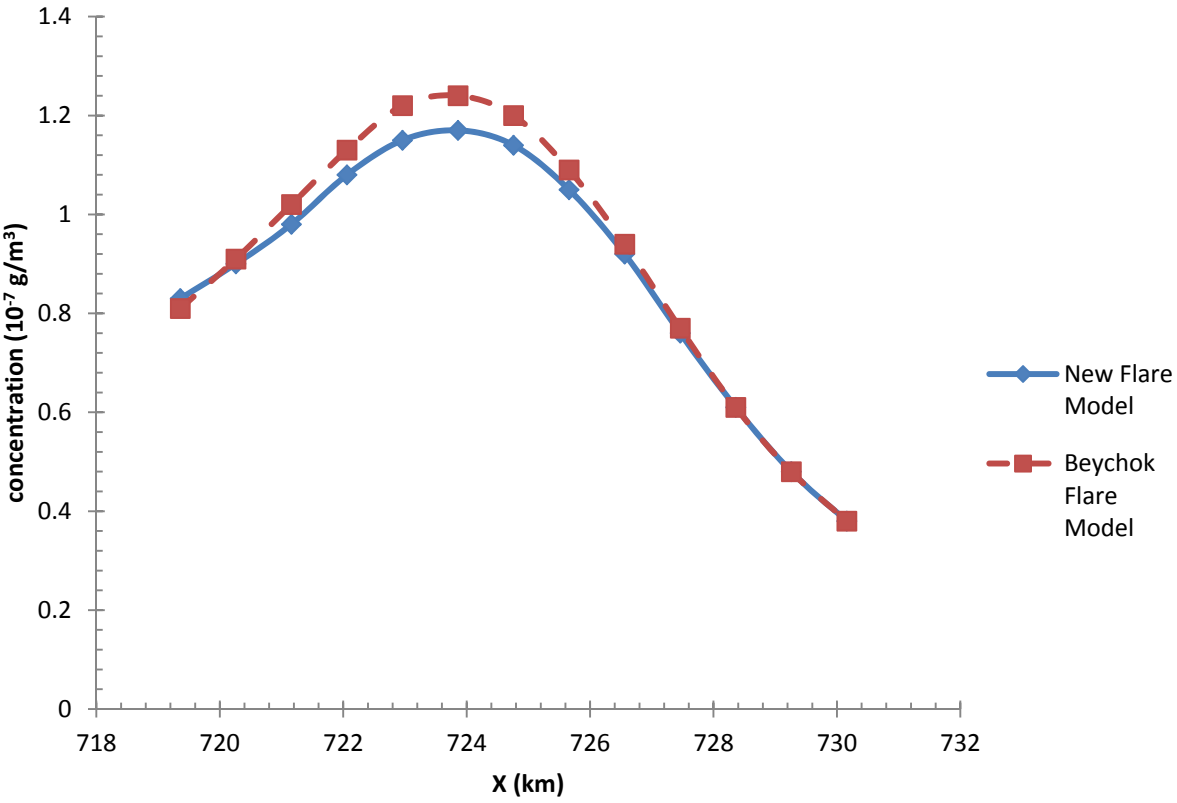

Figure 5-12: Concentration of SO_2 at hr 19:00 for Y=5754.06 km

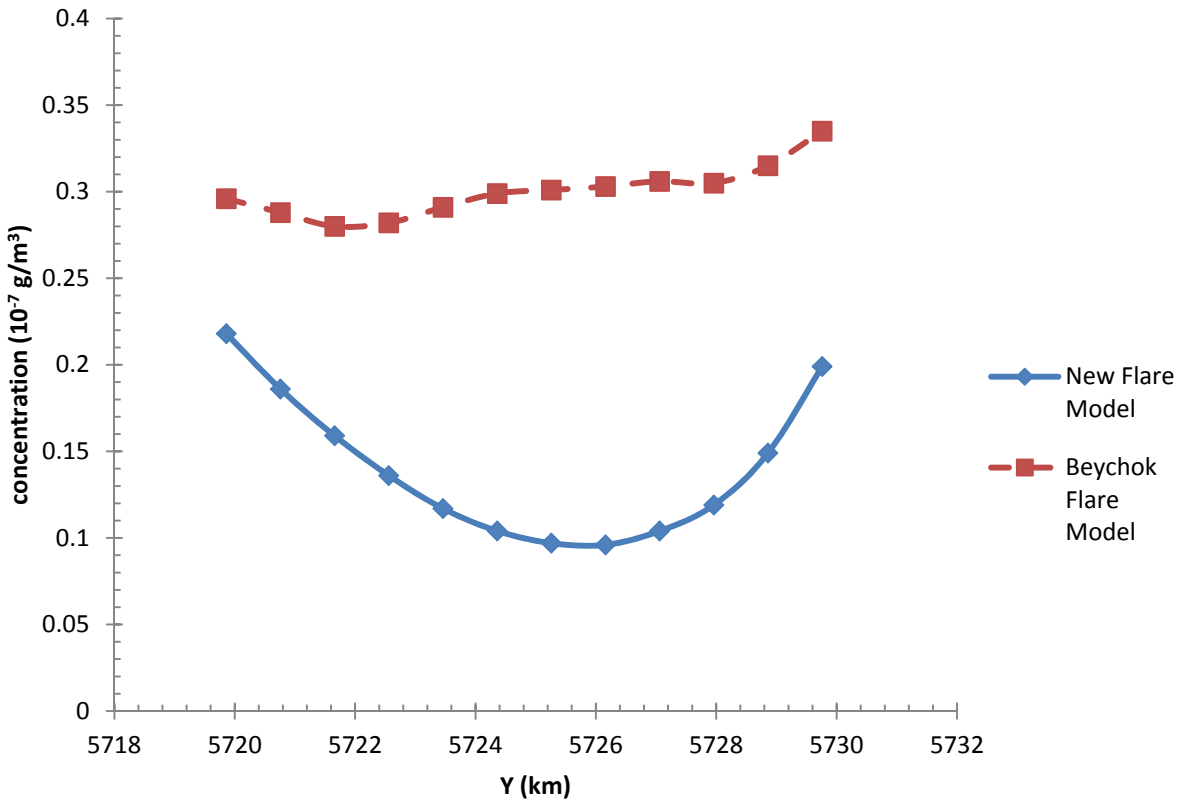

Figure 5-13: Concentration of SO_2 at hr 06:00 for X=714.86 km

Since the discussed flare model is sensitive to the wind speed, at low wind speed it predicts greater flame heights than the Beychok model. In contrast, for high wind speed, the discussed model predicts less flame height.

Chapter Six: **Conclusion and Future Work**

6.1 Conclusion

In this study a simple and comprehensive flare model was developed. This model is based on simple (one-dimensional) momentum, mass, and energy balances. All equations were combined and formed a set of differential equations which need to be solved along with some auxiliary equations. These auxiliary equations are responsible for calculating the emissivity, entrainments parameters, and including the rate of reaction into the model.

This research consists of three main sections. In the first part, the basic model was developed based on the previous work by De Visscher (2009). The basic model predicts the characteristics of the flare assuming that 25% of heat produced by flaring is emitted by radiation. It was also assumed that the combustion reaction occurs instantaneously. These two simplifying assumptions prevented the use of a complete formulation for calculating the emissivities of separate species in the flare, and the reaction rate of combustion. These assumptions make the basic model simple and fast to run, however the model is still able to reproduce observed flame lengths and angles accurately. The fit between the measurement data and the model values was optimized by adjusting the entrainment parameters and the relationship between the fraction of entrained air mixed into the burning part of the flame and the flare gas/wind velocity ratio.

In the second section, the basic model was improved to include the rate of the reactions. For the sake of simplicity, reactions in the combustion of pure methane were considered. Moreover, the emissivity of the flare was calculated in a more comprehensive method. In the improved model, emissivities of the gaseous species in the flare were considered separately from the emissivity of particulate matter, and the total emissivity was calculated according to the total optical density of species. Comparing the basic and improved model illustrates that the combustion reactions in the flaring of pure methane is close to instantaneous. As a result, the temperature profile and also the flare parameters such as height and length predicted are almost the same in the both models. The model predicts that the emissivity of the flame is predominantly due to particulate matter, and the contributions of water and carbon monoxide are negligible. In typical flaring conditions, the model predicts that about 10% of the produced heat is lost as radiation, which corresponds with

the value used in the GPSA Handbook. It follows that the new emissivity calculation is a marked improvement of the model, whereas the inclusion of reaction kinetics is a non-essential part of the model, and was not retained in the next section of this work.

In the last part the effect of implementing the basic flare model in the CALPUFF air dispersion model was investigated. A different flare model by Beychok (2005) was taken into account to compare the results of its effects in the CALPUFF simulation with the proposed model. Concentration profiles for each simulation show that the dispersion simulation based on the proposed model tends to predict higher concentrations of contaminants in the near field while the simulation based on the Beychok method shows the concentration of contaminants higher than the proposed model for the far field of sources. These differences in some cases are more than 100 percent, which is considerable.

This simple structure of the new proposed flare model allows it to be embedded into the air dispersion modeling software (such as CALPUFF) easily. Currently, regulatory models use variants of Beychok's (2005) approach which is not as accurate as the discussed model. More sophisticated models exist (e.g. based on CFD), but these are too complex to be used in combination with air dispersion models.

6.2 Future Work

In this study f_{mix}, a variable that described the fraction of air mixed into the flame that takes part in the combustion, is a function of ratio of the wind speed to the exit stack gas velocity. To calculate its value, results of the basic model were calibrated to some observed data. Computing values for f_{mix} for different exit stacks and wind speeds could be improved by calibrating to more experimental and observed data with a greater variety of wind speeds and exit stack velocities.

In this study of flames from flares it is assumed that flaring achieves complete combustion. However, flaring is rarely successful in burning with 100% efficiency. EPA (2000) has reported a value of 98% for flare combustion efficiency for properly operated flares, however flaring gases with low heats of combustion has been shown to have efficiencies as low as 65% (Blackwood, 2000). Since efficiency of the flare directly affects the calculation of the heat

generation and the flame length in the model, including the efficiency of flaring into the model could improve the accuracy of the model. Although relatively accurate CFD models for the efficiency of flaring have been provided by Blackwood (2000), Castineira and Edgar (2008), and Singh et al. (2012), these models cannot be included in this flare model due to their complexity and computation time. Instead, the empirical models of Johnson and Kostiuk (2002) or Leahey and Preston (2001) for the efficiency of flaring can be applied for this purpose.

To validate the results in the CALPUFF air dispersion model, the flare model could be compared to other flare models such as the flare model which is used by the Energy Resources Conservation Board (ERCB). In addition, the resolution of the terrain in the CALPUFF simulation also can be increased for a better understanding of local effects of flaring to the dispersion of contaminants.

Finally, the main goal of this study is to improve the accuracy of dispersion modeling in air dispersion model such as CALPUFF. Hence, the next step would be embedding this model into the dispersion model code. This would enable the dispersion models to model the flare stacks directly. For example, translating this model into the Fortran programing language and compiling the code with CALPUFF dispersion codes, would prepare a flare module in the CALPUFF model. Therefore, CALPUFF would be able to simulate air dispersion from the flare stacks more accurately.

References

American Petroleum Institute (1969), “Guide for pressure relief and depressuring systems”, API RP 521, First Edition

Argyropoulos, C.D., Sideris, G.M., Christolis, M.N., Nivolianitou, Z., Markatos N.C. (2009), “Modelling pollutants dispersion and plume rise from large hydrocarbon tank fires in neutrally stratified atmosphere”, Atmos. Environ., Vol. 44, pp. 803-813

Arya, S.P. (1999), “Air Pollution Meteorology and Dispersion”, Oxford University Press, New York

Benson, P.E. (1979), “CALINE3-A versatile dispersion model for predicting air pollutant levels near highway and arterial streets”, Interim Report, Washington, D.C.

Beychok, M.R. (2005), “Fundamentals of Stack Gas Dispersion”, 4th edition, Beychok, Newport Beach, CA

Bjorklund, J.R., Bowers, J.F. (1982), “User’s instructions for the SHORTZ and LONGZ computer programs”, EPA-903/9-82-004a and b, U.S. Environmental Protection Agency, Philadelphia

Blackwood, R.B. (2000), “An evaluation of flare combustion efficiency using open-path Fourier transform infrared technology”, J. Air Waste Manage. Assoc., Vol. 50, pp. 1714-1722

Bowers, J.R., Bjorklund, J.R., Cheney, C.S. (1979), “Industrial source complex (ISC) dispersion model user’s guide”, EPA-450/4-79-030 and 031, U.S. Environmental Protection Agency, Research Triangle Park, N.C.

Briggs, G.A. (1965), “A plume rise model compared with observations” J. Air Pollut. Control Assoc., Vol. 15, pp. 433

Briggs, G.A. (1968), “Concawe meeting: Discussion of the comparative consequences of different plume rise formulas”, Atmos. Environ., Vol. 2, pp. 228-232

Briggs, G.A. (1969), "Plume Rise", AEC Critical Review Series, U.S. AEC Technical Information Center, Oak Ridge, TN

Briggs, G.A. (1972), “Discussion: chimney plumes in neutral and stable surroundings”, Atmos. Environ., Vol. 6, pp. 507-510

Briggs, G.A. (1975), “Plume rise prediction”, Lectures on Air Pollution and Environmental Impact Analyses, pp. 59-111, Am. Met. Soc., 34 Beacon Street, Boston, MA 02108, USA

Brzustowski, T.A. (1976), “Flaring in the energy industry”, Prog. Energy Combust. Sci., Vol. 2, pp. 129-141

Burt, E.W. (1977), “VALLEY model user’s guide”, EPA-450/2-77-018, U.S. Environmental Protection Agency, Research Triangle Park, N.C.

Castineira, D., Edgar, T.F. (2008), “CFD for simulation of crosswind on the efficiency of high momentum jet turbulent combustion flames”, J. Environ. Eng., Vol. 7, pp. 561871

Catalano, J.A., Turner, D.B., Novak, J.H. (1987), “User’s guide for RAM”, 2nd Edition, EPA-600/3-87-046, U.S. Environmental Protection Agency, Research Triangle Park, N.C.

Colbeck, I., Atkinson, B., Johar, Y. (1997), “The morphology and optical properties of soot produced by different fuels”, J. Aerosol Sci., Vol. 28, pp. 715–723

Cooper, C.D., Alley, F.C. (2011), “Air Pollution Control”, Waveland Press Inc., Long Grove, Illinois

Cooper, C.D., Alley, F.C., Overcamp, T.J. (1982), “Hydrocarbon Vapor Incineration Kinetics”, Environ. Prog., Vol. 1, pp. 129-133

De Visscher, A. (2009), “Extending the prime plume rise model to include flare combustion”, Proceedings 8th World Congress of Chemical Engineering, Montreal, Canada

De Visscher, A. (2013), “Air Dispersion Modeling. Foundations and Applications”, J.Wiley & Sons, forthcoming

DiCristofaro, D.C., Hanna, S.R. (1989), “OCD: The offshore and coastal dispersion model”, Version 4, Vols. 1 and 2, Westford, MA

Dobbins, R.A., Mulholland, G.W., Bryner, N.P. (1994), "Comparison of a fractal smoke optics model with light extinction measurements", Atmos. Environ., Vol. 28, pp. 889–897

Dobbins, R.A., Megaridis, M. (1991), "Absorption and scattering of light by polydisperse aggregates", Appl. Optics, Vol. 30, pp. 4747–4754

Dryer, F.L., Glassman, I. (1973), "High-temperature oxidation of CO and CH_4", 14th Symposium (International) on Combustion, Pittsburgh, PA: The Combust. Inst., pp. 987

Environment Canada website (2012), viewed September 01, 2012 <http://www.ec.gc.ca/ges-ghg/default.asp?lang=En&n=DDCA72D0-1>

EPA (1988), "Screening producers for estimating the air quality impact of stationary sources, draft for public comment", EPA-450/4-88-010, U.S. Environmental Protection Agency, Research Triangle Park, N.C.

EPA (1989), "User's guide to the complex terrain dispersion model plus algorithms for unstable situation (CTDMPLUS)", Vol. 1, EPA-600/8-89-041, U.S. Environmental Protection Agency, Research Triangle Park, N.C.

EPA (1990a), "User's guide to the urban airshed model", Vols. 1-8, EPA-454/B-93-004, U.S. Environmental Protection Agency, Research Triangle Park, N.C.

EPA (1990b), "User's guide to TSCREEN: A model for screening toxic air pollutant concentrations", EPA-450/4-91-013, U.S. Environmental Protection Agency, Research Triangle Park, N.C.

EPA (1992a), "The SCREEN2 model user's guide", EPA-450/4-92-006, U.S. Environmental Protection Agency, Research Triangle Park, N.C.

EPA (1992b), "User's guide for the industrial source complex (ISC2) dispersion model", Vols. 1-3, EPA-450/4-92-008a, b, and c, U.S. Environmental Protection Agency, Research Triangle Park, N.C.

EPA (1995), "User's guide for the industrial source complex (ISC3) dispersion models", Vols. 1-3, EPA-454/B-95-003a, b, and c, U.S. Environmental Protection Agency, Research Triangle Park, N.C.

EPA (2003), “Appendix W to part 51-Guideline on Air Quality Models”, U.S. Environmental Protection Agency, 68 FR 18448, Research Triangle Park, N.C.

Ezzati, M., Lopez, A.D., Vander Hoorn, S., Murray, C.J.L. (2002), “Selected major risk factor and global and regional burden of disease”, Lancet, Vol. 360, pp. 1347-1360

Fairweather, M., Jones, W.P., Lindstedt, R.P., Marquis, A.J. (1991), “Prediction of a turbulent reacting jet in a cross-flow”, Combust. Flame, Vol. 84, pp. 361-375

Forster, P., Ramaswamy, V., Artaxo, P., Berntsen, T., Betts, R., Fahey, D.W., Haywood, J., Lean, J., Lowe, D.C., Myhre, G., Nganga, J., Prinn, R., Raga, G., Schulz, M., Van Dorland, R. (2007), “Changes in atmospheric constituents and in radiative forcing. In: climate change 2007: The physical science basis. Contribution of working group I to the fourth assessment report of the intergovernmental panel on climate change [Solomon, S., D. Qin, M. Manning, Z. Chen, M. Marquis, K.B. Averyt, M.Tignor and H.L. Miller (eds.)]”, Cambridge University Press, Cambridge, United Kingdom and New York, NY, USA

Fraser, S. (2011), “Estimating intake fraction by loose-coupling an air dispersion model and a geospatial information system (GIS)”, Master of Science Thesis, University of Calgary, Calgary, Alberta

GPSA (2012), GPSA Data Book, 13th Ed., Gas Processors Supplies Association

Hernandez, J., Crespo, A., Duijm, N.J. (1995), “Numerical modeling of turbulent jet diffusion flames in the atmospheric surface layer”, Combust. Flame, Vol. 101, pp. 113-131

Hewitt, C. (2001), “The atmosphere chemistry of sulfur and nitrogen in power station plumes”, Atmos. Environ., Vol. 35, pp. 1155-1170

Hottel, H.C., Egbert, R.B. (1942), Trans. Am. Inst. Chem. Eng., Vol. 38, pp. 531

Hoult, D.P., Weil, J.C. (1972), “Turbulent plume in laminar cross flow”, Atmos. Environ., Vol. 6, pp. 513-531

Howard, J.B., Williams, G.E., and Fine, D.H. (1973), “Kinetics of carbon monoxide oxidation in postflame gases”, 14th Symposium (International) on Combustion, Pittsburgh, PA: Combust. Inst., pp. 975

Irwin, J.S., Chico, T., Catalano, J. (1985), "CDM 2.0 (climatological dispersion model) user's guide", U.S. Environmental Protection Agency, Research Triangle Park, N.C.

Johnson, M. (2010) "Measuring PM emission in the upstream oil and gas industry", presentation in Petroleum Technology Alliance of Canada Air Issues Forum, Calgary, AB, Canada

Johnson, M.R., Devillers, R.W., Yang, C., Thomson, K.A. (2010) "Sky-scattered solar radiation based plume transmissivity measurement to quality soot emissions from flares", Environ. Sci. Technol., Vol. 44, pp. 8196-8202

Johnson, M.R., Kostiuk, L.W. (2002), "A parametric model for the efficiency of a flare in crosswind", Proc. Combust. Inst., Vol. 29, pp. 1943-1950

Jones, H.R.N., (2000) "Radiation Heat Transfer", Oxford University Press Inc., New York

Kalghatgi, G.T. (1983) "The visible shape and size of a turbulent hydrocarbon jet diffusion flame in a cross wind", Combust. Flame, Vol. 52, pp. 91-106

Lawal, M.S., Fairweather, M., Ingham, D.B., Ma, L., Pourkashanian, M., Williams, A. (2010), "Numerical study of emission characteristics of a jet flame in cross-flow", Combust. Sci. Technol., Vol. 182, pp. 1491-1510

Leahey, D.M., Paskall, H.G., Schroeder, M.B., Zelensky, M.J. (1985), "A preliminary study of the chemical composition and combustion efficiency of a sour gas flare", Alberta Environment, Research Management Division Report 85/30, Edmonton, Alberta, Canada

Leahey, D.M., Preston, K. (2001), "Theoretical and observational assessments of flare efficiencies", J. Air Waste Manage. Assoc., Vol. 51, pp. 1610-1616

Leahey, D.M., Schroeder, M.B. (1987), "Observations and predictions of jet diffusion flame behavior", Atmos. Environ., Vol. 21, No. 4, pp. 777-784

Leahey, D.M., Schroeder, M.B. (1990), "Observations and predictions of jet diffusion flame behavior - reply", Atmos. Environ., Vol. 24a, pp. 2527-2529

Leckner, B. (1972), “Spectral and total emissivity of water vapor and carbon monoxide”, Combust. Flame, Vol. 19, pp. 33-48

Liousse, C., Cashier, H., Jennings, S.G. (1993), “Optical and thermal measurements of black carbon aerosol content in different environments: variation of specific attenuation cross section, sigma (σ)”, Atmos. Environ., Vol. 27, pp. 1203-1211

Liu, D.H.F., Liptak, B.G. (2000), “Air Pollution”, Lewis Publishers, Boca Raton, FL

Lorimer, G. (1986), “The AUSPLUME Gaussian plume dispersion model”, Environmental Protection Authority of Victoria, Melbourne, Victoria, Australia

Moosmuller, H., Arnott, W.P., Rogers, C.F., Chow, J.C., & Frazier, C.A. (1998), “Photoacoustic and Filter measurements related to aerosol light absorption during the Northern Front Range Air Quality Study (Colorado 1996/1997)”, J. Geophys. Res., Vol. 103, pp. 28149–28157

National Institute of Water and Atmospheric Research, Aurora Pacific Limited, and Earth Tech Incorporated (2004), “Good practice guide for atmospheric dispersion modeling”, a report for Ministry for the Environment, ISBN: 0-478-18941-9, Wellington, New Zealand

Nuclear Regulatory Commission (1972), “Safety Guide 123, onsite meteorological programs”, EPRI Report EC-137

Paine, R.J. Strimaitis, D.G., Dennis, M.G., Yamartino, R.J., Mills, M.T., Insley, E.M. (1987), “User’s guide to the complex terrain dispersion model”, Vol. 1, EPA-600/8-87-058a, U.S. Environmental Protection Agency, Research Triangle Park, N.C.

Paine, R.J., Egan, B.A. (1987), “User’s guide to the rough terrain diffusion model (RTDM)”, Rev. 3.20

Perry, R.H, Green, D. (1984), “Perry’s Chemical Engineers’ Handbook”, McGraw-Hill, 5th Edition, Singapore

Perry, S.G, Burns, D.J., Adams, L.H., Paine, R.J., Dennis, M.G., Mills, M.T., Strimaitis, D.G., Yamartino, R.J., Insley, E.M. (1989), “User’s guide to the complex terrain dispersion model plus algorithm for unstable situation (CTDMPLUSS)”, Vol. 1, EPA-600/8-89-041, U.S. Environmental Protection Agency, Research Triangle Park, N.C.

Perry, S.G., Burns, D.J., Adams, L.H., Paine, R.J., Dennis, M.G., Mills, M.T., Strimaitis, D.G., Yamarantino, R.J., Insley, E.M. (1989), "User's guide to the complex terrain dispersion model plus algorithm for unstable situation (CTDMPLUS) volume 1: model description and user instruction", EPA-600/8-89/041, U.S. Environmental Protection Agency, Research Triangle Park, NC

Perry, S.G., Burns, D.J., Cimorelli, A.J. (1990), "User's guide to CDTMPLUS", Vol. 2, EPA-600/8-90-087, U.S. Environmental Protection Agency, Research Triangle Park, N.C.

Sandler, S.I. (1999), "Chemical, Biological and Engineering Thermodynamic", 3rd Edition, USA, Wiley

Schnaiter, M., Horvath, H., Mohler, O., Naumann, K.H., Saathoff, H., Schock, O.W. (2003), "UV-VIS-NIRspectral optical properties of soot and soot-containing aerosols", J. Aerosol Sci., Vol. 34, pp. 1421-1444

Schulman, L.L., Scire, J.S. (1980), "Buoyant line and point source (BLP) dispersion model user's guide", Doc. P-7304B, Concord, Mass.

Schulman, L.L., Strimaitis, D.G., Scire, J.S. (2000), "Development and evaluation of the PRIME plume rise and building downwash model", J. Air Waste Manage. Assoc., Vol. 50, pp. 378–390

Scire, J.S., Lurman, F.W., Bass, A., Hanna, S.R (1984b), "User's guide to the MESOPUFF II model and related processor programs", EPA-600/8-84-013, U.S. Environmental Protection Agency, Research Triangle Park, N.C.

Scire, J.S., Lurman, F.W., Bass, A., Hanna, S.R. (1984a), "Development of the MESOPUFF II dispersion model", EPA-600/3-84-057, U.S. Environmental Protection Agency, Research Triangle Park, N.C.

Scire, J.S., Strimaitis, D.G., Yamartino, R.J. (1990a), "Model formulation and user's guide for the CALMET meteorological model", Prepared for California Air Resource Board by Sigma Research Corporation, Concord, MA

Scire, J.S., Strimaitis, D.G., Yamartino, R.J. (1990b), "Model formulation and user's guide for the CALPUFF dispersion model", Prepared for California Air Resource Board by Sigma Research Corporation, Concord, MA

Scire, J.S., Strimaitis, D.G., Yamartino, R.J. (2000), "A user's guide for the CALPUFF dispersion Model (Version 5)", Earth Tech, Inc.

Segal, H.M. (1988), "A microcomputer pollution model for civilian airports and air force basis - Model application and background", FAA-EE-88-5, Washington, D.C.

Segal, H.M. (1991), "EDMA - Microcomputer pollution model for civilian airports and air force basis: User's guide", FAA-EE-91-3, Washington, D.C.

Segal, H.M., Hamilton, P.L. (1988), "A Microcomputer pollution model for civilian airports and air force basis - Model description", FAA-EE-88-4, Washington, D.C.

Seigel, R., Howel, J.R. (2002), "Thermal Radiation Heat Transfer", 4th edition, Taylor & Francis, New York

Singh, K.D., Dabade, T., Vaid, H., Gangadharan, P., Chen, D., Lou, H.H., Li, X., Li, K., Martin, C.B. (2012), "Computational fluid dynamics modeling of industrial flares operated in stand-by mode", Ind. Eng. Chem. Res., Vol. 51, pp. 12611-12620

Smith, P.T., Thurston, C.M., Chambers, A. (2009), "Large eddy simulation of industrial flares", viewed November 1, 2012, <http://www.flaresimulation.org/arc/>

Turner, B.C., Schulze, R.H. (2007), "Practical Guide to Atmospheric Dispersion Modeling", Trinity Consultants, Inc. and Air & Waste Management Association, Dallas, TX

Turner, D.B. (1994), "Workbook of Atmospheric Dispersion Estimates: An Introduction to Dispersion Modeling", 2nd Edition, Lewis Publishers

Turner, D.B., Novak, J.H. (1978), "User's guide for RAM", Vols. 1 and 2, Report EPA-600/8-78-016a and b, U.S. Environmental Protection Agency, Research Triangle Park, N.C.

Wendt, J.F. (1992), "Computational Fluid Dynamics – An Introduction", Springer-Verlag Berlin and Heidelberg GmbH & Co. K, Berlin

Williams, G.C., Hottel, H.C., Morgan, A.C. (1969), "The combustion of methane in a jet-mixed reactor", 12th Symposium (International) on Combustion, Pittsburgh, PA: The Combustion Institute, pp. 913

World Health Organization (2012), “Estimated deaths & DALYs attributable to selected environmental risk factors, by WHO Member State, 2002”, viewed July 1, 2012. <http://www.who.int/entity/quantifying_ehimpacts/countryprofilesebd.xls>

Appendices

Appendix A

Adiabatic Lapse Rate

This derivation is the calculation of the altitude dependence of temperature of what is called a neutral atmosphere, or adiabatic atmosphere.

Start from the energy conservation law:

$dU = dq + dW$ .....equation 1

U is the internal energy (J) of the air parcel, q is the heat added to the air parcel (J), and W is the work added to the air parcel (J). For adiabatic conditions it can be assumed that $dq = 0$.

$dU = dW$.....equation 2

On the other hand

$U = H - pV$.....equation 3

Differentiation leads to:

$dU = d(H - pV) = dH - pdV - Vdp$ .....equation 4

The enthalpy change with temperature at constant pressure is the definition of the heat capacity at constant pressure:

$dH = mc_{p,air}dT$ .....equation 5

Where m is the mass of the air parcel (kg), $c_{p,air}$ is the specific heat of air (J/kg K), and T is the absolute temperature (K). Mechanical work is due to compression/expansion, and is given by:

$dW = -pdV$.....equation 6

The minus sign indicates that the work exerted on the air parcel is positive in compression. Substitution of the energy conservation law equation with the above equation leads to:

$dU = -pdV$.....equation 7

Substitution of equations 5 and 7 into equation 4 leads to:

$$-\mathrm{pdV} = \mathrm{mc_{p,air}dT} - \mathrm{pdV} - \mathrm{Vdp}$$

or

$$\mathrm{mc_{p,air}dT} = \mathrm{Vdp}$$ .....equation 8

The hydrostatic equation defines the altitude dependence of barometric pressure. This equation, which is a force balance for a thin layer of area 1 m^2, is given by:

$$(p + dp) + \rho g dz = p$$

Where p is barometric pressure (Pa), ρ is the density of the air (kg/m^3), g is acceleration of gravity (9.80665 m/s^2), and z is the altitude (m). Canceling out p and rewriting leads to the following equation:

$$dp = -\rho g dz$$

Substituting the hydrostatic equation into equation 8 leads to:

$$\mathrm{mc_{p,air}dT} = -\mathrm{V\rho gdz}$$.....equation 9

Since $m = V.p$:

$$\mathrm{c_{p,air}dT} = -\mathrm{gdz}$$

Or

$$\frac{\mathrm{dT}}{\mathrm{dz}} = -\left(\frac{\mathrm{g}}{\mathrm{c_{p,air}}}\right)$$ .....equation 10

The term $\left(\frac{g}{c_{p,air}}\right)$ which is called the adiabatic Lapse Rate, is applied only for dry air. In the presence of clouds or fog, the adiabatic Lapse Rate is given by:

$$\frac{\mathrm{dT}}{\mathrm{dz}} = -\left(\frac{\mathrm{g}}{c_{\mathrm{p,air}} + \Delta_{vap} H \frac{\mathrm{dw}}{\mathrm{dt}}}\right)$$.....equation 11

Where w is the water to air mass ratio

Appendix B

<u>Coefficients to be used in Equation 4.45 for water vapor and carbon dioxide (Leckner, 1972)</u>

Deviation from values calculated with spectral data is max ±5%.

Water vapor, T 400, M=2, N=2			
i	c_{0i}	c_{1i}	c_{2i}
0	-2.2118	-1.1987	0.035596
1	0.85667	0.93048	-0.14391
2	-0.10838	-0.17156	0.045915

Carbon dioxide, Hottels's diagram, M=2, N=3				
i	c_{0i}	c_{1i}	c_{2i}	c_{3i}
0	-3.3390	1.1996	-1.0604	0.16454
1	0.90786	0.086726	0.13797	-0.035144
2	-0.15563	-0.10292	0.064443	-0.014128

Appendix C

The basic flare model code

Data File:

```
tend = 20;
step = 0.01;
tspan = 0:step:tend;

Uatm = 2;                              %wind speed (m/s)

Tatm = 288;                            %T of atmosphere at height 0 (K)

Patm = 101325;                         %atmosphere pressure (pa)

lapse = -0.00975;                      %temperature lapse in the atmosphere
                                       dTatm/dz)

MO2 = 0.232;                           %mass fraction of oxygen in air

Mgas = 0.016;                          %molar mass of gas in kg/mol

Mair = 0.029;                          %molar mass of air in kg/km

ROatm = Mair*Patm/8.314472/Tatm;       %density of atmosphere (kg/m3)

ROflame = Mgas*Patm/8.314472/Tatm;     %density of flame (kg/m3)

correction = 1.6;                      %correction for entertainment parameters
                                       alpha and beta

epsf = 0.0116;                         %emissivity of the flame

epsair = epsf;                         %emissivity of the air

thf = -log(1-epsf);                    %Flame Optical thickness

thair = -log(1-epsair);                %Air optical thickness

th = thf + thair;                      %Overall Optical thickness


sig = 5.67e-8;                         %Stefan-Boltzmann constant

alpha = correction* 0.11;

beta = correction*0.6;
```

```
n = 4;
g = 9.81;

dUatmdz=0;
dstack = 0.10695;                   %diameter of stack(m)
rstack = dstack/2;                  %radius of stack(m)
hstack = 20;                        %height of stack(m)
Qc = 10000;                         %heating value in kJ/s
H = 50000;                          %heat of combustion in kJ/kg

m = Qc/H;                           %mass flow rate (kg/s)
Vrate = m/ROflame;                  %volumetric flow rate (m3/s)
Area = pi*rstack*rstack;
Ustk = Vrate/Area;                  %stack exit velocity
p1 = Uatm/Ustk;
Usc = Vrate/Area;                   %velocity of plume
fmix = 0.0362*exp(4.5679*p1);       %fraction of air mixing into the  plume
Tair = 288;                         %T of non-burning fraction of the flame
Tf = 288;                           %T of burning fraction of the plume
cpf = 1000;                         %specific heat of burning fraction of the
                                    plume air (J/kg K)
cpair = 1000;                       %specific heat of non-burning fraction of
                                    the flame air (J/kg K)

y0(1) = ROflame*Usc*rstack*rstack;
y0(2) = 0;
y0(3) = hstack;
y0(4) = y0(1)*(0-Uatm);
y0(5) = y0(1)*Usc;
y0(6) = 0;
```

```
y1init = y0(1);

y0(7) = y0(1);

y0(8) = 0;

y0(9) = 0;

y0(10) = 0;
```

Function file:

```
function dydt = f
(t,y,Uatm,Tatm,Patm,lapse,epsf,epsair,eps,thf,thair,th,sig,alpha,beta,n,g,dUa
tmdz,MO2,H,fmix,y1init,Mgas)


x = y(2);

z = y(3);

u = Uatm + y(4)/y(1);

w = y(5)/y(1);


frac = y(7)/y(1);

Tf = Tatm+y(8)/y(1)/frac;
    if frac == 1
        Tair = Tf;
    else
        Tair = Tatm+y(9)/y(1)/(1-frac);
    end

Tatm = Tatm+z*lapse;

ROatm = 0.029*Patm/8.314472/Tatm;

ROair = 0.029*Patm/8.314472/Tair;

MWf = (Mgas*y1init + 0.029*(y(7) - y1init))/y(7);

ROf = MWf*Patm/8.314472/Tf;

RO = 1/(frac/ROf+(1-frac)/ROair);

Usc = sqrt(u*u+w*w);

cpf = 1.9327e-10*Tf^4-7.9999e-7*Tf^3+1.1407e-3*Tf^2-4.4890e-1*Tf+1.0575e+3;

cpair = 1.9327e-10*Tair^4 - 7.9999e-7*Tair^3 + 1.1407e-3*Tair^2 - 4.4890e-
1*Tair + 1.0575e+3;

r = sqrt(y(1)/(RO*Usc));


dydt = zeros(10,1);

dydt(1) = 2*r*alpha*ROatm*abs(Usc-Uatm*u/Usc)+2*r*beta*ROatm*abs(Uatm*w/Usc);

dydt(2) = u/Usc;
```

```
dydt(3) = w/Usc;

dydt(4)=-r*r*RO*w*dUatmdz;

dydt(5)=g*r*r*(ROatm-RO);

dydt(7) = fmix*dydt(1);

dydt(6) = MO2/n/y1init*dydt(7);
if y(6) > 1
    dydt(6) = 0;
end

dydt(8) = y1init*(H*1000/cpf)*dydt(6)-frac*(lapse+g/cpf)*RO*w*r*r-
(2*eps*sig*r*frac/cpf)*(Tf^4-Tatm^4);

dydt(9) = -(1-frac)*(lapse+g/cpair)*RO*w*r*r;

dydt(10) = (2*sig*(1-exp(-th))*r*(Tf^4-Tatm^4))/(cpf*y1init*H*(1000/cpf));
```

Main File:

```
data

options = odeset('RelTol', 1e-6, 'AbsTol', 1e-8, 'InitialStep', 0.01);

[T,Y] =
ode45(@f,tspan,y0,options,Uatm,Tatm,Patm,lapse,epsf,epsair,eps,thf,thair,th,s
ig,alpha,beta,n,g,dUatmdz,MO2,H,fmix,y1init,Mgas);


figure(1)

plot(T,Y(:,6),'k','linewidth',2)
title('X vs S')
xlabel('S (distance aong the plume centerline, m)')
ylabel('X-CH4 (conversion of combustion to CH4)')


[s1,s2] = size(T);

for i=1:s1
    frac(i) = Y(i,7)/Y(i,1);
    Ta = Tatm + lapse*Y(i,3);
    Tf(i) = Ta + Y(i,8)/Y(i,1)/frac(i);
end

hold on

figure(2)

plot(T,Tf,'k','linewidth',2)
title('Tf vs S')

xlabel('S (distance along the plume centerline, m)')
ylabel('Tf (temperature of the flare, T)')


jj=0;
uu=0;
for i=1:100*tend+1
    if Y(i,6)>0.999 & jj==0
        jj=i;
        uu(jj)=T(i);
    end
end


flamelenght = uu(jj);

flameheight = Y(jj,3)-20;
```

Appendix D

The improved flare model code

Data file:

```
tend = 10;
step = 0.01;
tspan = 0:step:tend;

Uatm = 2;                          %wind speed (m/s)

Tatm = 288;                        %T of atmosphere at height 0 (K)

Patm = 101325;                     %atmosphere pressure (pa)

lapse = -0.00975;                  %temperature lapse in the atmosphere
                                   (dTatm/dz)

MO2 = 0.232;                       %mass fraction of oxygen in air

Mgas = 0.016;                      %molar mass of gas in kg/mol

Mair = 0.029;                      %molar mass of air in kg/km

ROatm = Mair*Patm/8.314472/Tatm;   %density of atmosphere (kg/m3)

ROflame = Mgas*Patm/8.314472/Tatm; %density of flame (kg/m3)

correction = 1.6;                  %correction for entertainment parameters
                                   alpha and beta

epsf = 0.0085;                     %emissivity of the flame

epsair = 0.0085;                   %emissivity of the air

thf = -log(1-epsf);                %Flame Optical thickness

thair = -log(1-epsair);            %Air optical thickness

th = thf + thair;                  %Overall Optical thickness


sig = 5.67e-8;                     %Stefan-Boltzmann constant

alpha = correction*0.11;

beta = correction*0.6;
```

```
n = 4;

g = 9.81;

dUatmdz=0;

dstack = 0.10695;                   %diameter of stack(m)

rstack = dstack/2;                  %radius of stack(m)

hstack = 20;                        %height of stack(m)

Qc = 10000;                         %heating value in kJ/s

H1 = 32500;                         %heat of combustion in kJ/kg CH4 (to CO)

H2 = 17500;                         % heat of combustion in kJ/kg CH4 (CO to
                                    CO2)

m = Qc/(H1+H2);                     %mass flow rate (kg/s)

Vrate = m/ROflame;                  %volumetric flow rate (m3/s)

Area = pi*rstack*rstack;

Ustk = Vrate/Area;                  %stack exit velocity

p1 = Uatm/Ustk

Usc = Vrate/Area;                   %velocity of plume

fmix = 0.0362*exp(4.5679*p1);       %fraction of air mixing into the  plume


Tair = 288;                         %T of non-burning fraction of the flame

Tf = 288;                           %T of burning fraction of the plume

cpf = 1000;                         %specific heat of burning fraction of the
                                    plume air (J/kg K)

cpair = 1000;                       %specific heat of non-burning fraction of
                                    the flame air (J/kg K)


y0(1) = ROflame*Usc*rstack*rstack;

y1init = y0(1);

y0(2) = 0;

y0(3) = hstack;

y0(4) = y0(1)*(0-Uatm);
```

```
y0(5) = y0(1)*Usc;

y0(6) = 0;

y0(7) = y0(1);

y0(8) = 0;

y0(9) = 0;

y0(10) = 0;

y0(11) = 0;
```

Function file:

```
function dydt =
f3(t,y,Uatm,Tatm,Patm,lapse,epsf,epsair,eps,thf,thair,th,sig,alpha,beta,n,g,d
Uatmdz,MO2,H1,H2,fmix,y1init,Mgas)


dydt = zeros(11,1);


x = y(2);

z = y(3);


u = Uatm + y(4)/y(1);

w = y(5)/y(1);


frac = y(7)/y(1);

Tf = Tatm+y(8)/y(1)/frac;
    if frac == 1
        Tair = Tf;
    else
        Tair = Tatm+y(9)/y(1)/(1-frac);
    end

Tatm = Tatm+z*lapse;

ROatm = 0.029*Patm/8.314472/Tatm;

ROair = 0.029*Patm/8.314472/Tair;

MWf = (Mgas*y1init + 0.029*(y(7) - y1init))/y(7);

ROf = MWf*Patm/8.314472/Tf;

RO = 1/(frac/ROf+(1-frac)/ROair);

ROinit = Mgas*Patm/8.314472/Tatm;   %density of burning gas in the initial
point pf stack

Usc = sqrt(u*u+w*w);

cpf = 1.9327e-10*Tf^4-7.9999e-7*Tf^3+1.1407e-3*Tf^2-4.4890e-1*Tf+1.0575e+3;

cpair = 1.9327e-10*Tair^4 - 7.9999e-7*Tair^3 + 1.1407e-3*Tair^2 - 4.4890e-
1*Tair + 1.0575e+3;

r = sqrt(y(1)/(RO*Usc));
```

```
%KINETIC CALCULATION

if (y(6) < 1)
    yCH4 = y1init*(1-y(6));
else
    yCH4 = 0;
end

if (y(6) - y(11) > 0)
    yCO = y1init*(y(6) - y(11))*1.75;           % mass flow rate of CO
else
    yCO = 0;
end

yCO2 = y1init*y(11)*2.75;           % mass flow rate of CO2

yH2O = y(6)*y1init*2.25;

yO2 = (frac*y(1)-y1init)*MO2 - y1init*(3*y(6) + y(11));

yN2 = (frac*y(1)-y1init)*(1-MO2);


ymCH4 = yCH4/0.016;

ymCO2 = yCO2/0.044;

ymH2O = yH2O/0.078;

ymO2 = yO2/0.032;

ymN2 = yN2/0.028;

ymCO = yCO/0.028;

ymsum = ymCH4 + ymCO2 + ymH2O + ymO2 + ymN2 + ymCO;

ymfO2 = ymO2/ymsum;

ymfCH4 = ymCH4/ymsum;

ymfCO = ymCO/ymsum;

ymfH2O = ymH2O/ymsum;


Z = 1.011e11;                       %collision factor

S = 1;                              %steric factor: S=16/MW

R = 8.314;                          %gas constant (j/mol.k)

RR = 0.08206;                       %gas constant (L.atm/mol.k)
```

```
E = (-0.00966*Mgas+46.1)*4.184*1000;      %activation energy (j)

A = (Z*S*ymfO2*Patm)/(RR);


CCH4 = ymfCH4*Patm/R/Tf;

CCO = ymfCO*Patm/R/Tf;

CH2O = ymfH2O*Patm/R/Tf;

dydt(1) = 2*r*alpha*ROatm*abs(Usc-Uatm*u/Usc)+2*r*beta*ROatm*abs(Uatm*w/Usc);

dydt(7) = fmix*dydt(1);

if t<1 && Tf<1000;
    k1 = Z*S*R*Tf/RR*exp(-E/8.314/1000);
    k2 = 1.3e8*exp(-30000*4.184/R/1000)*sqrt(CH2O);
    C_O2sqrt = (-0.032*0.5*k2*CCO+sqrt((0.032*0.5*k2*CCO)^2 +
4*0.032*1.5*k1*CCH4*dydt(7)*MO2/r/r))/(2*0.032*1.5*k1*CCH4);
    C_O2 = C_O2sqrt^2;
    rCH4 = k1*C_O2*CCH4;
    rCO2 = k2*CCO*C_O2sqrt;
else
    k1 = Z*S*R*Tf/RR*exp(-E/8.314/Tf);
    k2 = 1.3e8*exp(-30000*4.184/R/Tf)*sqrt(CH2O);
    if CCH4 == 0
        C_O2sqrt = (dydt(7)*MO2/r/r)/(0.032*0.5*k2*CCO);
    else
        C_O2sqrt = (-0.032*0.5*k2*CCO+sqrt((0.032*0.5*k2*CCO)^2 +
4*0.032*1.5*k1*CCH4*dydt(7)*MO2/r/r))/(2*0.032*1.5*k1*CCH4);
    end
    C_O2 = C_O2sqrt^2;
    rCH4 = k1*C_O2*CCH4;
    rCO2 = k2*CCO*C_O2sqrt;
end


%EMISSIVITY CALCULATION

%SOOT EMISSIVITY CALCULATION

c = 3e8;                              %speed of light (meter/sec)

h = 6.626e-34;                        %Planck constant (J*sec)

k = 1.38e-23;                         %Boltzman constant (J/K)

landa = (c*h)/(4.96*k*Tf);

cprime = 4000;                        %constant in: sigmaA=cprime/landa

sigmaA = cprime/(landa*1e9);

EF = 0.2;                             %emission factor (kg soot/1000m3 fuel)
```

```
cnst = (y1init*RO*EF*y(6))/(y(1)*ROinit*1000)*1000;
                                    %concentration of soot (g soot/m3 plume)

ODsoot = cnst*2*r*sigmaA;

epssoot = 1 - exp(-ODsoot)


%PARTIAL PRESSURE CALCULATION

molCO2 = y1init*frac*0.044/0.016/0.044;         %number of CO2 moles

molH2O = y1init*frac*0.036/0.016/0.018;         %number of H2O moles

molT = y(1)*frac/MWf;                           %total number of moles in the
flame

pCO2 = (Patm/100000)*(molCO2/molT);             %partial pressure of CO2(bar)

pH2O = (Patm/100000)*(molH2O/molT);             %partial pressure of HO2
(bar)


%H2O EMISSIVITY CALCULATION

if Tf>750
    taw = Tf/1000;
else
    taw = 0.75;
end
taw = abs(taw);
if taw>2.4
    taw = 2.4;
end
landaP = log10(abs(pH2O/100000*2*r*100*frac));
                                    %constant used in other equations

A  = 1.888 - 2.053*log10(taw);      %constant used in other equations

B = 1.10*taw^(-1.4);                %constant used in other equations

a0 = -2.2118 - 1.1987*taw + 0.035596*taw^2;
                                    %a0-a2 constant used in other equations

a1 = 0.85667 + 0.93048*taw - 0.14391*taw^2;

a2 = -0.10838 - 0.17156*taw + 0.045915*taw^2;

eps0H2O  = exp(a0 + a1*landaP + a2*landaP^2);
                                    %emissivity at pressure of 1 bar

PEH2O = Patm/100000*(1 + 4.9*pH2O/(Patm/100000)*sqrt(273/Tf));
                                    %equivalent pressure of H2O
```

```
epH2O = (A*PEH2O + B)/(PEH2O + A + B  -1);
                                    %portion of actual emissivity to
                                    emissivity at pressure of 1 bar

epsH2O = epH2O*eps0H2O;             %actual emmisivity of H2O


%CO2 EMISSIVITY CALCULATION

if Tf>750
    taw = Tf/1000;
else
    taw = 0.75;
end
taw = abs(taw);
if taw>2.4
    taw = 2.4;
end

landaP = log10(abs(pCO2/100000*2*r*100*frac));
                                    %constant used in other equations

A = 0.1*taw^(-1.45) + 1;
                                    %constant used in other equations

B = 0.23;                           %constant used in other equations

a0 = -3.3390 + 1.1996*taw - 1.0604*taw^2 + 0.16454*taw^3;
                                    %a0-a3 constant used in other equations

a1 = 0.90786 + 0.086726*taw + 0.13797*taw^2 - 0.035144*taw^3;

a2 = -0.15563 - 0.10292*taw + 0.064443*taw^2 - 0.0141128*taw^3;

eps0CO2 = exp(a0 + a1*landaP + a2*landaP^2);
                                    %emissivity at pressure of 1 bar

PECO2 = Patm/100000*(1 + 4.9*pCO2/(Patm/100000)*sqrt(273/Tf));
                                    %equivalent pressure of H2O

epCO2 = (A*PECO2 + B)/(PECO2 + A + B  -1);
                                    %portion of actual emissivity to
                                    emissivity at pressure of 1 bar

epsCO2 = epCO2*eps0CO2;             %actual emissivity of CO2


%TOTAL EMISSIVITY OF CO2/H2O/SOOT

x = pH2O/(pH2O + pCO2);            %constant used in other equation

landaP = log10(abs((pCO2+pH2O)/100000*2*r*100*frac));
                                    %constant used in other equations

if landaP < 0
```

```
    landaP = 0;
end

deltae = (x/(10.7 + 101*x) - 0.0089*x^10.4)*landaP^2.76;
                                    %overlap correction

epsCO2H2O = epsH2O + epsCO2 - deltae;

ODCO2H2O = -log(1-epsCO2H2O);       % Optical density of carbon monoxide

ODtotal = ODsoot + ODCO2H2O;        %Total optical density

eps = 1-exp(-ODtotal);              %total emissivity


%DIFFERENTIAL EQUATIONS

dydt(1) = 2*r*alpha*ROatm*abs(Usc-Uatm*u/Usc)+2*r*beta*ROatm*abs(Uatm*w/Usc);

dydt(2) = u/Usc;

dydt(3) = w/Usc;

dydt(4)=-r*r*RO*w*dUatmdz;

dydt(5)=g*r*r*(ROatm-RO);

if y(6) > 1
   dydt(6) = 0;
else
    dydt(6) = Mgas*r*r*rCH4/y1init;
end

dydt(7) = fmix*dydt(1);

if y(11) > 1
   dydt(11) = 0;
else
    dydt(11) = Mgas*r*r*rCO2/y1init;
end

dydt(8) = y1init*(H1*1000/cpf)*dydt(6)+y1init*(H2*1000/cpf)*dydt(11)-
frac*(lapse+g/cpf)*RO*w*r*r-(2*eps*sig*r*frac/cpf)*(Tf^4-Tatm^4);

dydt(9) = -(1-frac)*(lapse+g/cpair)*RO*w*r*r;

dydt(10) = (2*sig*(1-exp(-th))*r*(Tf^4-
Tatm^4))/(cpf*y1init*(H1+H2)*(1000/cpf));
```

Main file:

```
data

options = odeset('RelTol', 1e-6, 'AbsTol', 1e-8, 'InitialStep', 0.01);

[T,Y] =
ode45(@f3,tspan,y0,options,Uatm,Tatm,Patm,lapse,epsf,epsair,eps,thf,thair,th,
sig,alpha,beta,n,g,dUatmdz,MO2,H1,H2,fmix,y1init,Mgas);


figure(1)

plot(T,Y(:,6),':b','linewidth',2)

title('X vs S')

xlabel('S (distance along the plume centerline, m)')

ylabel('X-CH4 (conversion of combustion to CH4)')

hold on

figure(3)

plot(T,Y(:,11),'--r','linewidth',2)

title('X-CO2 vs S')

xlabel('S (distance along the plume centerline, m)')

ylabel('X-CO2 (conversion of combustion to CO2)')

[s1,s2] = size(T);

for i=1:s1
    frac = Y(i,7)/Y(i,1);
    Ta = Tatm + lapse*Y(i,3);
    Tf(i) = Ta + Y(i,8)/Y(i,1)/frac;
end

hold on

figure(2)

plot(T,Tf,'-.m','linewidth',2)

title('Tf vs S')

xlabel('S (distance aong the plume centerline, m)')

ylabel('Tf (temperature of the flare, T)')
```

```
jj=0;

uu=0;

for i=1:100*tend+1
    if Y(i,11)>0.999 && jj==0
        jj=i;
        uu(jj)=T(i);
    end
end

flamelenght = uu(jj);

flameheight = Y(jj,3)-20;
```